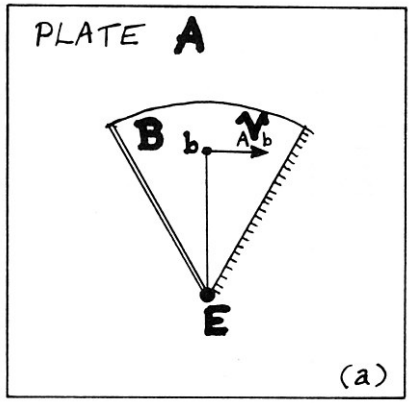
PLATE A
B
b
V_{Ab}
E
(a)

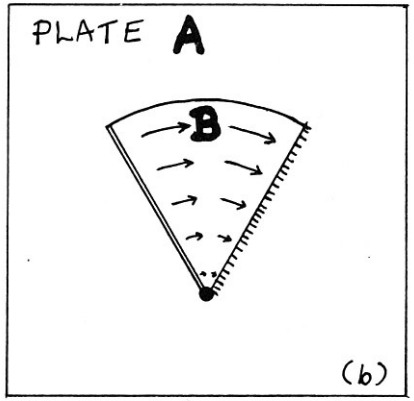
PLATE A
B
(b)

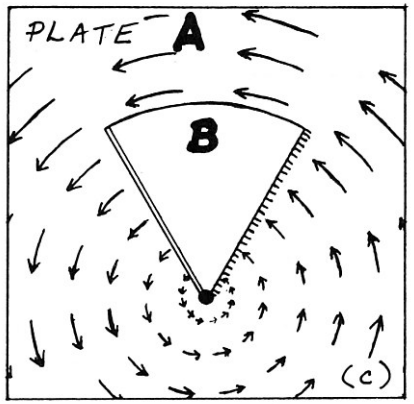
PLATE A
B
(c)

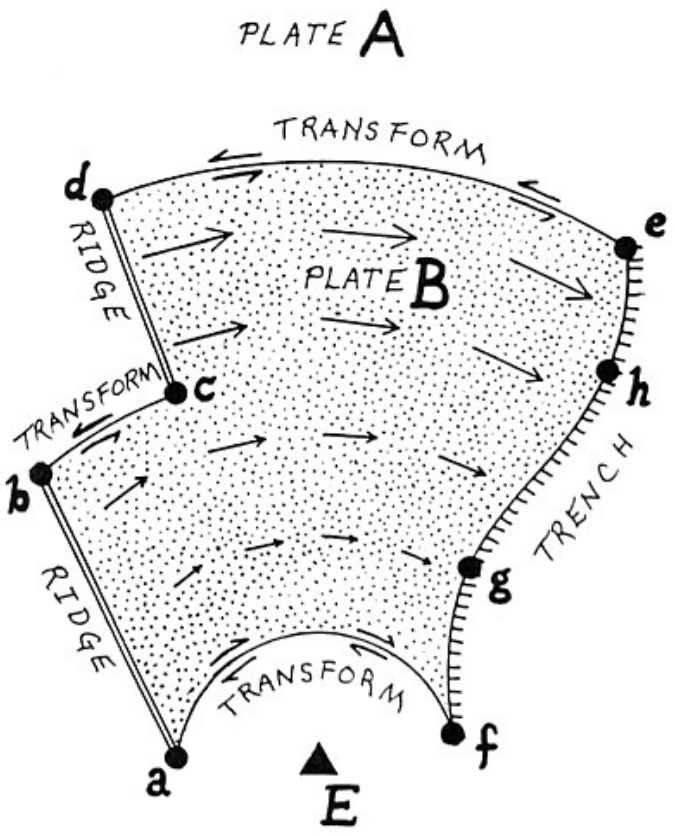
PLATE A
TRANSFORM
d
e
RIDGE
PLATE B
TRANSFORM
c
h
b
TRENCH
RIDGE
g
TRANSFORM
f
a
E

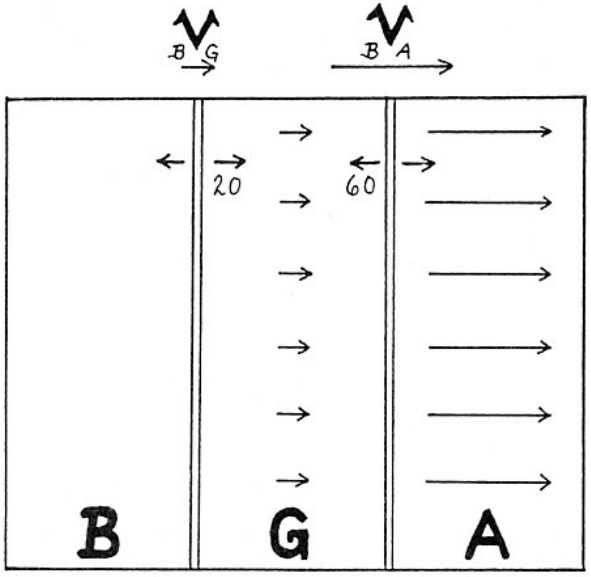
B G
B A
20
60
B
G
A

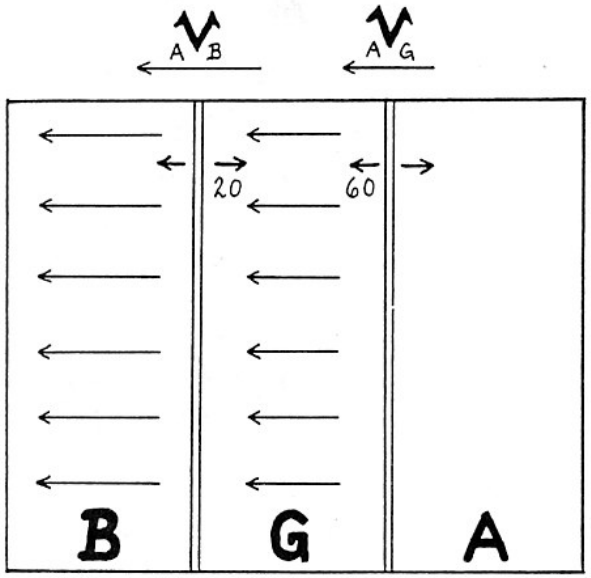
A B
A G
20
60
B
G
A

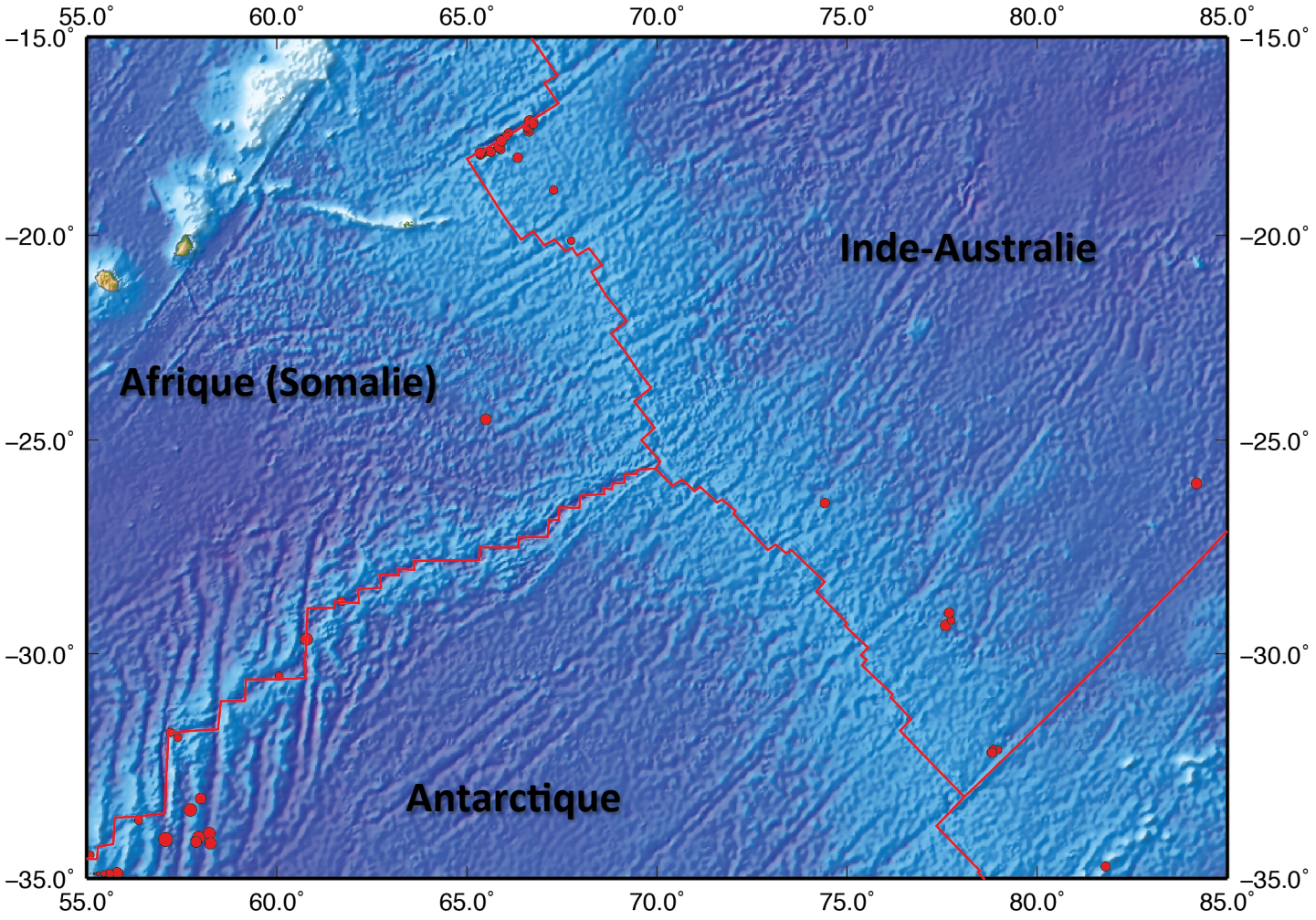
55.0°
60.0°
65.0°
70.0°
75.0°
80.0°
85.0°
−15.0°
−20.0°
−25.0°
−30.0°
−35.0°
Inde-Australie
Afrique (Somalie)
Antarctique

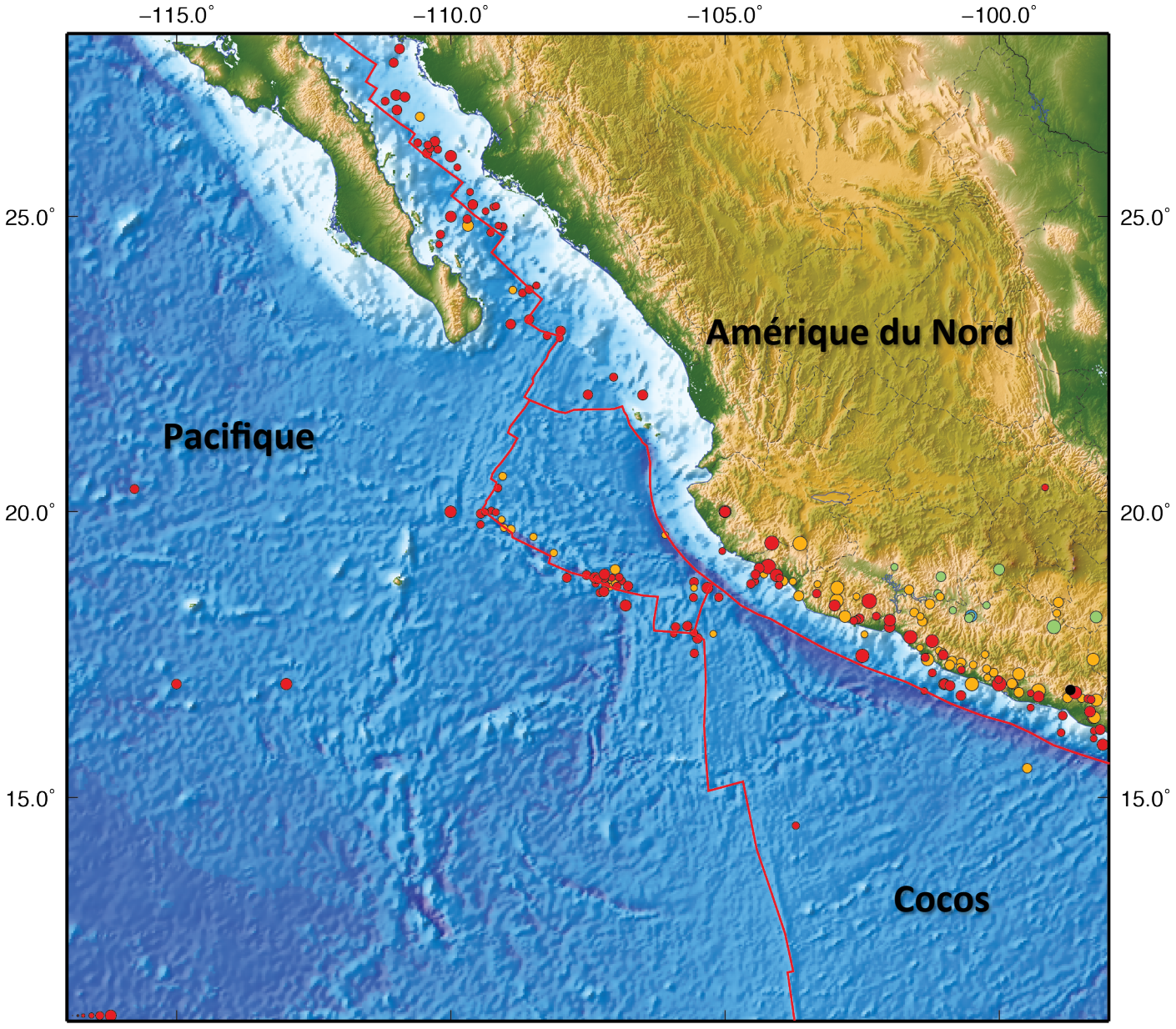
−115.0°
−110.0°
−105.0°
−100.0°
25.0°
20.0°
15.0°
Amérique du Nord
Pacifique
Cocos

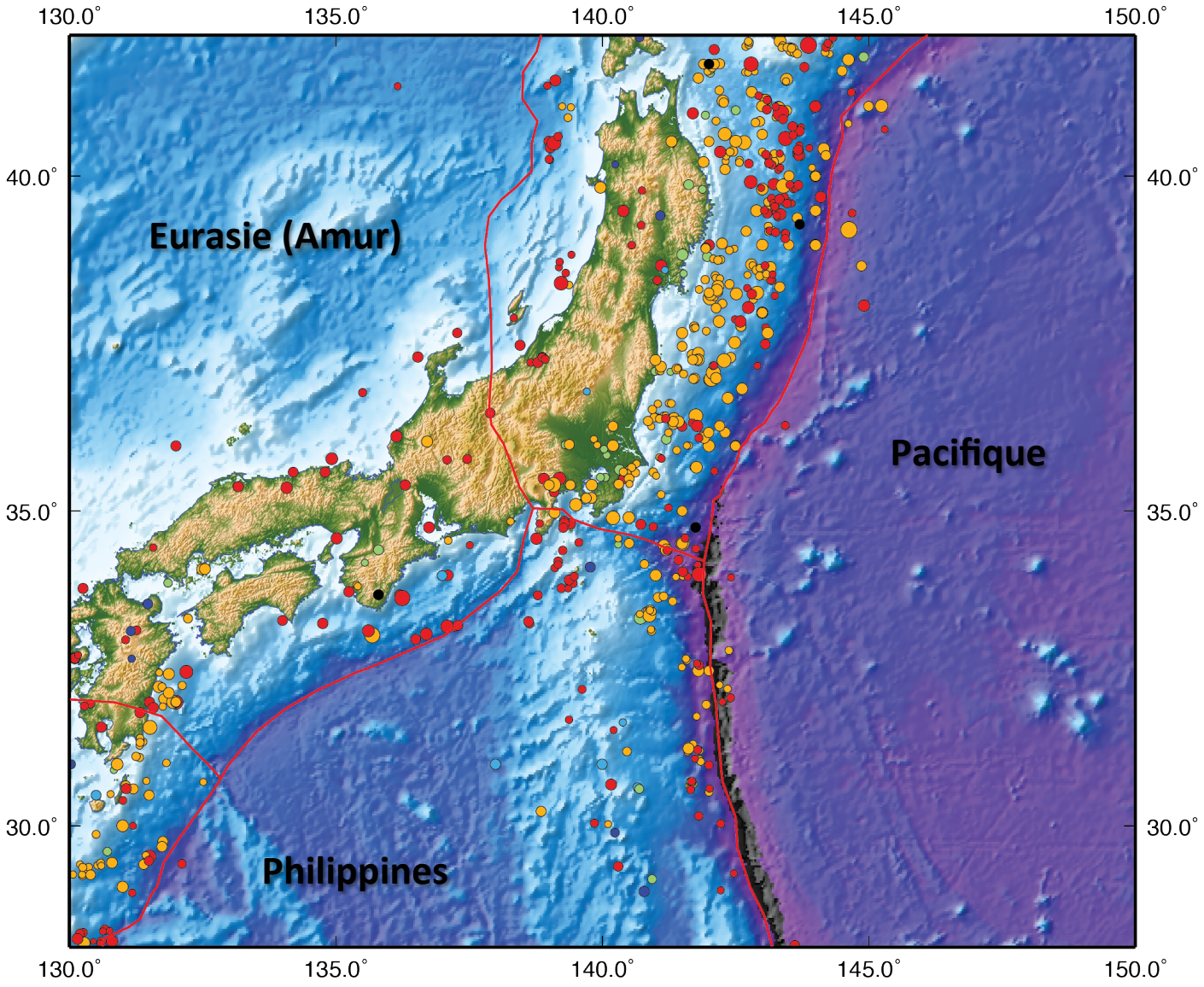
130.0°
135.0°
140.0°
145.0°
150.0°
40.0°
35.0°
30.0°
Eurasie (Amur)
Pacifique
Philippines

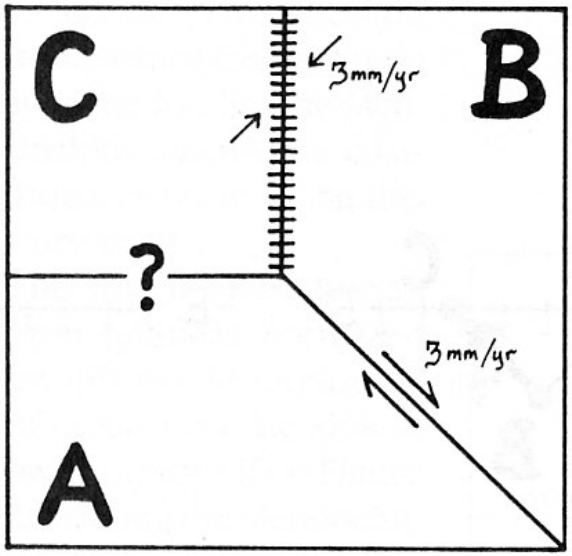
C
B
3mm/yr
?
3mm/yr
A

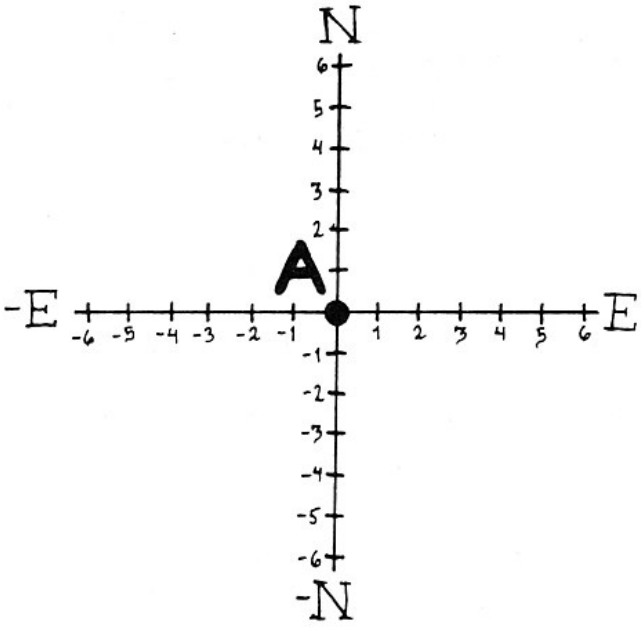
N
-E
E
-N
A
6
5
4
3
2
1
-1
-2
-3
-4
-5
-6

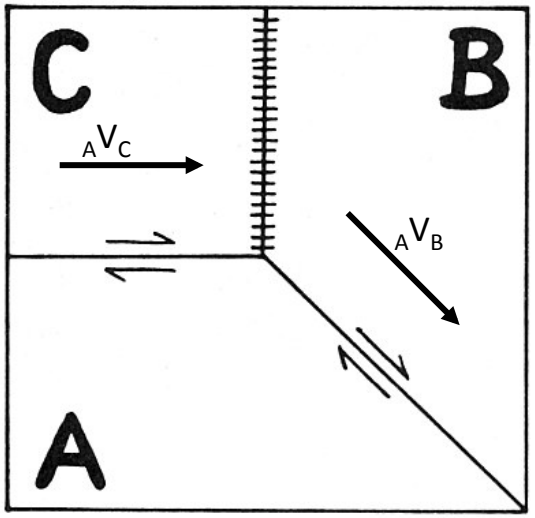
C
B
A
$_AV_C$
$_AV_B$

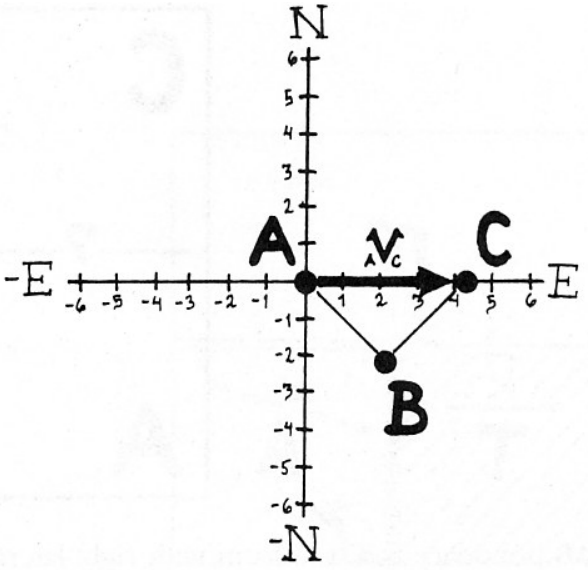
N
-N
E
-E
A
B
C
$_AV_C$

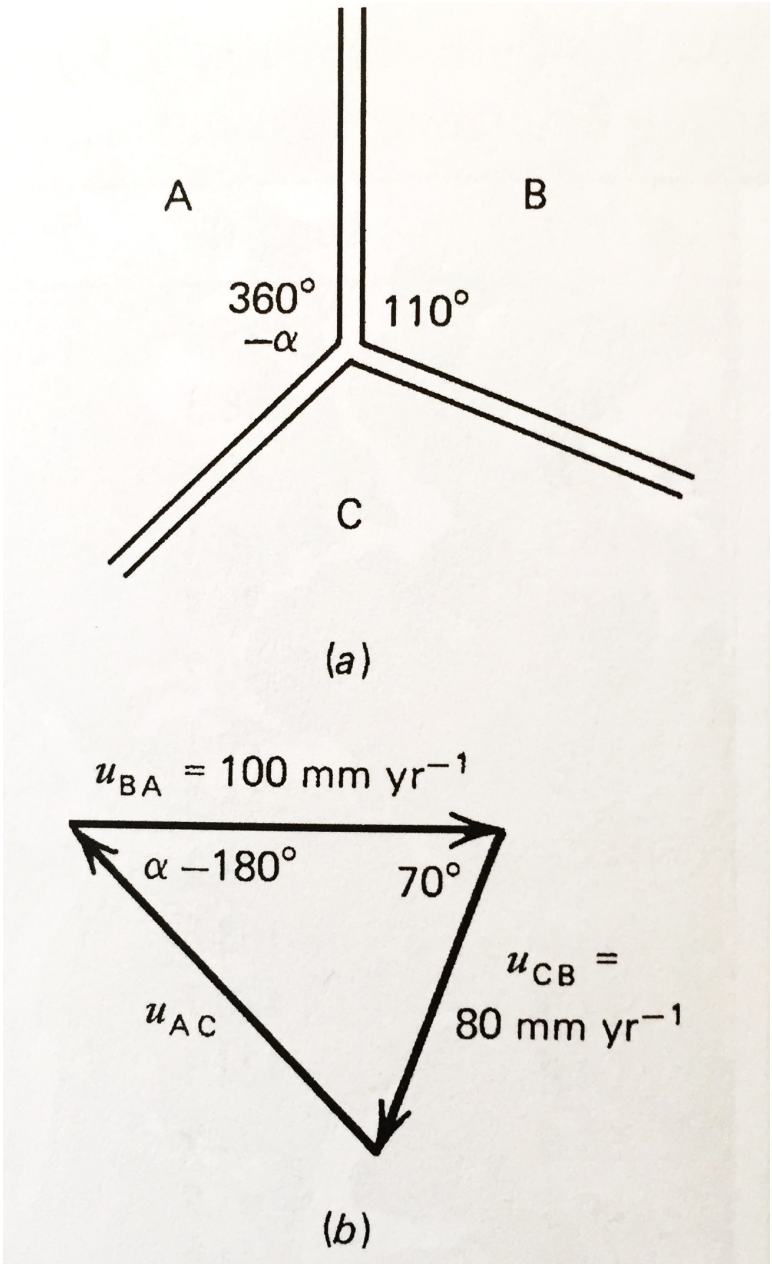
A
B
C
360°
−α
110°
(a)
u_{BA} = 100 mm yr^{-1}
α −180°
70°
u_{CB} =
80 mm yr^{-1}
u_{AC}
(b)

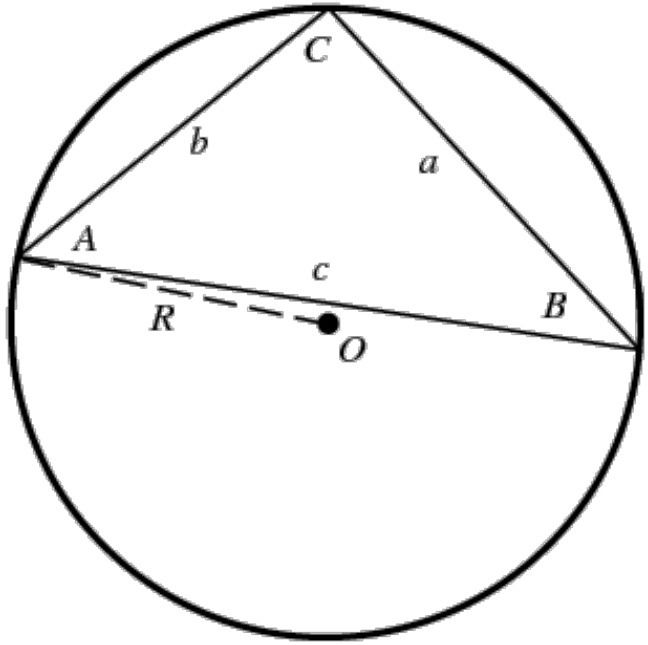

$$\cos A = \frac{c^2 + b^2 - a^2}{2bc}, \qquad \frac{a}{\sin A} = \frac{b}{\sin B} = \frac{c}{\sin C} = 2R,$$

$$a^2 = b^2 + c^2 - 2bc\cos A$$
$$b^2 = a^2 + c^2 - 2ac\cos B$$
$$c^2 = a^2 + b^2 - 2ab\cos C.$$

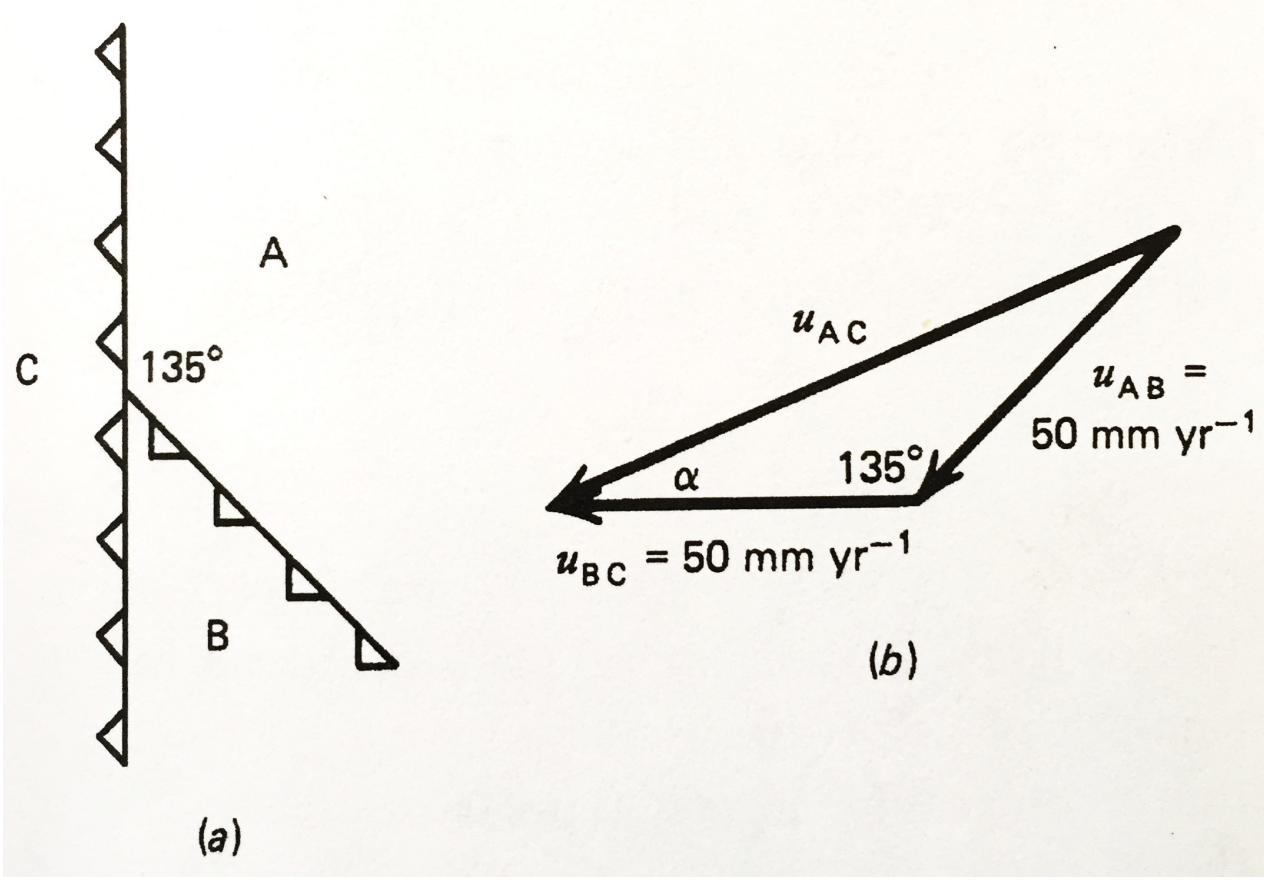
A
C
135°
B
(a)
u_{AC}
u_{AB} =
50 mm yr^{-1}
α
135°
u_{BC} = 50 mm yr^{-1}
(b)

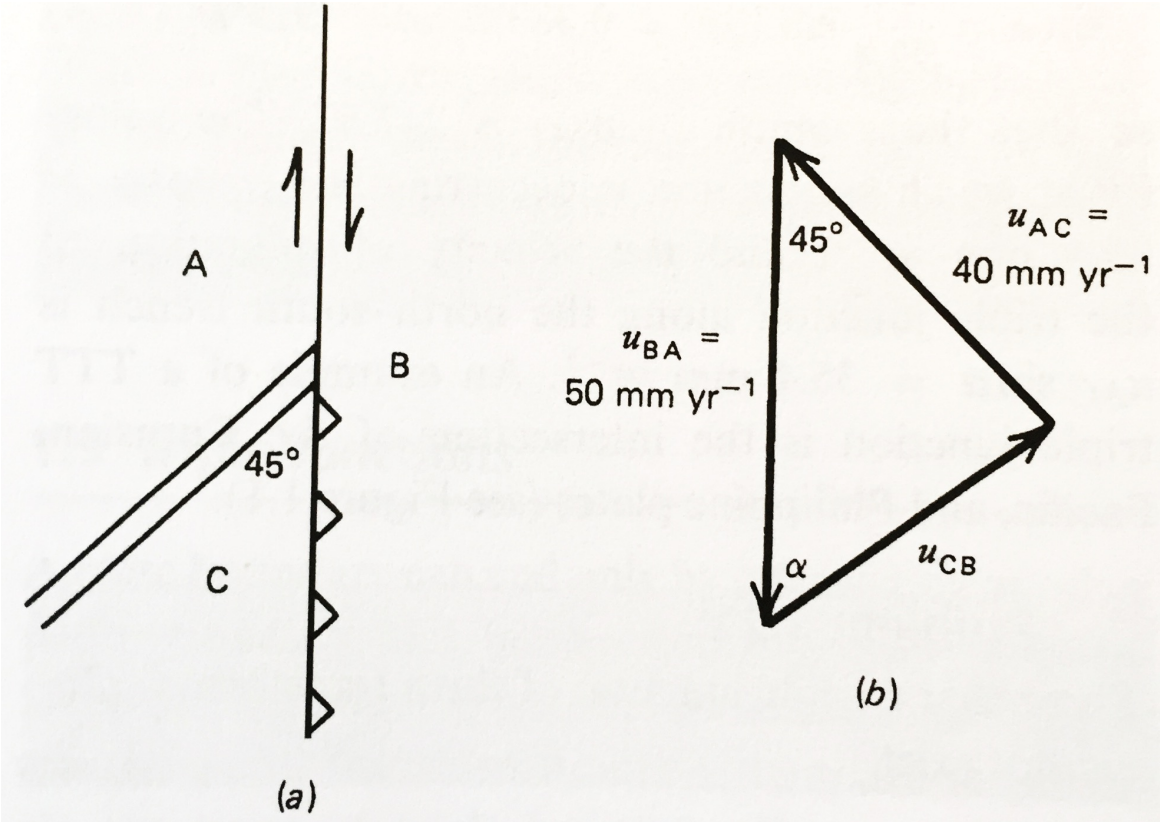
A
B
C
45°
(a)
45°
u_{AC} =
40 mm yr^{-1}
u_{BA} =
50 mm yr^{-1}
α
u_{CB}
(b)


Explorer Ridge
Explorer Plate
Sovanco Fracture Zone
Nootka Fracture Zone
Vancouver Island
BRITISH COLUMBIA
Vancouver
Seattle
WASHINGTON
Juan de Fuca Ridge
Juan de Fuca Plate
Portland
Newport
Blanco Fracture Zone
OREGON
Pacific Ocean
Gorda Ridge
Gorda Plate
Mendocino Fracture Zone
CALIFORNIA
0 100 200
miles

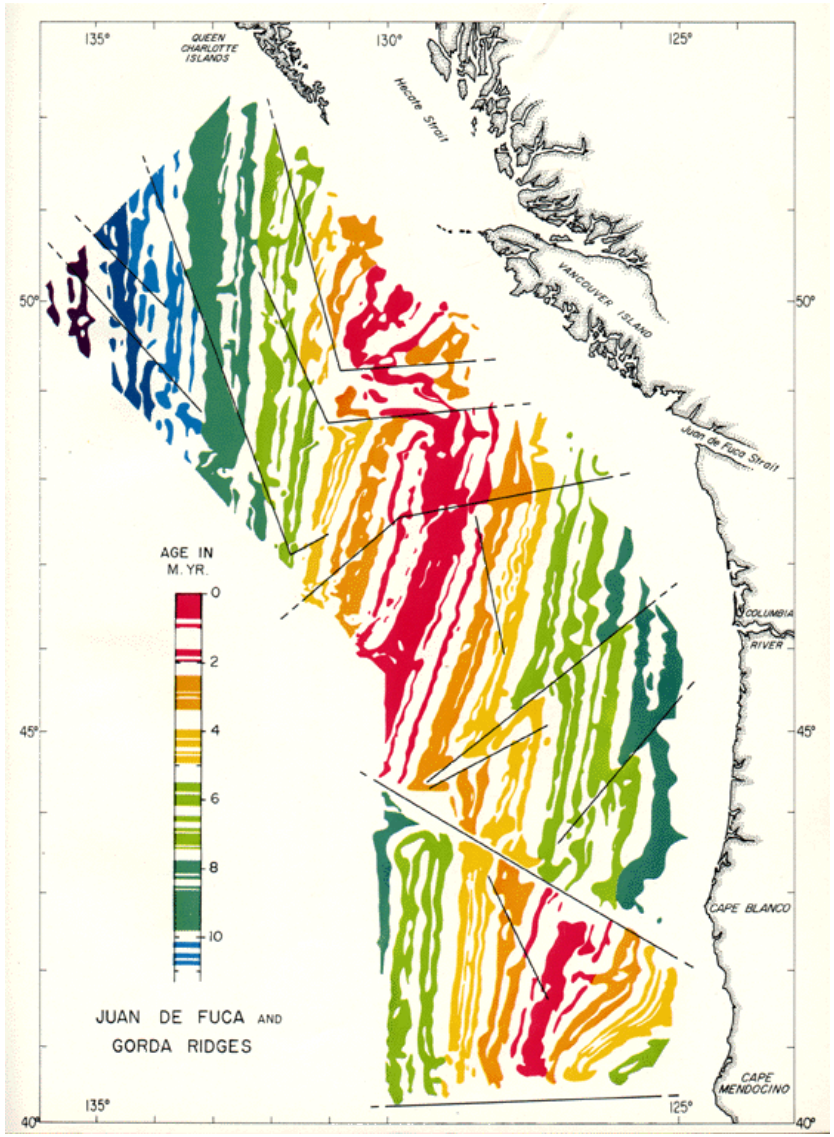
135°
130°
125°
QUEEN CHARLOTTE ISLANDS
Hecate Strait
VANCOUVER ISLAND
Juan de Fuca Strait
50°
45°
40°
COLUMBIA RIVER
CAPE BLANCO
CAPE MENDOCINO
AGE IN M.YR.
0
2
4
6
8
10
JUAN DE FUCA AND GORDA RIDGES

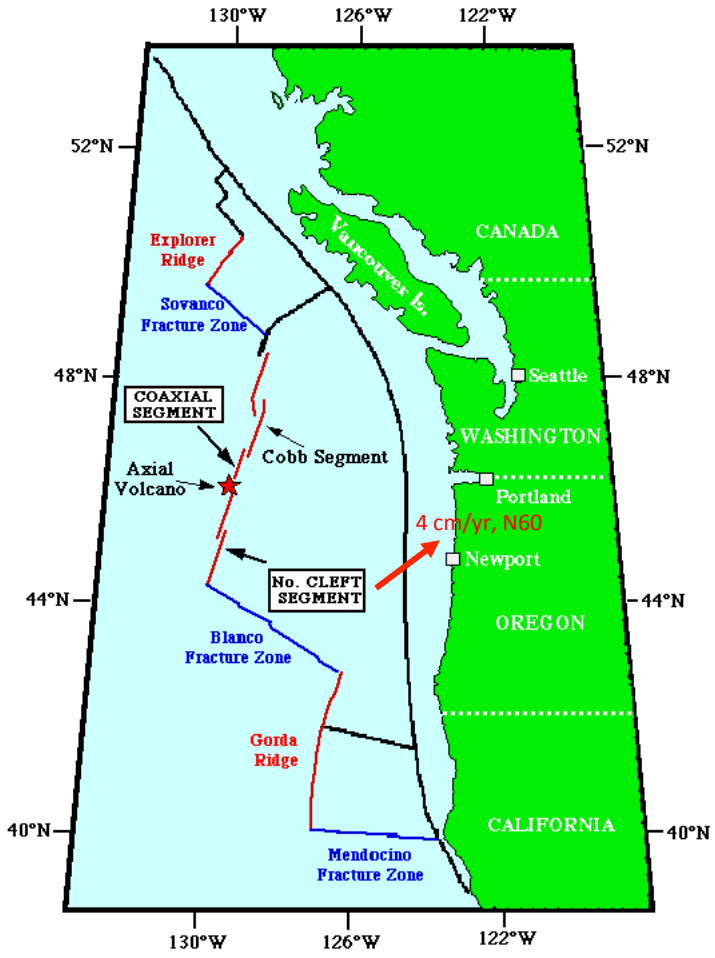
130°W
126°W
122°W
52°N
48°N
44°N
40°N
Explorer Ridge
Sovanco Fracture Zone
COAXIAL SEGMENT
Cobb Segment
Axial Volcano
No. CLEFT SEGMENT
Blanco Fracture Zone
Gorda Ridge
Mendocino Fracture Zone
CANADA
Vancouver Is.
Seattle
WASHINGTON
Portland
4 cm/yr, N60
Newport
OREGON
CALIFORNIA

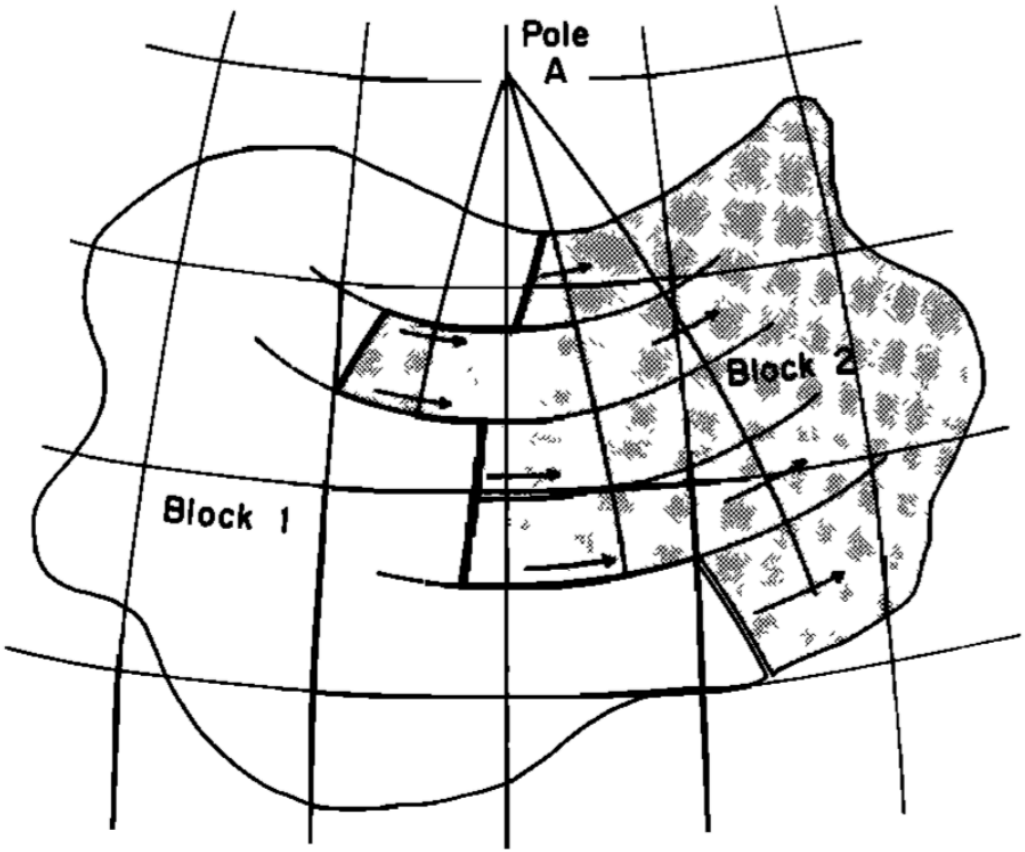

Fig. 4. On a sphere, the motion of block 2 relative to block 1 must be a rotation about some pole. All faults on the boundary between 1 and 2 must be small circles concentric about the pole A.

Morgan, 1968

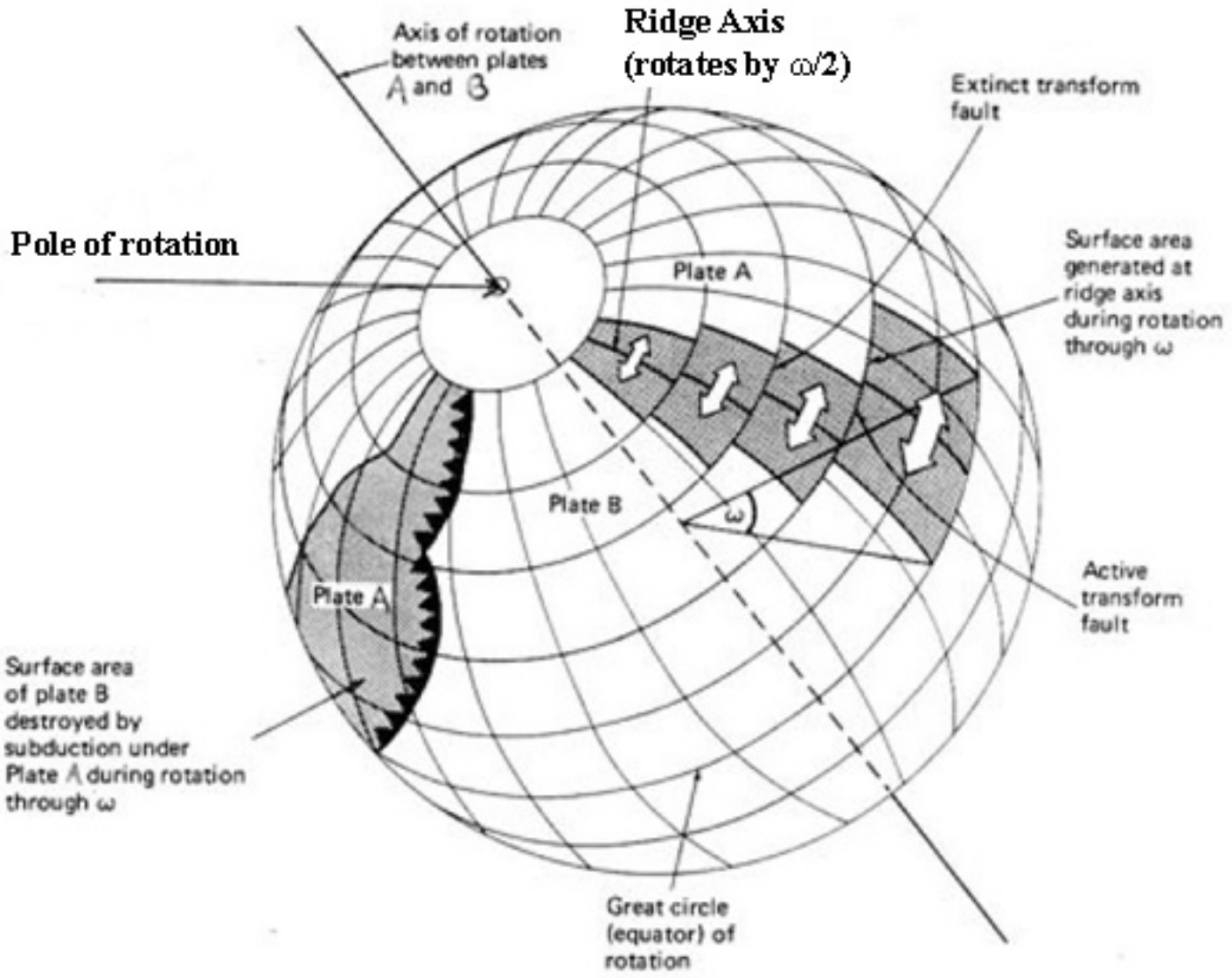
Axis of rotation between plates A and B
Ridge Axis (rotates by ω/2)
Extinct transform fault
Pole of rotation
Surface area generated at ridge axis during rotation through ω
Plate A
Plate B
ω
Active transform fault
Plate A
Surface area of plate B destroyed by subduction under Plate A during rotation through ω
Great circle (equator) of rotation

Maia et al., Nat. Geo, 2016

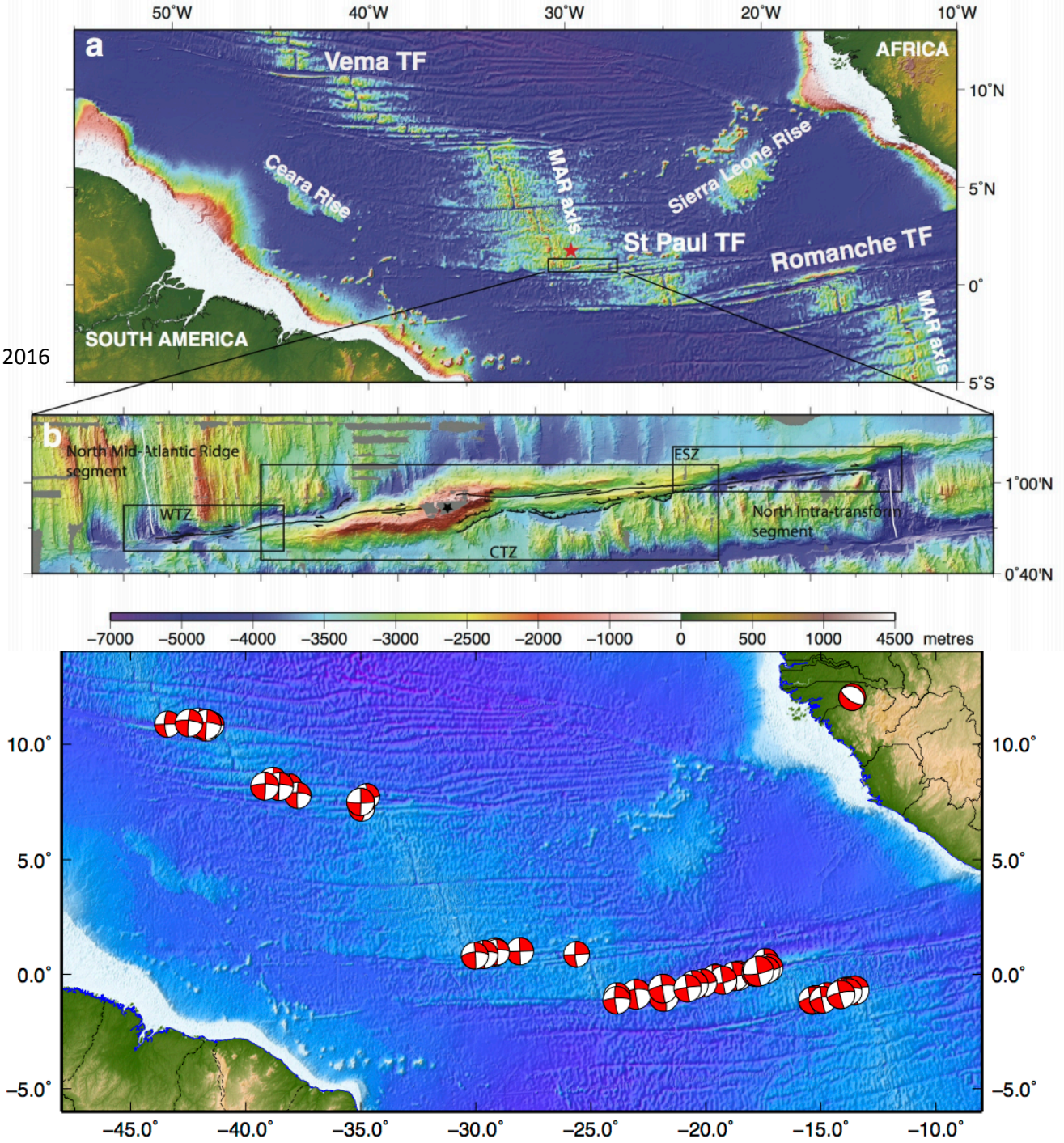

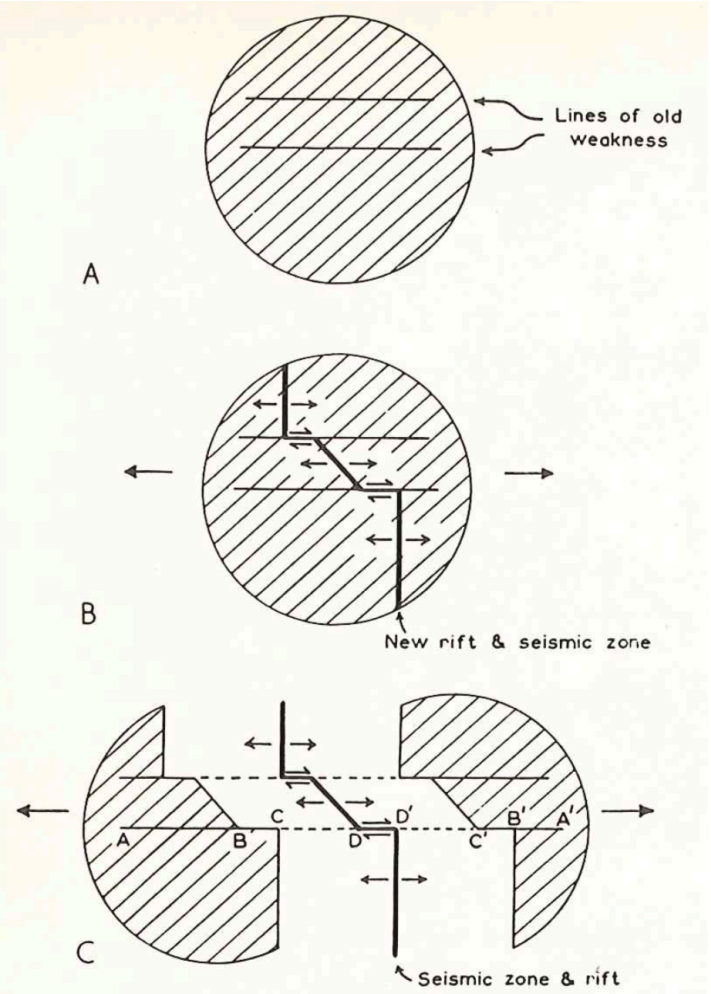

Figure 6-6
Diagram illustrating three stages in the rifting of a continent into two parts. This could represent South America and Africa. There will be seismic activity along the heavy lines only

Wilson et al., 1965

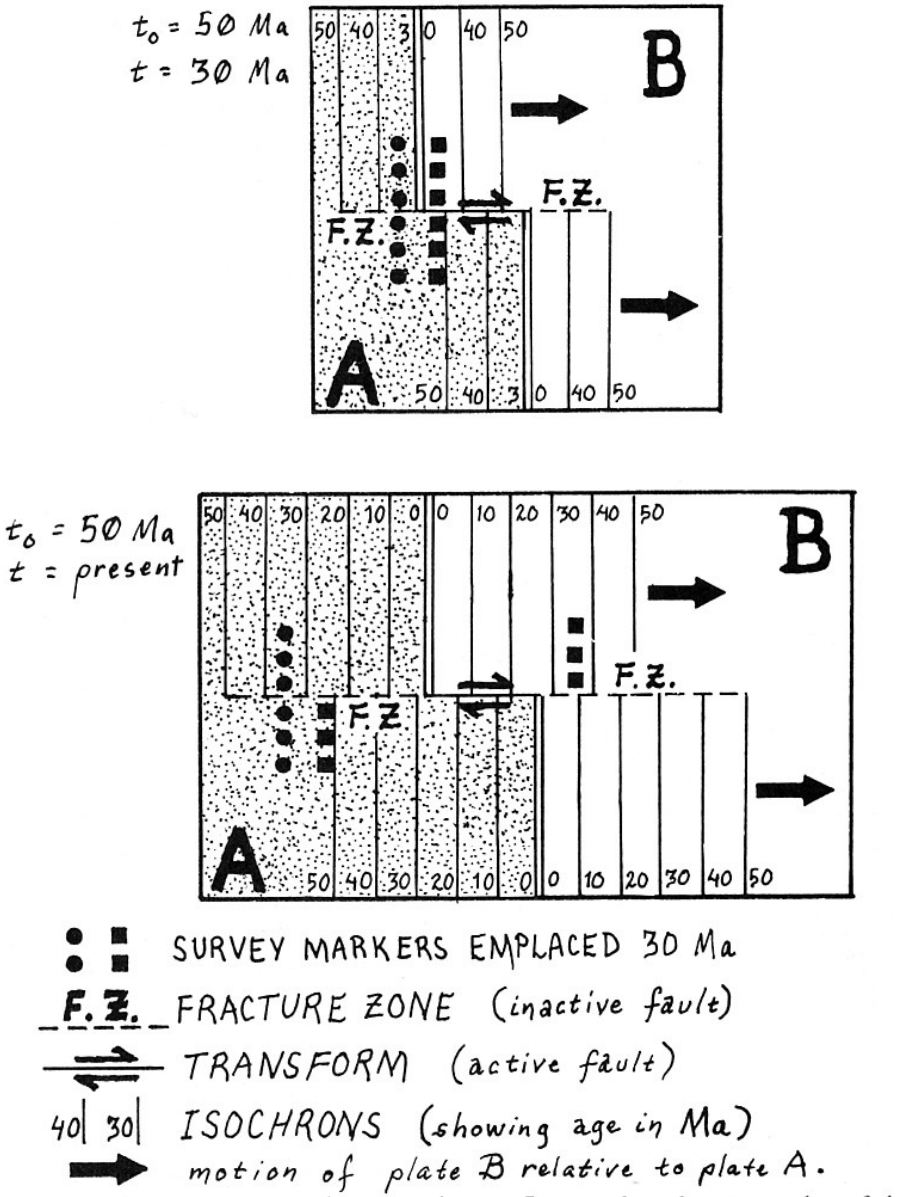

Cox, 1986, Plate Tectonics: how it works.

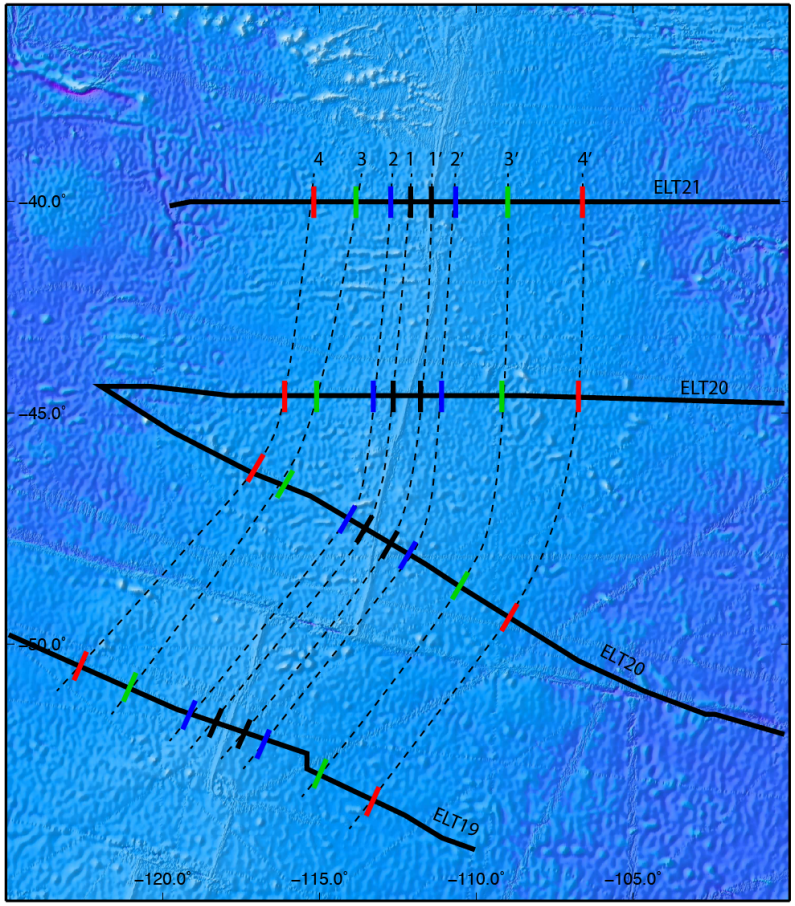

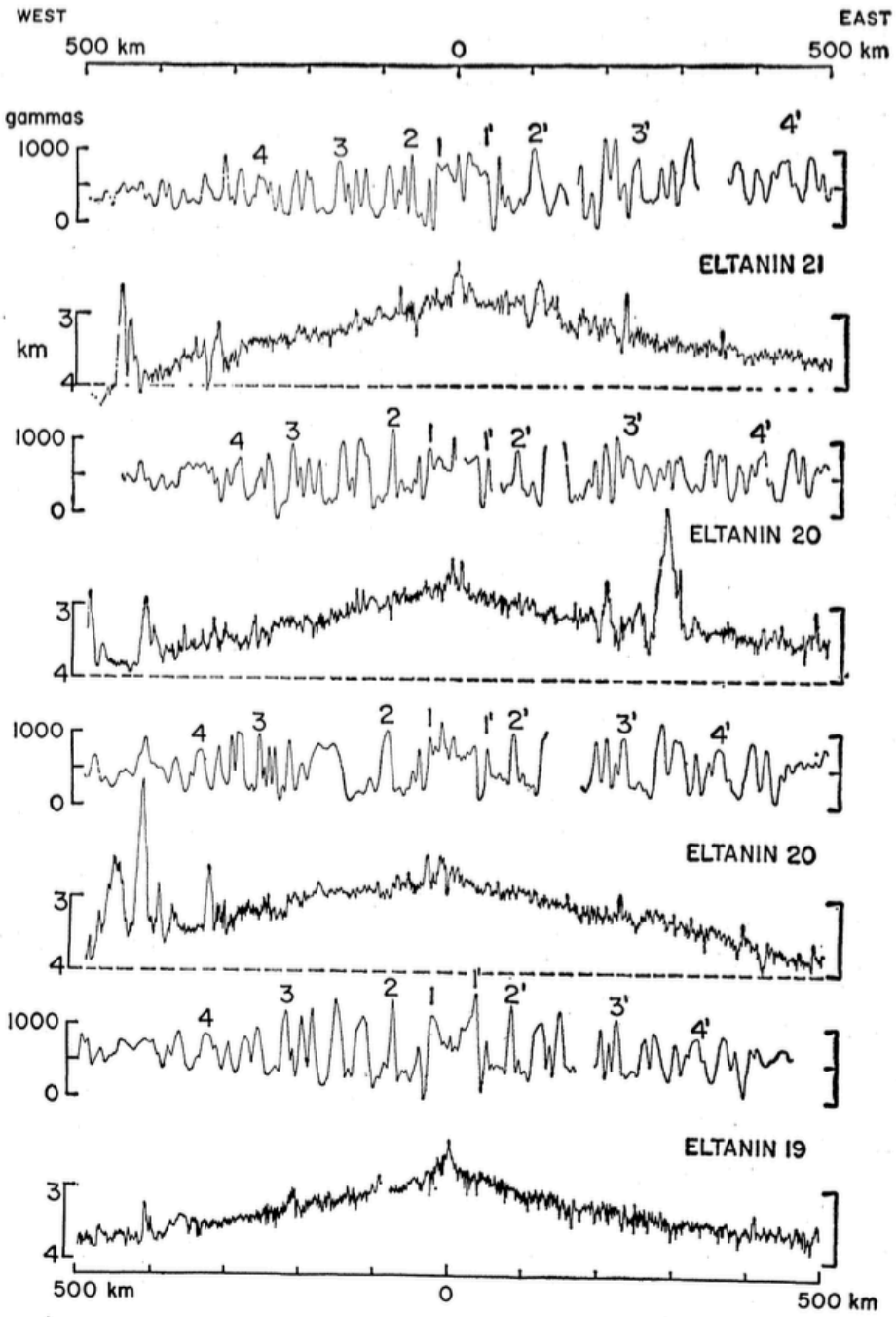

Fig. 2. Observed profiles, of magnetic anomalies and bathymetry, along the tracks shown in Fig. 1; they have been projected along an azimuth at right angles to the ridge axis. The numbers correspond with those in Fig. 1.

Pitman and Heirtzler, Science, 1966

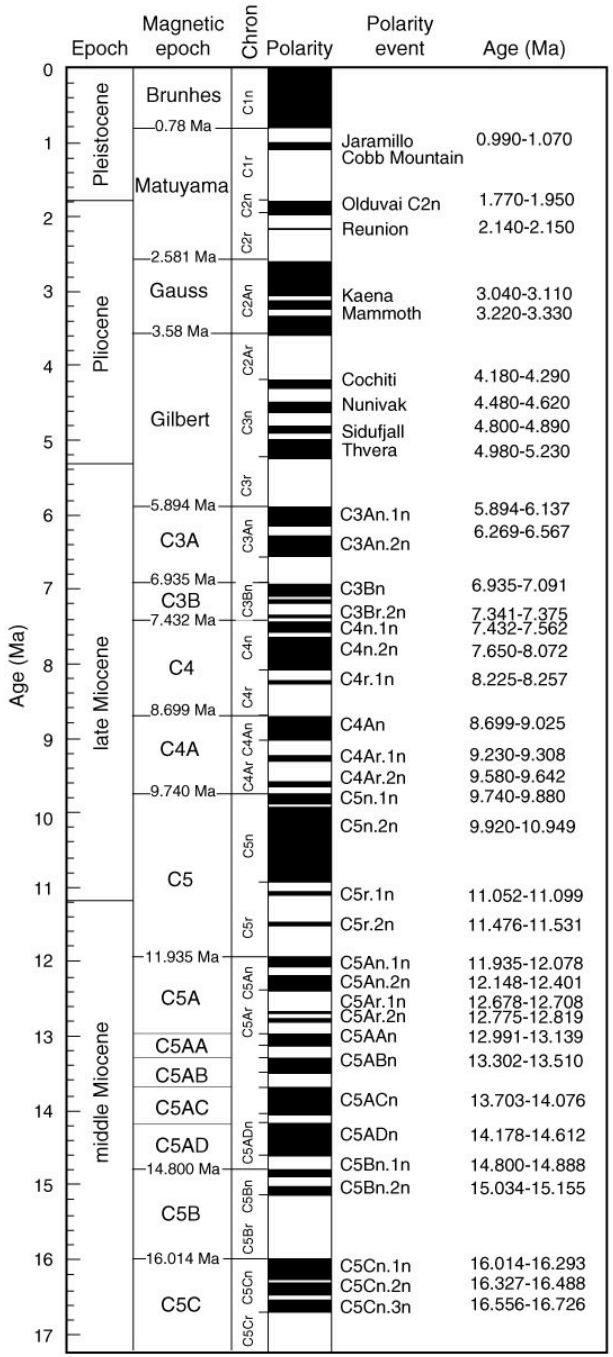

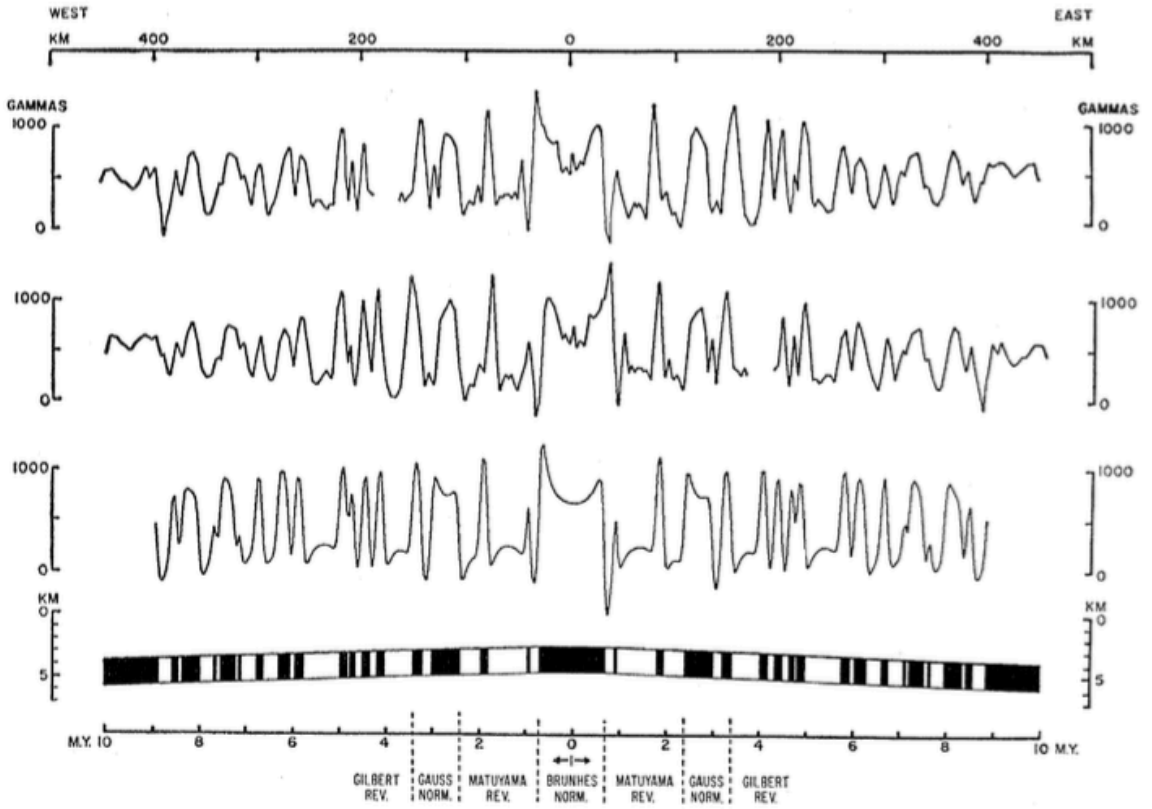

Fig. 3. The middle curve is the *Eltanin*-19 magnetic-anomaly profile; east is to the right. The upper anomaly profile is that of *Eltanin*-19 reversed; west is to the right. On the bottom is the model for the Pacific-Antarctic Ridge. The time scale (millions of years ago) is related to the distance scale by the spreading rate of 4.5 cm/yr. The previously known magnetic epochs since the Gilbert epoch are noted. The shaded areas are normally magnetized material; unshaded areas, reversely magnetized material. Above the model is the computed anomaly profile.

Pitman and Heirtzler, Science, 1966

http://publications.iodp.org/proceedings/327/102/102_f11.htm

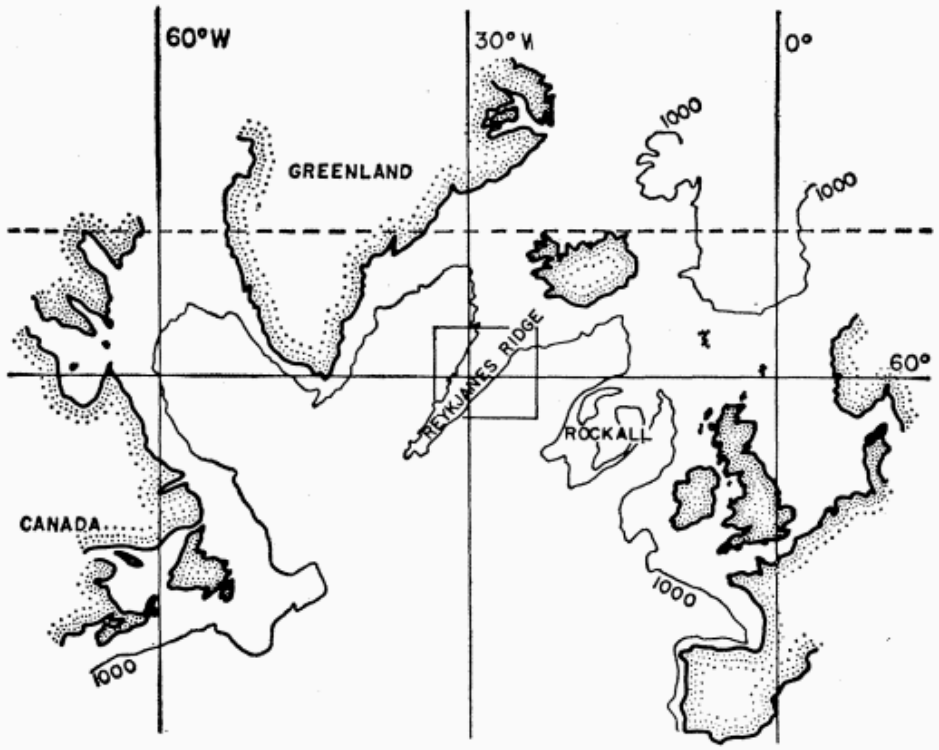

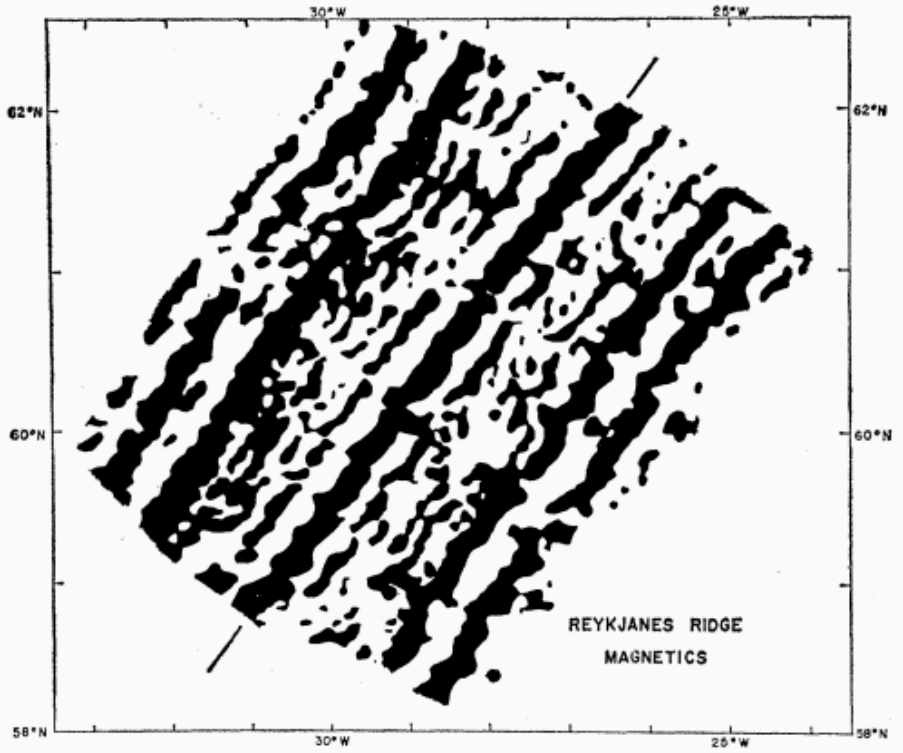

Fig. 2 (left). The location of Reykjanes Ridge, southwest of Iceland, and the area of Fig. 3. The 1000-fathom submarine contour is shown, together with the 500-fathom contours for Rockall Bank. Fig. 3 (right). Summary diagram of the magnetic anomalies observed over Reykjanes Ridge (see Fig. 2). Straight lines indicate the axis of the ridge and the central positive anomaly (*17*).

Vine, Science, 1966 (after Vine and Matthews, Nature, 1963)

TABLE 1. Strike of Faults on the Mid-Atlantic Ridge

Name	Latitude	Longitude	Strike	Reference
Atlantis	30.0°N	42.3°W	99°	*a*
	18.5°N	46.8°W	95°	*a*
	14.5°N	46.0°W	91°	*a*
Vema V	10.8°N	42.3°W	92°	*b*
Vema W	10.2°N	40.9°W	94°	*b*
Vema X	9.4°N	40.0°W	92°	*b*
Vema Y	8.8°N	38.7°W	92°	*b*
Vema Z	7.6°N	36.6°W	91°	*b*
	7.2°N	34.3°W	91°	*b*
	4.0°N	31.9°W	88°	*c*
	1.9°N	30.6°W	86°	*c*
St. Paul's	1.1°N	26.0°W	86°	*c*
	1.1°S	24.0°W	81°	*c*
Romanche	0.1°S	18.0°W	77°	*c*
Chain	1.3°S	14.5°W	75°	*c*
	1.9°S	12.9°W	82°	*c*
	2.9°S	12.5°W	73°	*c*
	7.5°S	12.3°W	73°	*a*

[a] *Heezen and Tharp* [1965].
[b] *Heezen et al.* [1964*b*].
[c] *Heezen et al.* [1964*a*].

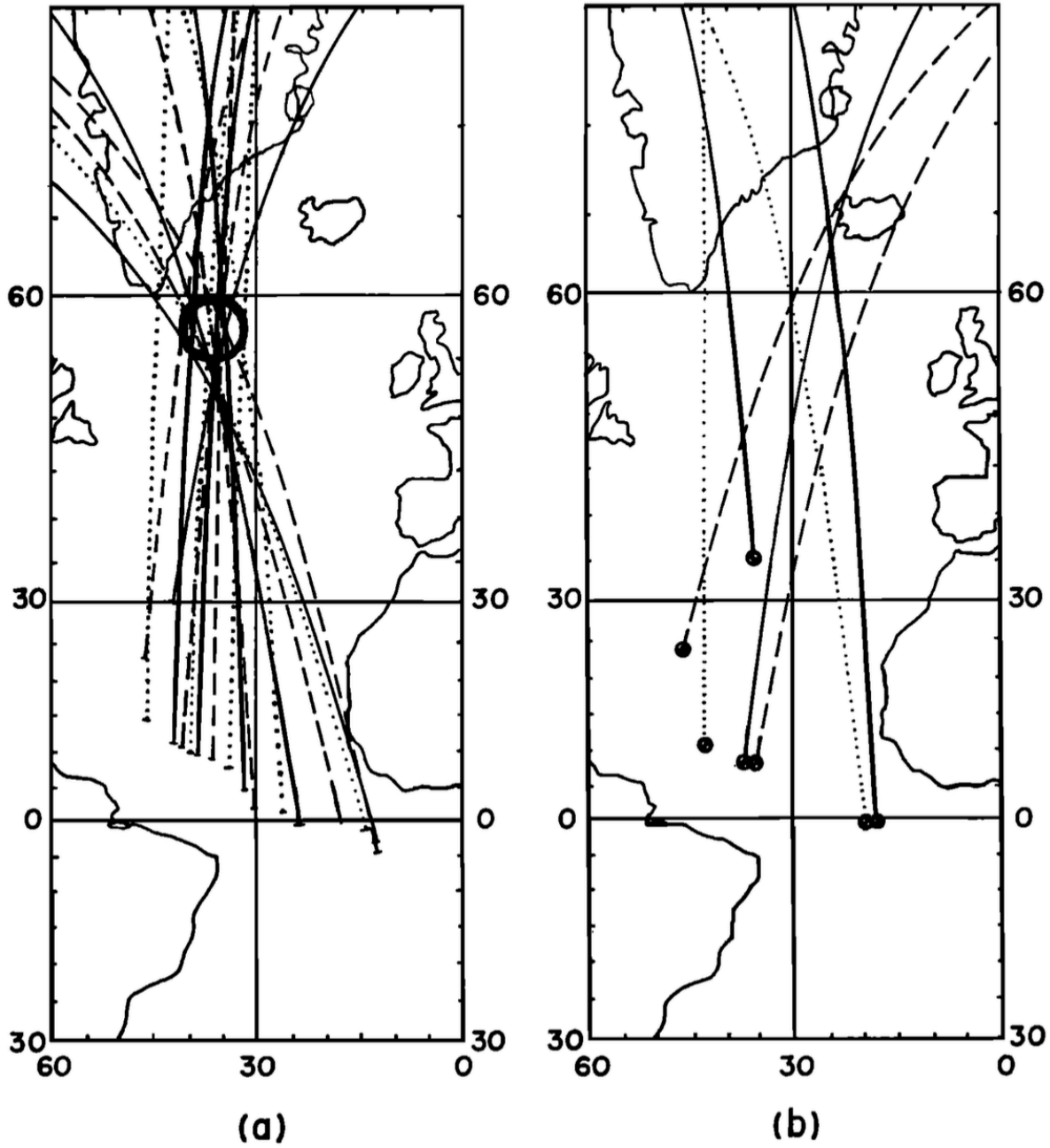

Fig. 8. Great circles perpendicular to the strike of offsets of the mid-Atlantic ridge are shown in (*a*). With one exception, all of these lines pass within the circle centered at 58°N, 36°W. Great circles perpendicular to the strike determined by earthquake mechanism solutions are shown in (*b*).

Morgan, 1968

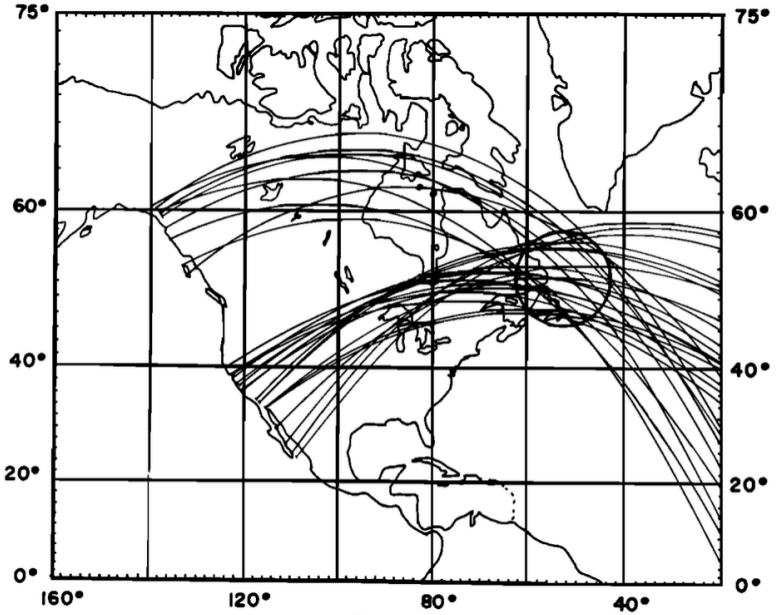

Fig. 14*e*

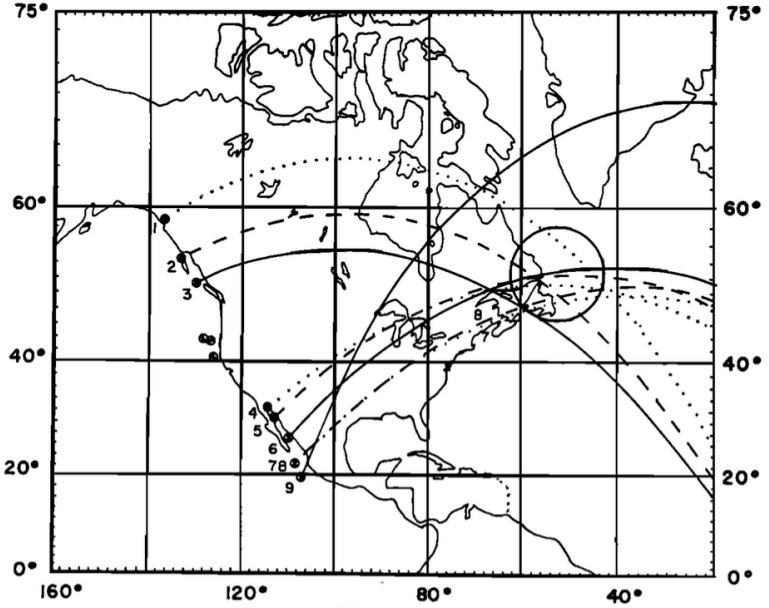

Fig. 14*f*

Fig. 14. Parts (*a*) through (*d*) show great circles constructed perpendicular to the strikes of fault segments observed in the Fairweather-Queen Charlotte, northern California, southern California, and Gulf of California regions. Part (*e*) is a composite of the four separate regions with the exceptions noted in the text. Part (*f*) shows great circles constructed perpendicular to strikes determined from earthquake mechanism solutions. The circle of intersection drawn has the coordinates 53°N (±6°), 53°W, (±10°).

Morgan, 1968

1

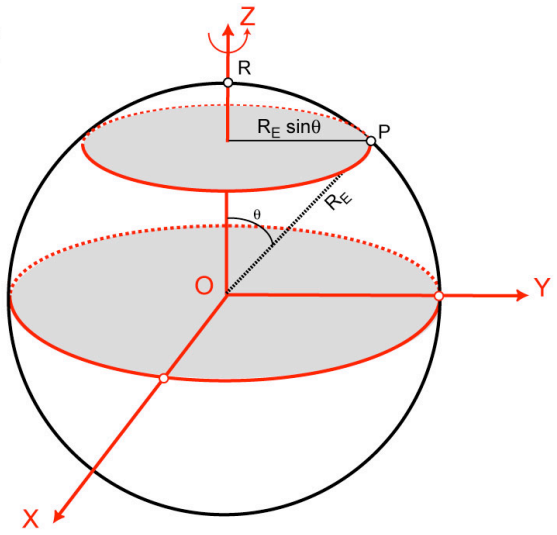
Z
R
$R_E \sin\theta$
P
R_E
θ
O
Y
X

2

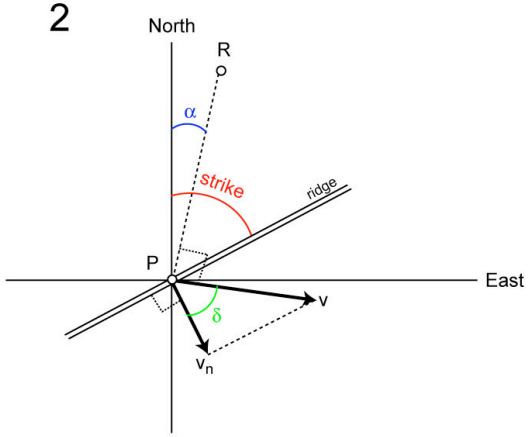
North
R
α
strike
ridge
P
East
v
δ
v_n

3

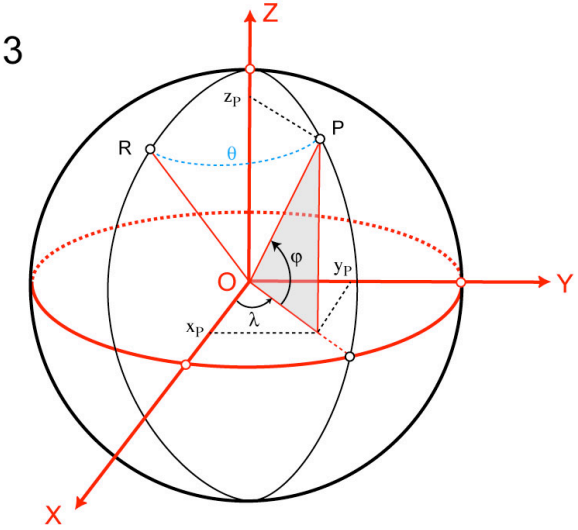
Z
z_P
P
R
θ
φ
y_P
O
Y
λ
x_P
X

4

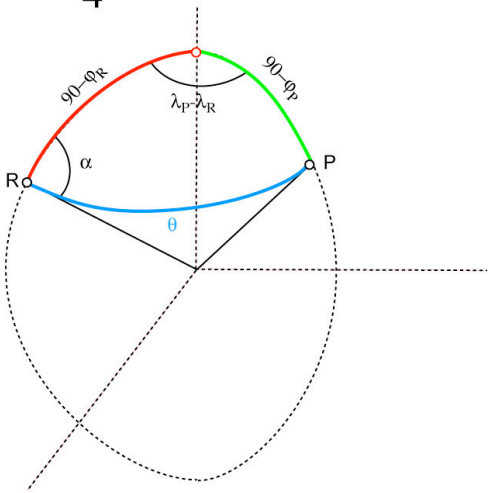
90–φR
λP–λR
90–φP
α
R
P
θ

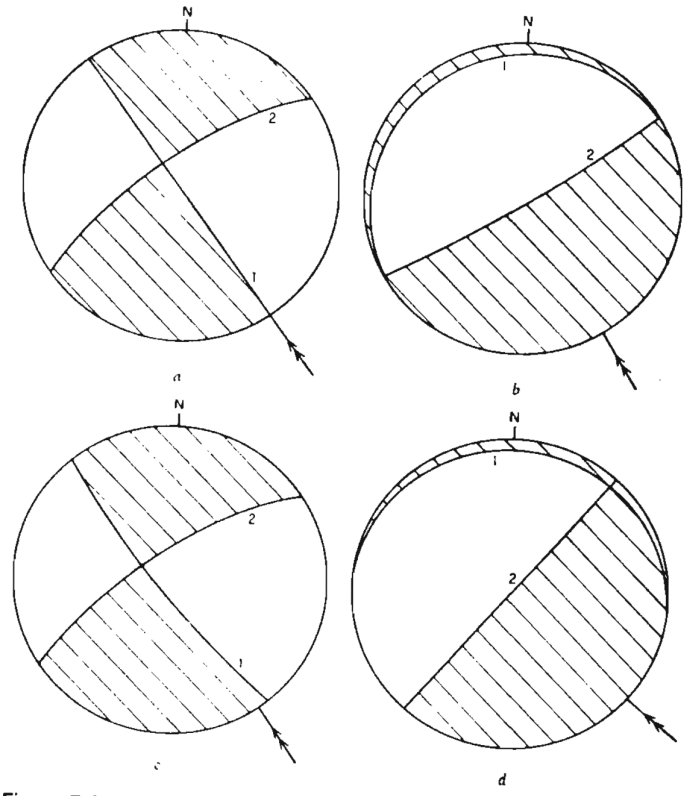

Figure 7-2
Mechanism diagrams for four circum-Pacific earthquakes. The lower half of the focal sphere is projected stereographically on to a horizontal surface, and the rarefraction quadrants are shaded. The horizontal projection of the slip vector in plane 1 is marked with a double arrow. (a) June 28, 1966, Parkfield (McEvilly, 1966a), strike slip; (b) September 4, 1964, Alaska (Stauder and Bollinger, 1966a), overthrust; (c) June 14, 1962, Near and Aleutian Islands (Stauder and Bollinger, 1964a), strike slip; (d) October 20, 1963, Kurile Islands (Stauder and Bollinger, 1966b), overthrust

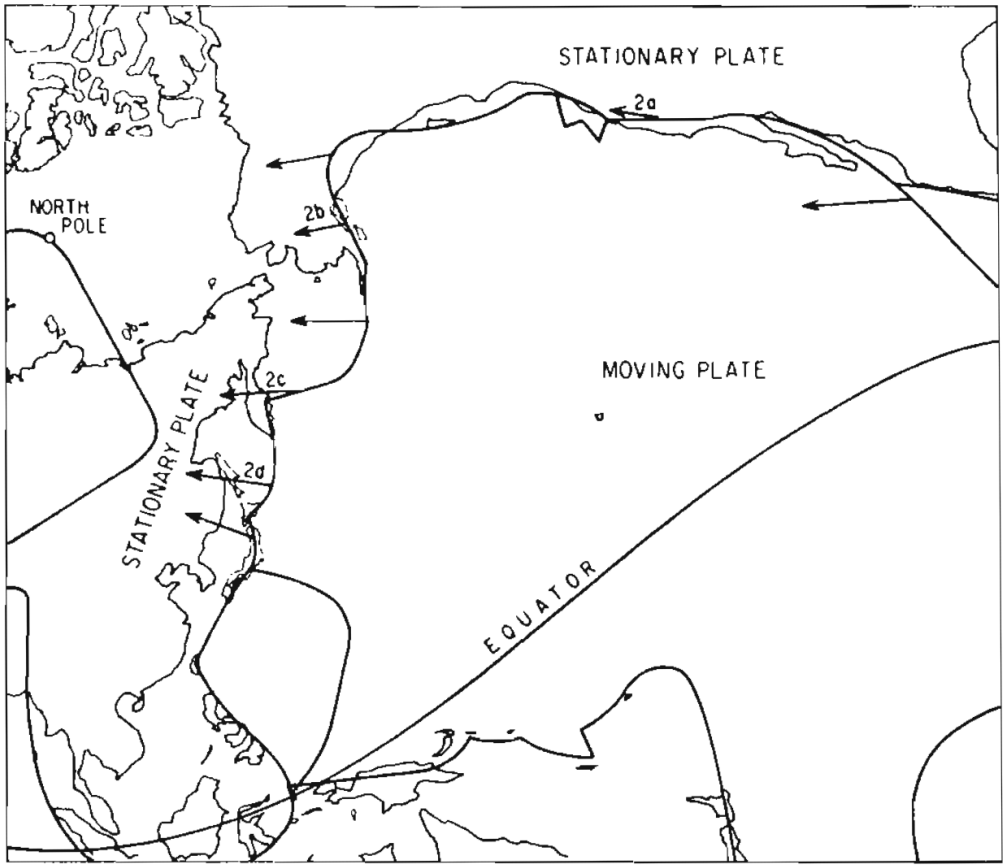

Figure 7-3
A Mercator projection of the Pacific with a pole at 50° N., 85° W. The arrows show the direction of motion of the Pacific plate relative to that containing North America and Kamchatka. If both plates are rigid all slip vectors must be parallel with each other and with the upper and lower boundaries of the figure. Possible boundaries of other plates are sketched

McKenzie and Parker, 1967

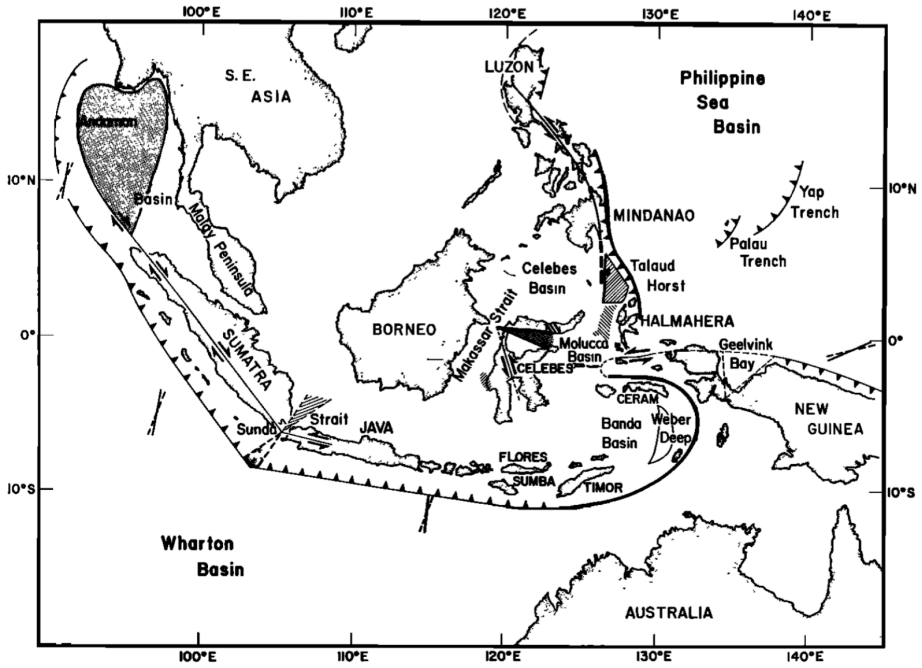

Fig. 4. Major fault zones adjacent to southeast Asia. Shading and striping mark regions of known or suspected extension and shortening, respectively. Locations of transcurrent faults in Celebes and Java and the sense of motion on them are from *Katili* [1970]. Saw-tooth curves mark zones of shallow underthrusting for which there is at least some seismic evidence. Smooth continuations of these curves represent zones of underthrusting along which at most only scattered concentrations of shallow earthquakes were recorded in recent years. Thin curves, dashed where there is little supporting evidence, mark fault zones that may or may not be part of a plate margin. Directions of relative motion between the major plates computed from rigid plate models are given by solid lines [*Morgan*, 1972] and dashed lines [*Le Pichon*, 1968].

Fitch et al., 1972

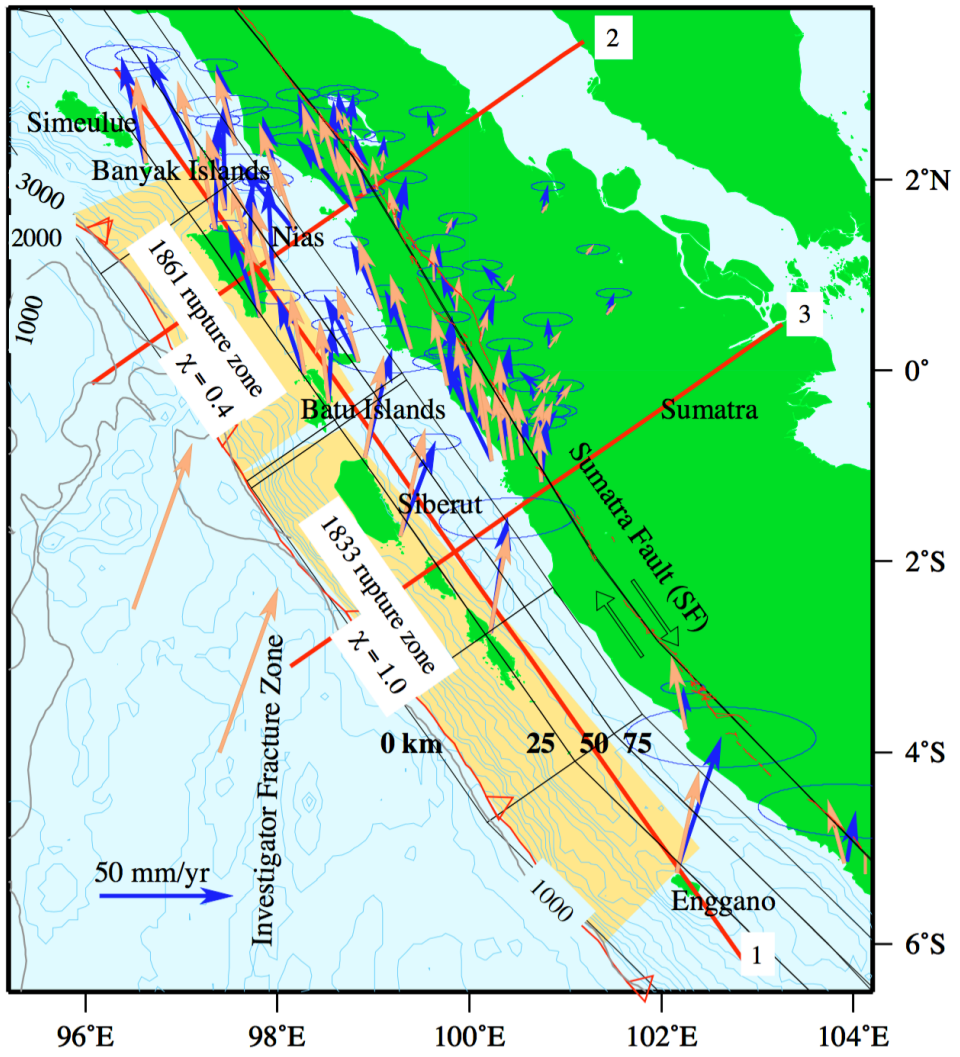

Prawirodirdjo et al., 1997

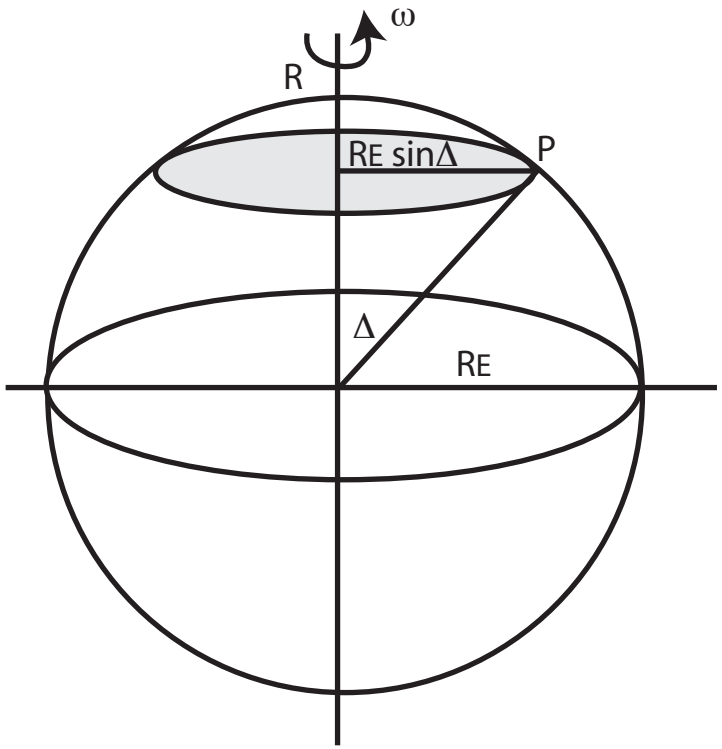
ω
R
RE sinΔ
P
Δ
RE

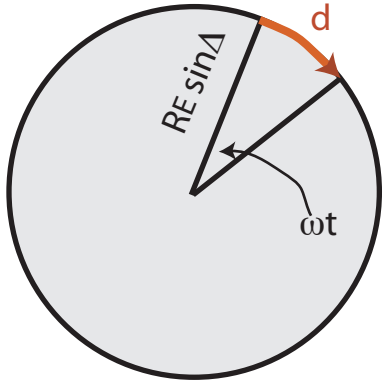
d
RE sinΔ
ωt

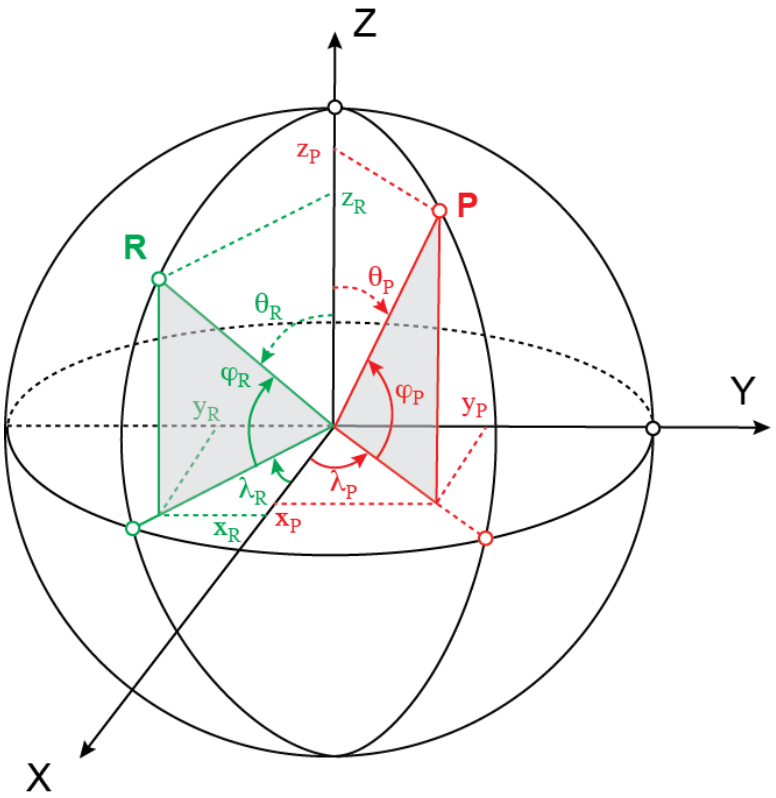
Z
Y
X
R
P
z_P
z_R
θ_P
θ_R
φ_R
φ_P
y_R
y_P
λ_R
λ_P
x_R
x_P

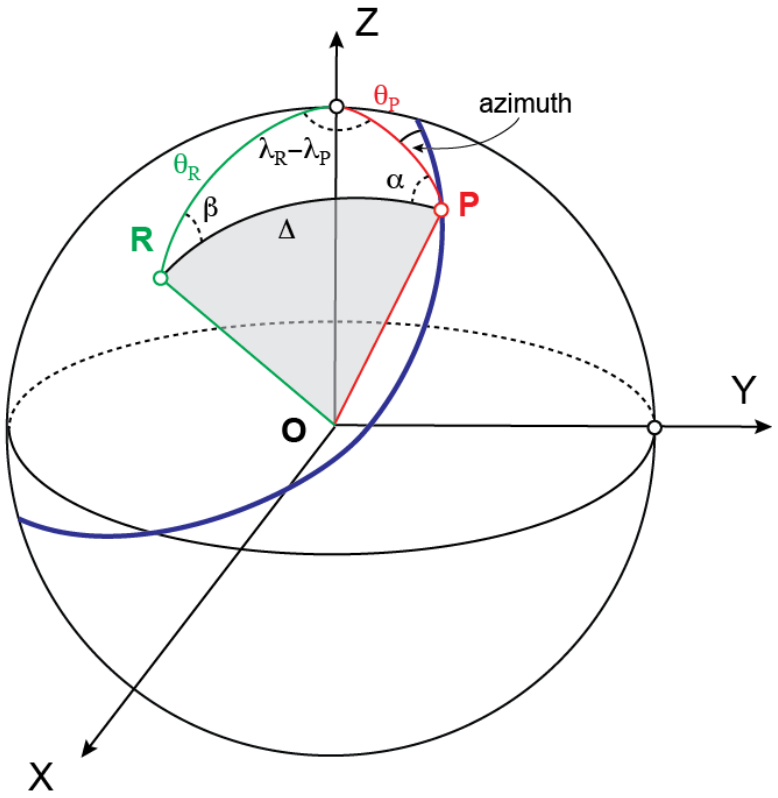
Z
Y
X
O
R
P
θ_P
azimuth
θ_R
$\lambda_R-\lambda_P$
α
β
Δ

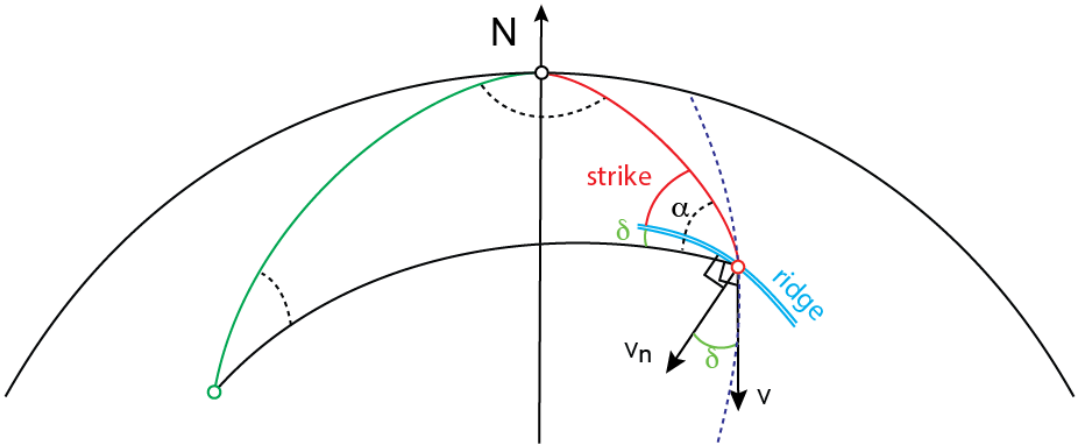
N
strike
α
δ
ridge
v_n
δ
v

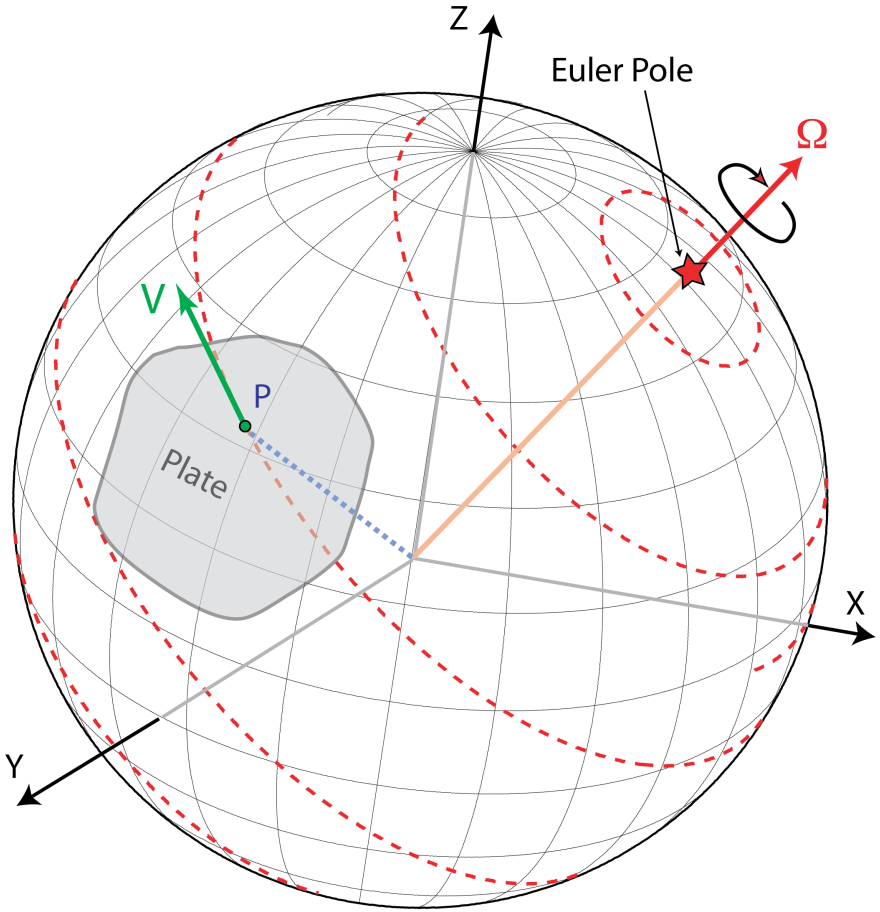
Z
Euler Pole
Ω
V
P
Plate
X
Y

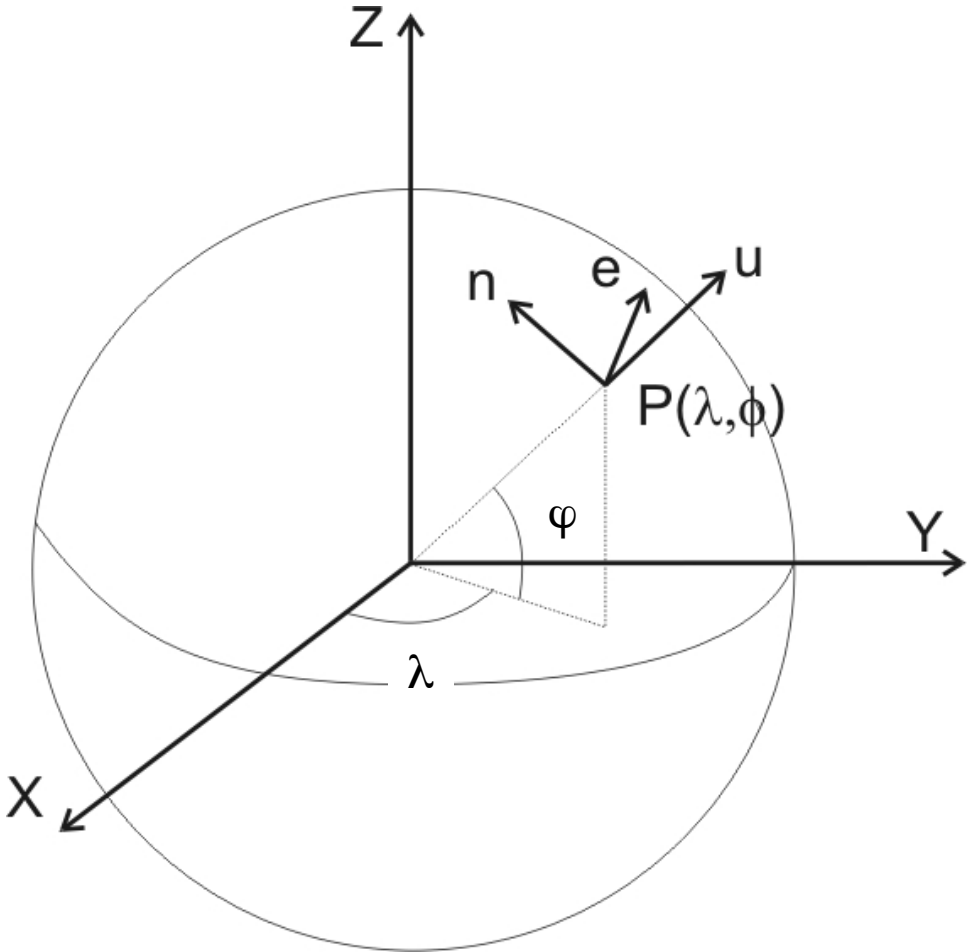
Z
n
e
u
P(λ,ϕ)
φ
Y
λ
X

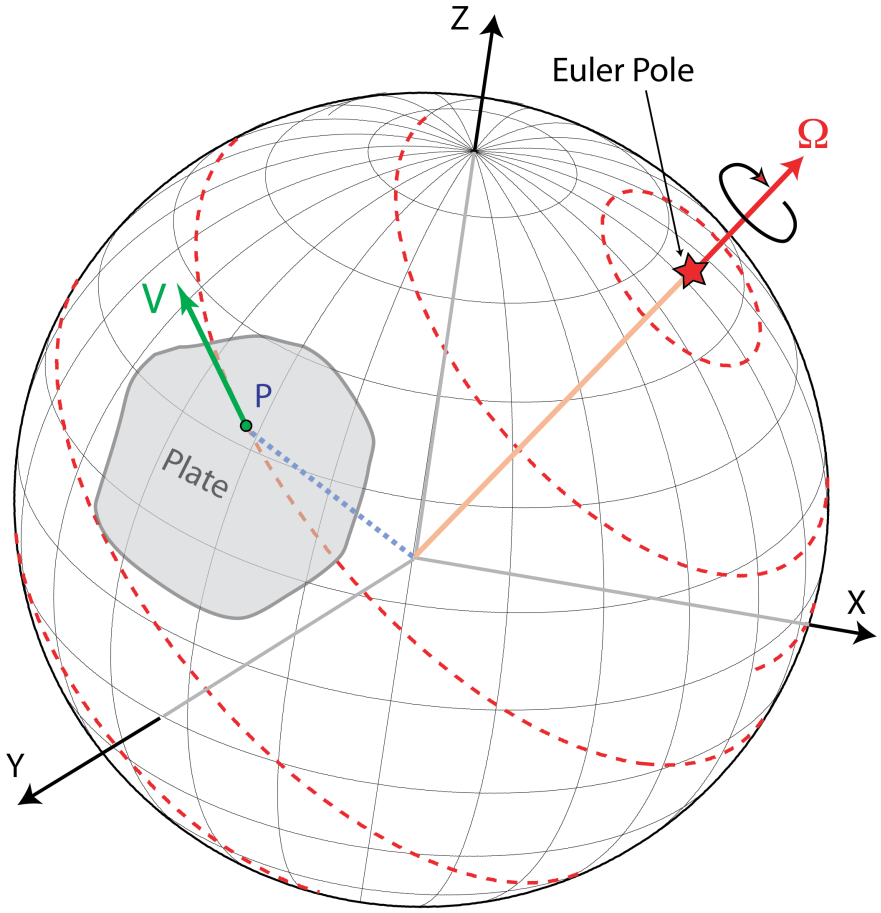
Z
Euler Pole
Ω
V
P
Plate
X
Y

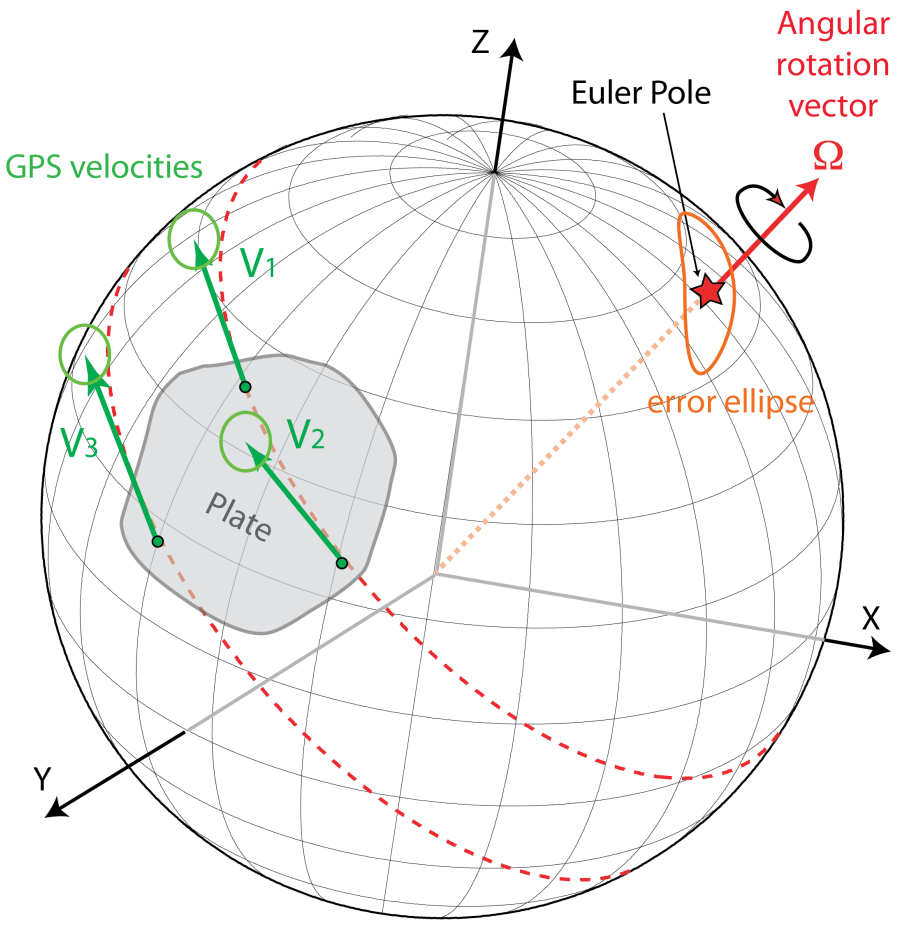
Z
Euler Pole
Angular
rotation
vector
Ω
GPS velocities
V1
V2
V3
Plate
error ellipse
X
Y

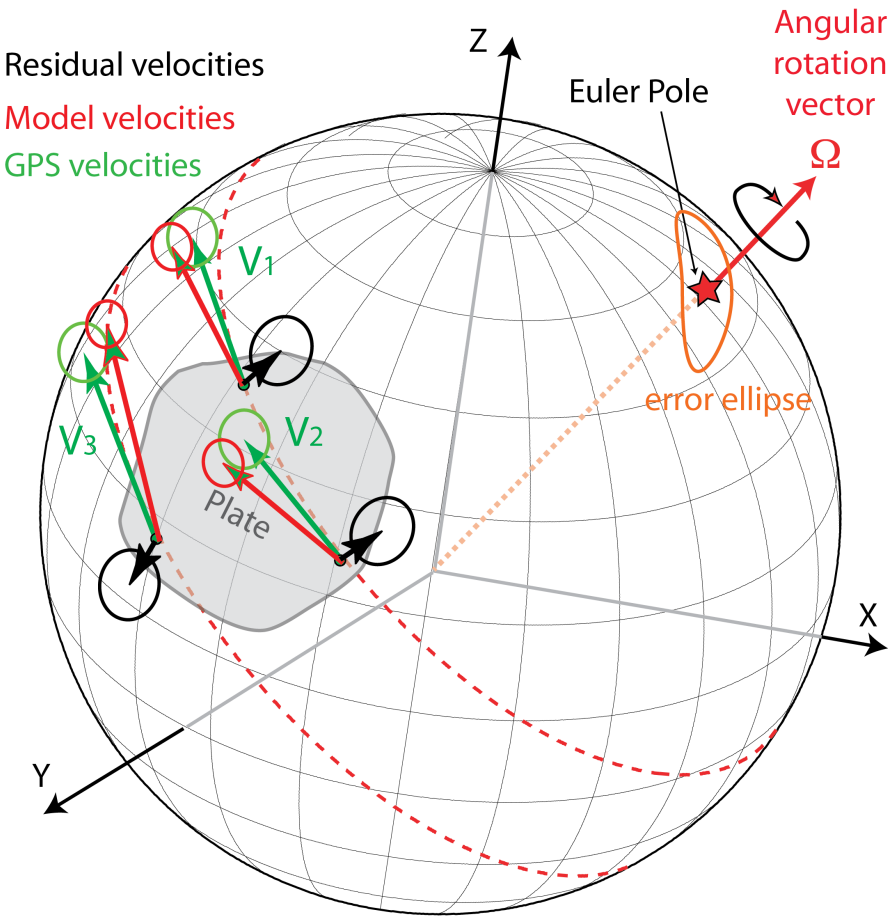
Residual velocities
Model velocities
GPS velocities
Z
Euler Pole
Angular
rotation
vector
Ω
V1
V2
V3
Plate
error ellipse
X
Y

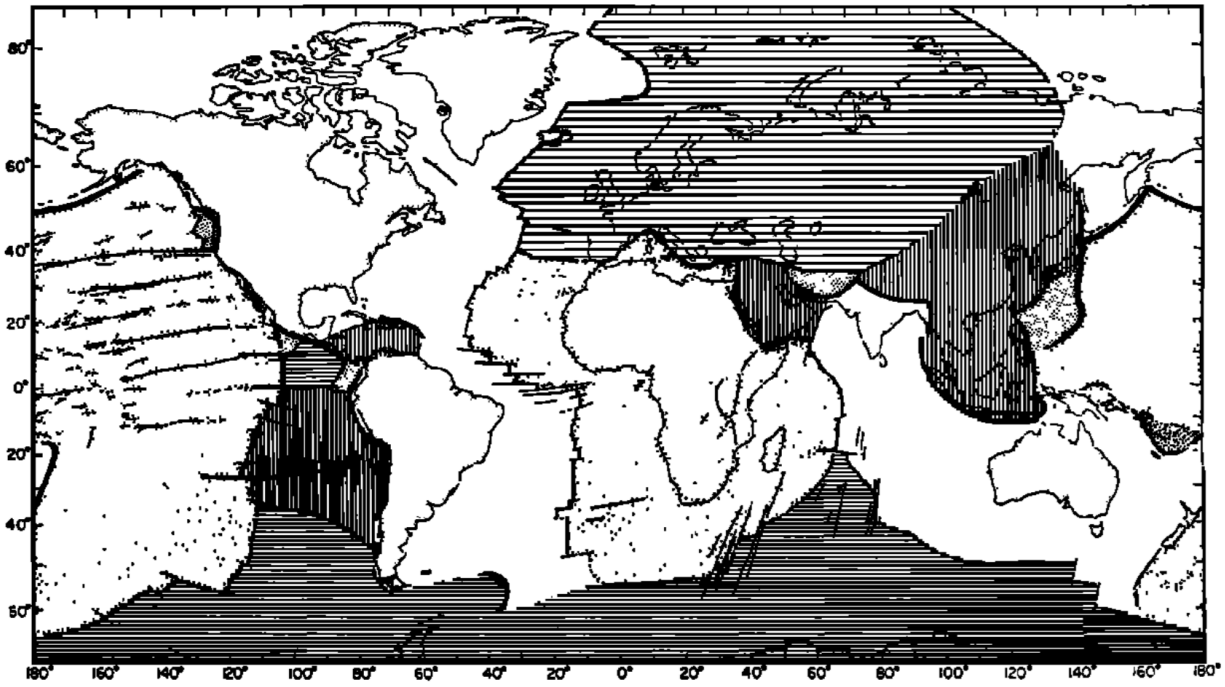

Fig. 1. The crust is divided into units that move as rigid blocks. The boundaries between blocks are rises, trenches (or young fold mountains), and faults. The boundaries drawn in Asia are tentative, and additional sub-blocks may be required. (Figure is based on *Sykes*'s [1968*b*] map of the ridge system with additional features from *Heezen and Tharp*'s [1965] tectonic map.)

Morgan, 1968

TABLE 5. Prediction of Antarctica–Africa Pole from Closure of Africa–North America–Pacific–Antarctica–Africa Circuit

	Latitude, °N	Longitude, °E	V_{max}, cm/yr	$\frac{1}{2}a\omega_x$, cm/yr	$\frac{1}{2}a\omega_y$, cm/yr	$\frac{1}{2}a\omega_z$, cm/yr
ω_{Am-Af}	62 ± 5	−36 ± 2	1.8 ± 0.1	0.7 ± 0.1	−0.5 ± .1	1.6 ± 0.1
ω_{Pac-Am}	53 ± 3	−53 ± 5	4.0 ± 0.6	1.4 ± 0.3	−1.9 ± .4	3.2 ± 0.5
$\omega_{Ant-Pac}$	−71 ± 2	118 ± 6	5.7 ± 0.3	−0.9 ± 0.2	1.6 ± .2	−5.4 ± 0.3
ω_{Ant-Af}	−25 ± 30	−35 ± 20	1.6 ± 0.5	1.2 ± 0.4	−0.8 ± .5	−0.6 ± 0.6

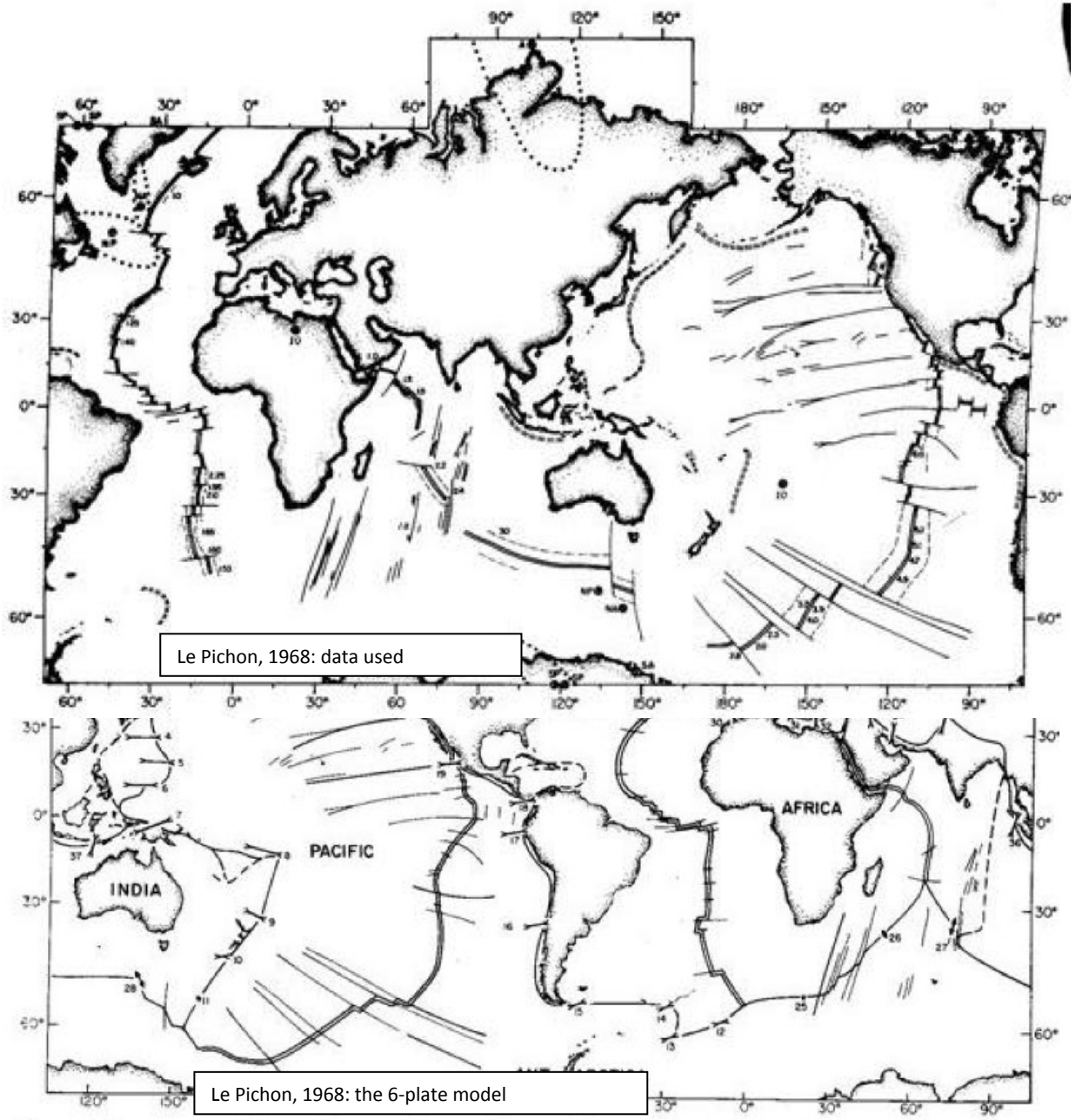

Figure 9-6
The locations of the boundaries of the six blocks used in the computations. The numbers next to the vectors of differential movement refer to Table 9-5. Note that the boundaries where the rate of shortening exceeds about 2 cm/yr account for most of the world earthquake activity

Le Pichon, 1968

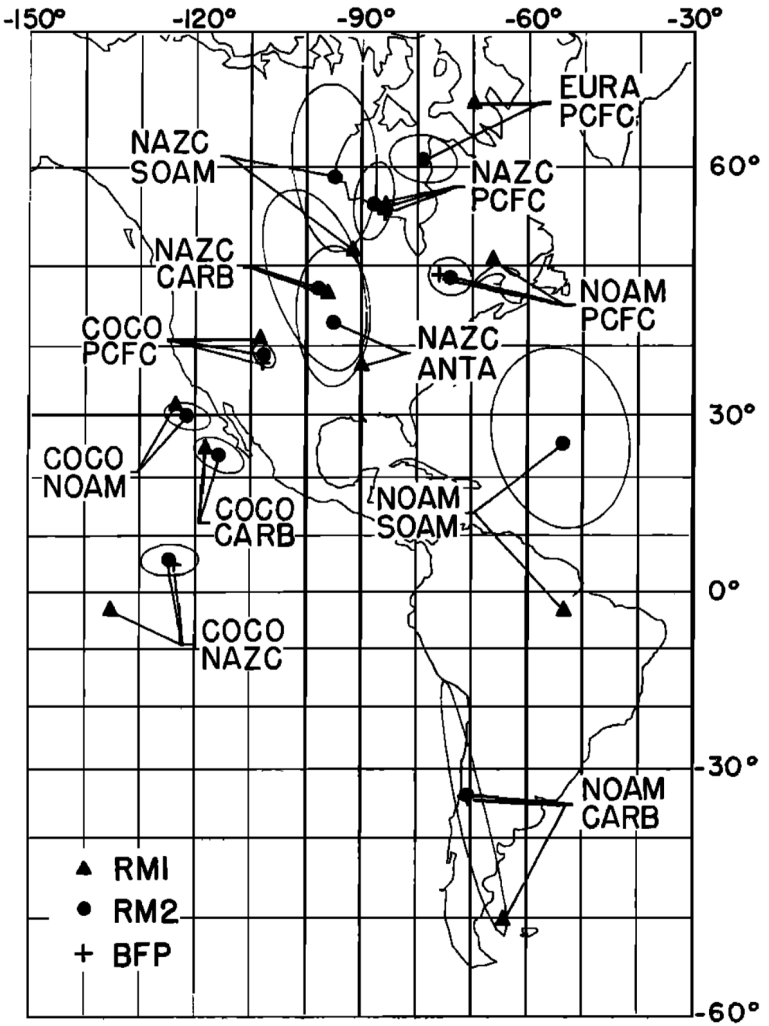

Fig. 4. Poles for model RM2, with their 95% (2σ) confidence ellipses. RM1 poles and best fitting poles (Table 3), where available, are also shown.

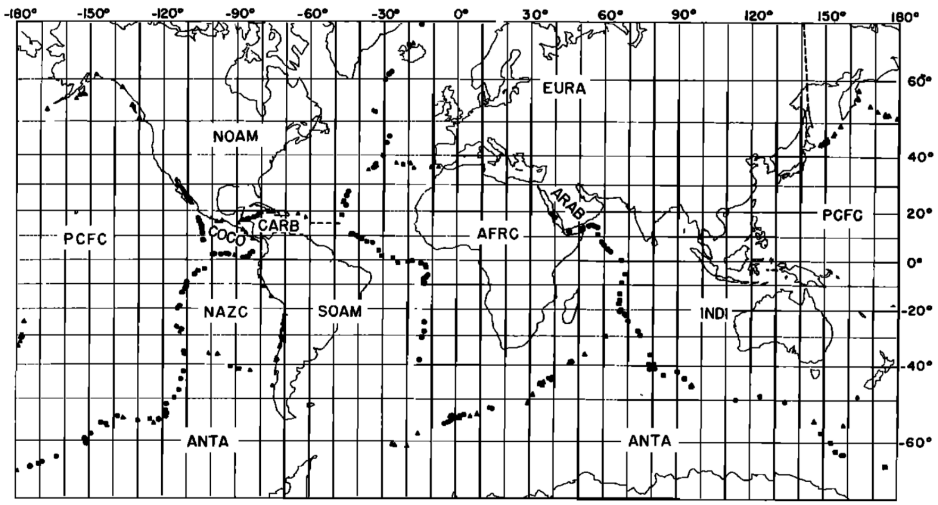

Fig. 1. Plate geometry and geographical distribution of the data used in producing model RM2. Circles are sea floor spreading rates, squares are transform faults, and triangles are slip vectors. Seven EURA-NOAM data at high latitudes are not shown on the figure.

	Relative Rotation Vector*						Error Ellipse†			Importance Distribution			
Plate Pair	θ °N	σ_θ deg	φ °E	σ_ϕ deg	ω deg/m.y.	σ_ω deg/m.y.	ζ_{max} deg	σ_{max} deg	σ_{min} deg	RA	TF	SV	Total
NOAM-PCFC	48.77	1.10	-73.91	1.94	0.852	0.025	S71°E	1.30	1.08	0.405	0.398	0.694	1.497
COCO-PCFC	38.72	0.89	-107.39	1.01	2.208	0.070	S37°E	1.00	0.63	0.977	0.272	0.009	1.258
NAZC-PCFC	56.64	1.89	-87.88	1.81	1.539	0.029	N09°E	1.91	0.96	0.849	0.341	0.038	1.228
EURA-PCFC	60.64	1.04	-78.92	3.04	0.977	0.027	S78°E	1.51	1.02	0	0	0	0
INDI-PCFC	60.71	0.77	-5.79	1.83	1.246	0.023	S82°E	0.90	0.76	0	0	0.246	0.246
ANTA-PCFC	64.67	0.90	-80.23	2.32	0.964	0.014	N52°E	1.11	0.75	1.200	0.811	0.039	2.050
COCO-NOAM	29.80	1.06	-121.28	2.07	1.489	0.070	S75°E	1.84	0.99	0	0	0.165	0.165
AFRC-NOAM	80.43	1.57	56.36	35.29	0.258	0.019	N86°E	5.88	1.51	0.851	0.246	0.091	1.188
EURA-NOAM	65.85	6.17	132.44	5.06	0.231	0.015	S14°E	6.36	1.39	1.055	0.626	0.366	2.047
NOAM-CARB	-33.83	9.19	-70.48	2.76	0.219	0.052	S13°E	9.42	0.97	0.952	1.741	0.253	2.946
COCO-CARB	23.60	1.48	-115.55	2.26	1.543	0.084	S63°E	2.24	1.21	0	0	0.111	0.111
NAZC-CARB	47.30	5.37	-97.57	4.57	0.711	0.056	S19°E	5.59	2.67	0	0	0	0
COCO-NAZC	5.63	1.40	-124.40	2.61	0.972	0.065	N89°E	2.60	1.40	1.829	0.732	0.076	2.637
NOAM-SOAM	25.57	7.12	-53.82	6.22	0.167	0.029	S14°E	7.22	5.49	0	0	0	0
CARB-SOAM	73.51	11.75	60.84	48.86	0.202	0.038	S52°E	16.84	6.84	0	0	0	0
NAZC-SOAM	59.08	3.76	-94.75	3.73	0.835	0.034	S05°E	3.77	1.90	0	0	0.464	0.464
AFRC-SOAM	66.56	2.83	-37.29	2.65	0.356	0.010	S08°E	2.85	0.98	1.201	1.108	0.072	2.381
ANTA-SOAM	87.69	1.30	75.20	79.29	0.302	0.018	N84°E	3.22	1.26	0.167	0.608	0.283	1.058
INDI-AFRC	17.27	0.97	46.02	1.06	0.644	0.014	S47°E	1.24	0.66	0.843	1.098	0	1.941
ARAB-AFRC	30.82	3.44	6.43	11.48	0.260	0.047	S79°E	10.02	2.93	1.989	0.934	0.077	3.000
AFRC-EURA	25.23	4.25	-21.19	0.98	0.104	0.036	S01°E	4.25	0.89	0	0.783	1.167	1.950
INDI-EURA	19.71	1.40	38.46	2.66	0.698	0.024	S65°E	2.72	0.90	0	0	0	0
ARAB-EURA	29.82	2.53	-1.64	9.57	0.357	0.054	S85°E	8.33	2.45	0	0	0	0
INDI-ARAB	7.08	2.15	63.86	2.30	0.469	0.066	S51°E	2.51	1.89	0	0	0	0
NAZC-ANTA	43.21	4.50	-95.02	3.28	0.605	0.039	S01°E	4.50	2.39	0.246	0.058	0.222	0.526
AFRC-ANTA	9.46	3.77	-41.70	3.55	0.149	0.009	S42°E	4.93	1.45	0.697	1.243	0.195	2.135
INDI-ANTA	18.67	1.16	32.74	1.41	0.673	0.011	S62°E	1.39	1.10	1.012	0.135	0.025	1.172
Total										14.273	11.134	4.593	30.000

*First plate named moves counterclockwise with respect to the second. Uncertainties are the standard deviations of marginal distributions.

†One-sigma error ellipses are specified by the azimuth ζ_{max} of the major axis; lengths of the axes are geocentric angles.

Minster and Jordan, 1978 (RM2)

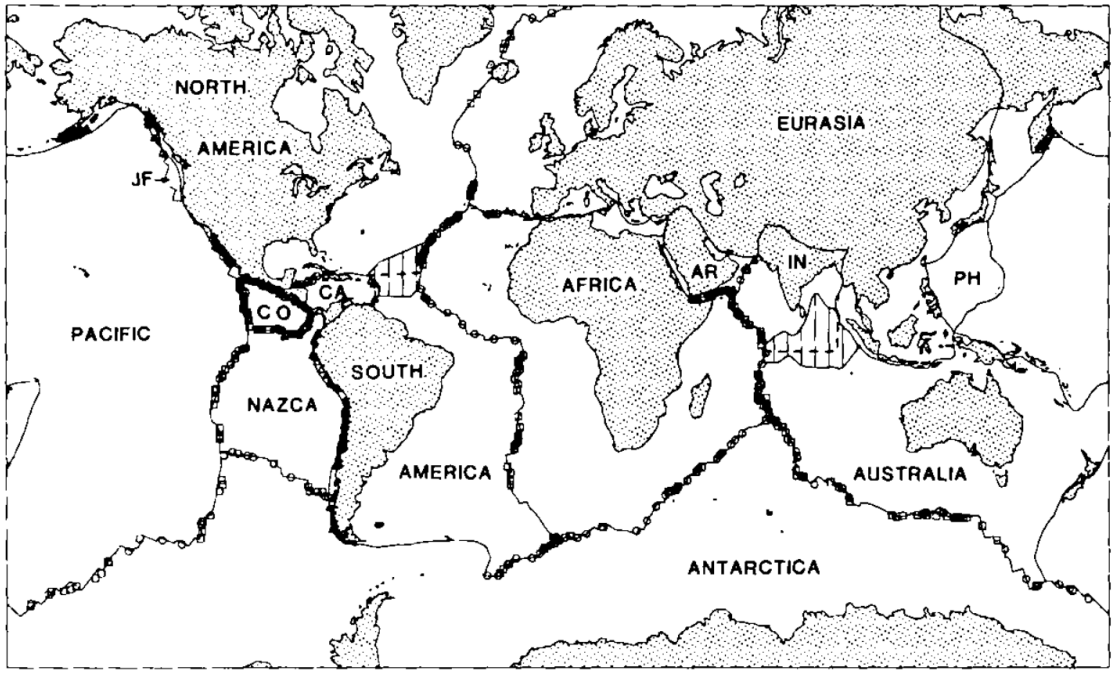

Figure 4. Data locations and plate geometry assumed for NUVEL-1. Regions with vertical lines mark diffuse plate boundaries between North and South America and between India and Australia. Within each of these diffuse boundaries a dashed line shows the discrete boundary assumed in NUVEL-1. Squares show locations of spreading rates, circles show locations of transform azimuths, and triangles show earthquake locations for slip vectors (except those along transform faults offsetting mid-ocean ridges, which are omitted for clarity). Also shown are two plates (Philippine and Juan de Fuca) omitted from NUVEL-1, but included in Table 1 for completeness. Plate name abbreviations: Cocos (CO), Caribbean (CA), Indian (IN), Arabian (AR), Philippine (PH), and Juan de Fuca (JF). Mercator projection.

reliably resolved. The 1122 data from 22 plate boundaries inverted to obtain NUVEL-1 consist of 277 spreading rates, 121 transform fault azimuths, and 724 earthquake slip vectors. We determined all rates over a uniform time interval of 3.0 m.y., corresponding to the centre of the anomaly 2A sequence, by comparing synthetic magnetic anomalies with observed profiles. The model fits the data well.

DeMets et al., 1990

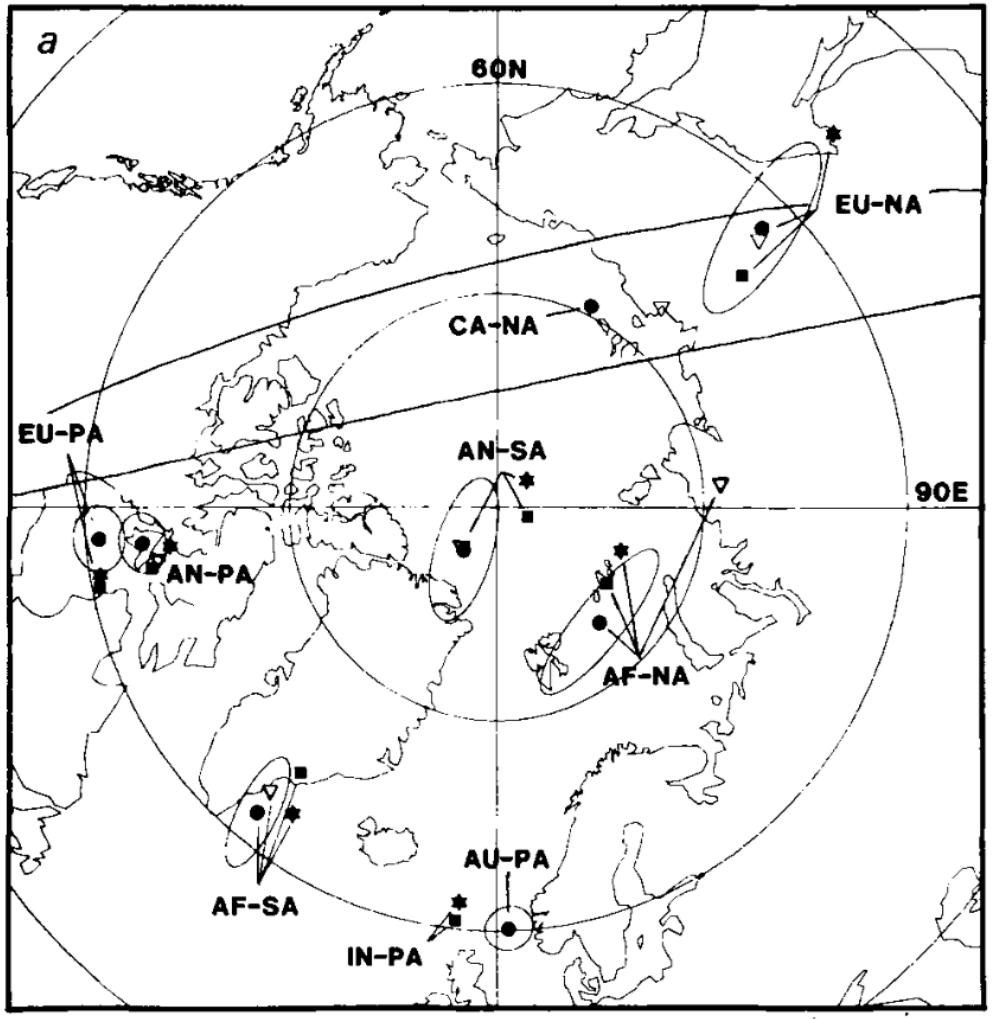

Figure 6(a). Location of some of the NUVEL-1 Euler poles (solid circles) and their 2-D 95 per cent confidence regions describing motion between the African (AF), Antarctic (AN), Australian (AU), Caribbean (CA), Eurasian (EU), Indian (IN), North American (NA), Pacific (PA), and South American (SA) plates. Best-fitting poles (open triangles), model P071 (Chase 1978) Euler poles (stars), and model RM2 (Minster & Jordan 1978) Euler poles (squares) are also shown. For each Euler pole, the first plate listed rotates counter-clockwise relative to the second plate.

DeMets et al., 1990

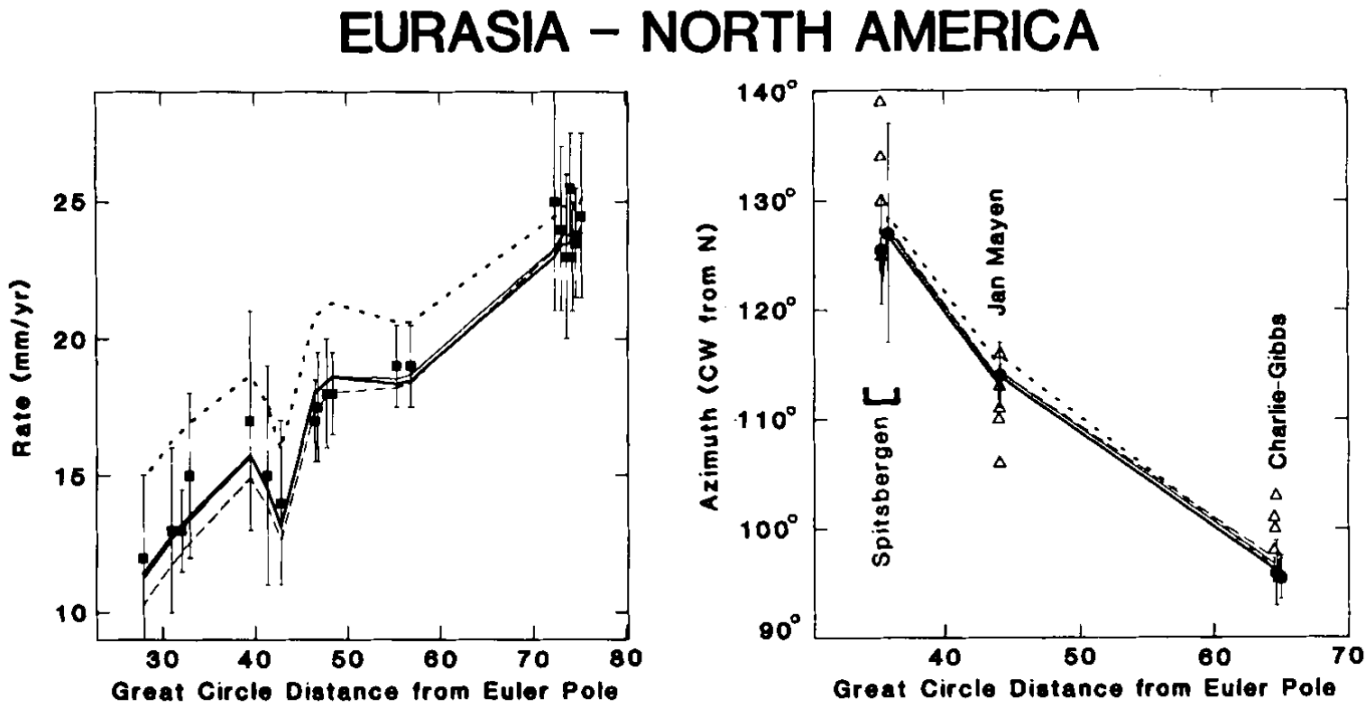

Figure 10. Spreading rates (squares), transform fault azimuths (circles), and slip vector azimuths (triangles) observed along the Arctic Ridge and northern Mid-Atlantic Ridge are compared with directions and rates from the NUVEL-1 (bold solid), best-fitting (thin solid), RM2 (long dashed), and P071 (short dashed) Eurasia–North America Euler vectors. The horizontal axis shows the angular distance from the best-fitting Euler vector (Table 4). Vertical error bars show 1-σ errors assigned to rates and transform fault azimuths.

DeMets et al., 1990

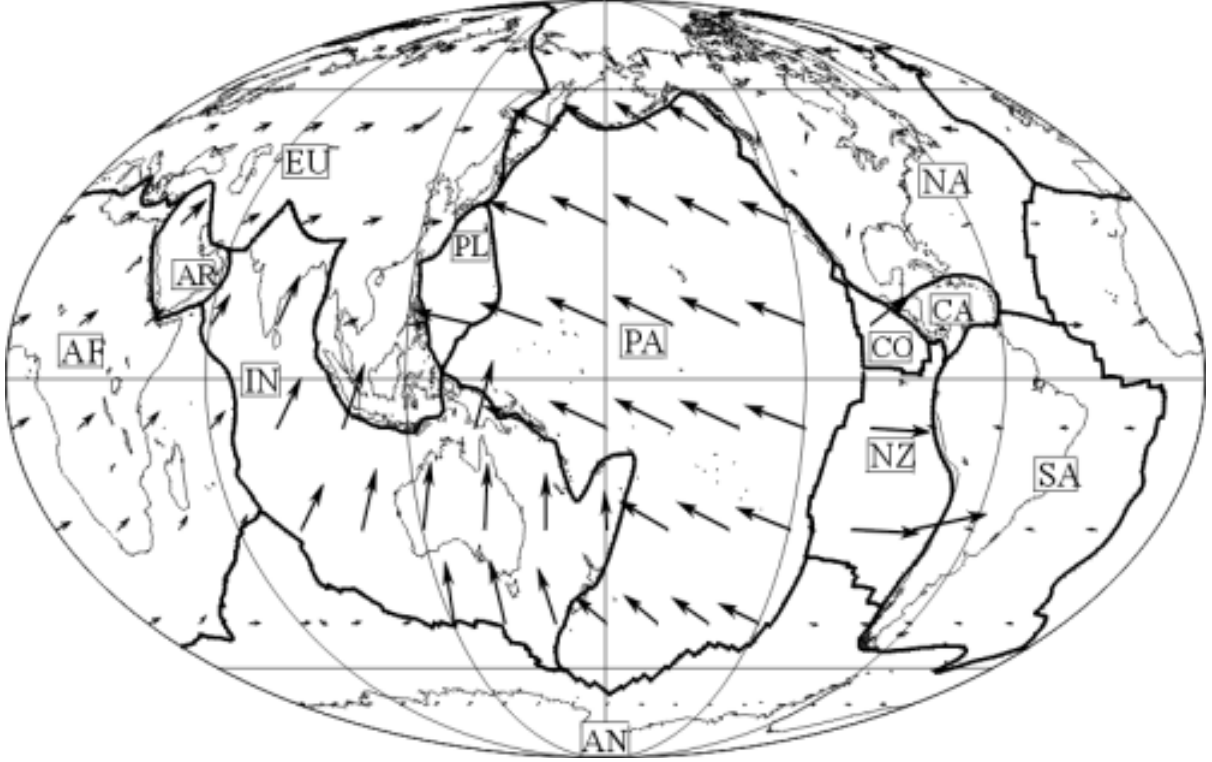

Table 2. Angular Velocities Describing Plate Motion

Plate Pair	Angular Velocity Lat. °N	Lon. °E	ω °/m.y.	Pole Error Ellipse σ_{max} °	σ_{min} °	ζ_{max} °	σ_ω °/m.y.
Eurasia–N. Amer.	78.5	122.0	.23	8.2	4.9	−8	.03
N. Amer.–Pacific	49.1	−73.0	.79	4.1	2.2	−83	.03
Africa–N. Amer.	80.9	16.7	.22	14.5	11.1	15	.04
Pacific–Australia	−57.2	−173.5	1.13	2.6	2.4	43	.04
Australia–Eurasia	9.9	47.4	.72	4.9	4.0	−53	.05
Africa–Eurasia	−11.7	−27.3	.07	41.7	36.1	36	.03
Eurasia–Pacific	60.2	−74.4	.95	3.3	2.2	−88	.05
Australia–Africa	11.2	52.6	.71	6.1	4.3	−22	.04
N. Amer.–S. Amer.	6.5	−55.6	.28	8.3	7.4	−55	.12
Africa–S. Amer.	39.9	−49.3	.38	16.2	7.4	−7	.10

The first plate moves counterclockwise relative to the second plate. The uncertainty in pole position is described by the one-sigma error ellipse, which is given by the angular lengths of the semi-principal axes (σ_{max} and σ_{min}) and azimuth of the semi-major axis (ζ_{max}, in degrees clockwise of North). The uncertainty in rotation rate is σ_ω.

DeMets et al., 1994

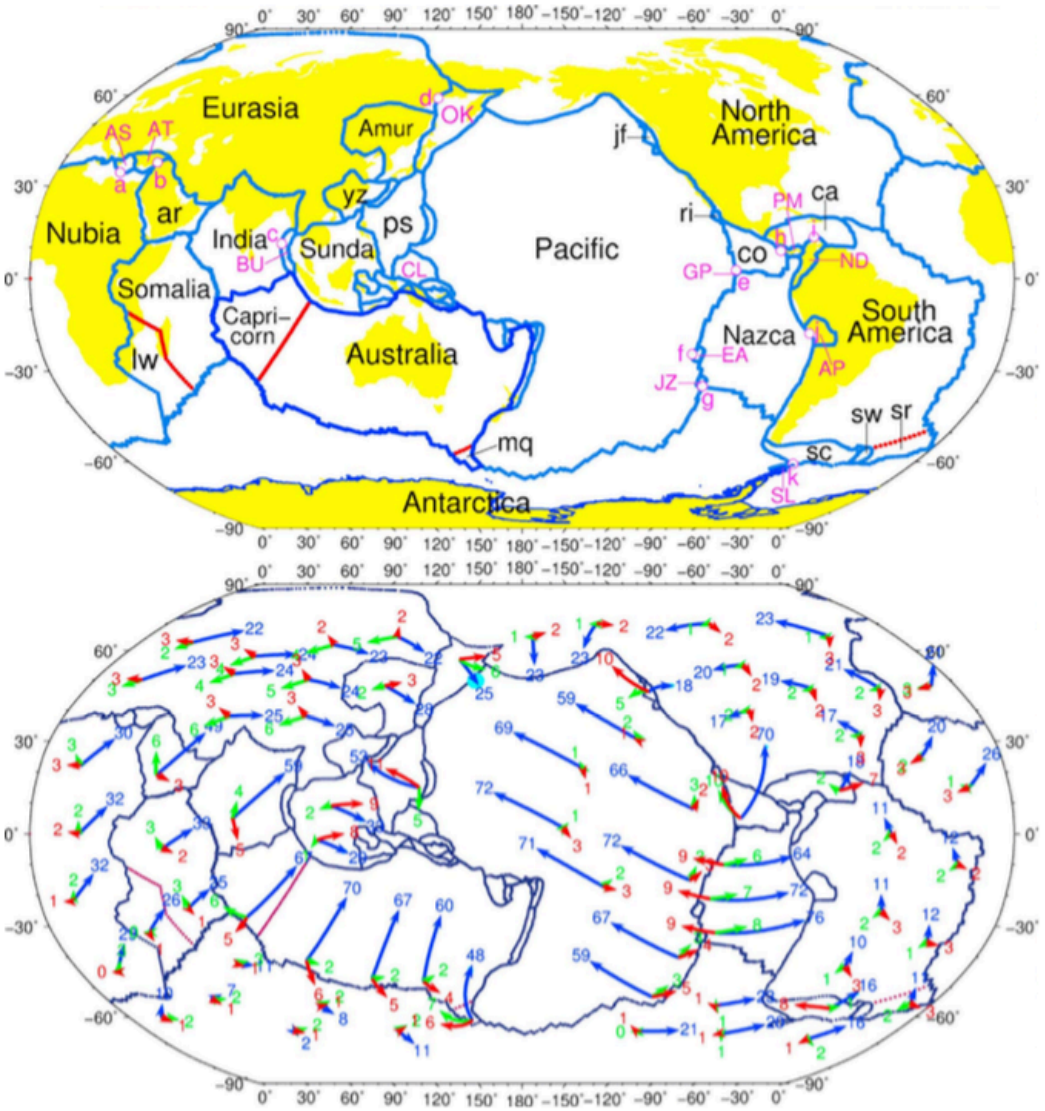

Figure 1. (top) The 56 plates in NNR-MORVEL56, which consist of the 25 plates in MORVEL (black text) [*DeMets et al.*, 2010] and 31 additional small plates from *Bird* [2003] (magenta text). Two-letter abbreviations (see Table 1) are lowercase for MORVEL plates and uppercase for the 31 plates from *Bird* [2003]. Plate boundaries are identical to those from *Bird* [2003] (in blue), except for (in red) the Lwandle-Somalia, Capricorn-Australia, Macquarie-Australia, and Sur-South America plate boundaries. MORVEL56 relative plate velocities at locations (a) through (k) are shown in Figure S1 of the auxiliary material. (bottom) The blue arrows and numerals show the NNR-MORVEL56 horizontal velocities and 95% confidence limits (light blue, imperceptible except for the Okhotsk plate). The red arrows and numerals show velocity differences between NNR-MORVEL56 and NNR-NUVEL1A. The green arrows and numerals show velocity differences between NNR-MORVEL56 and GSRM-NNR-2 [*Kreemer et al.*, 2006]. Speeds are in mm a^{-1}.

Argus et al., 2010

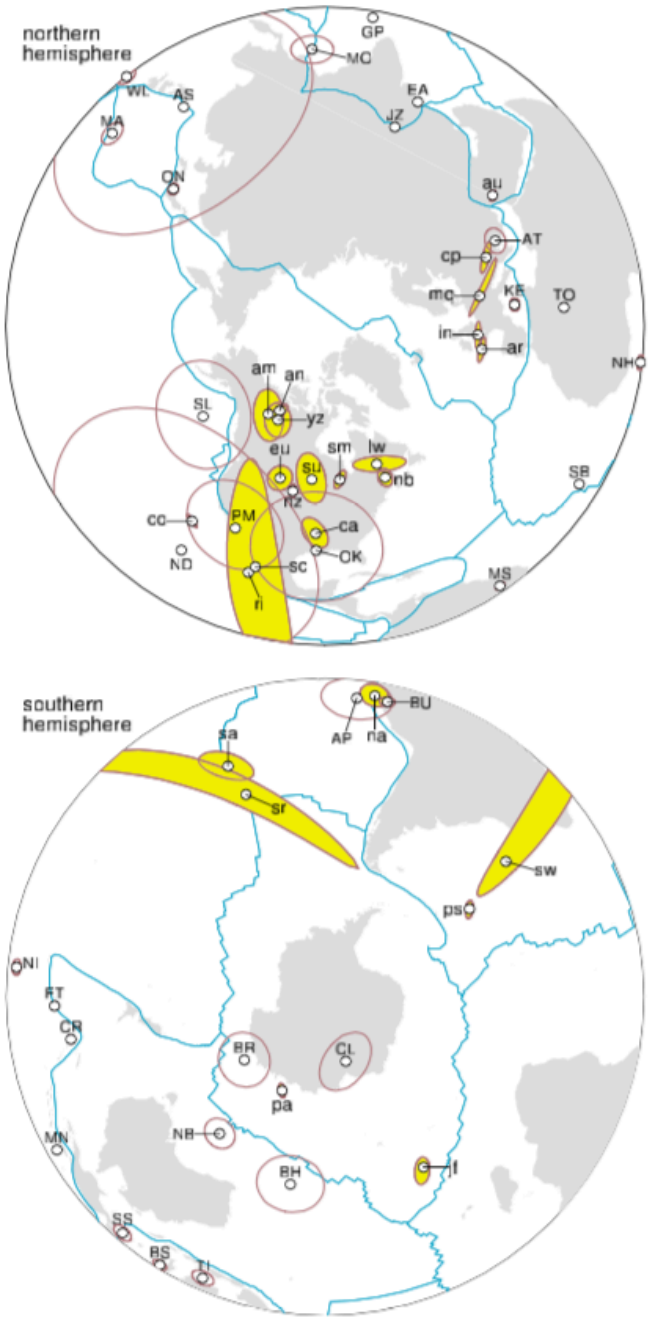

Argus et al., 2010

Figure 3. NNR-MORVEL56 rotation ples and 95% confidence limits. For many plates the 95% confidence limits are smaller than the circle marking the location of their rotation pole.

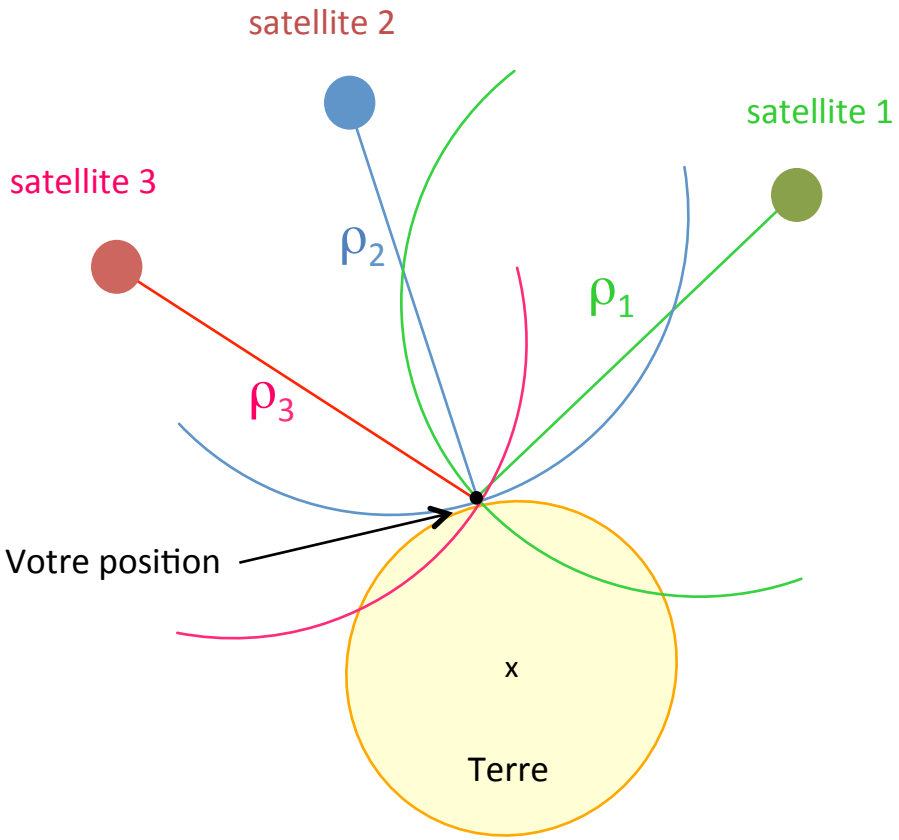
satellite 2
satellite 1
satellite 3
ρ2
ρ1
ρ3
Votre position
x
Terre

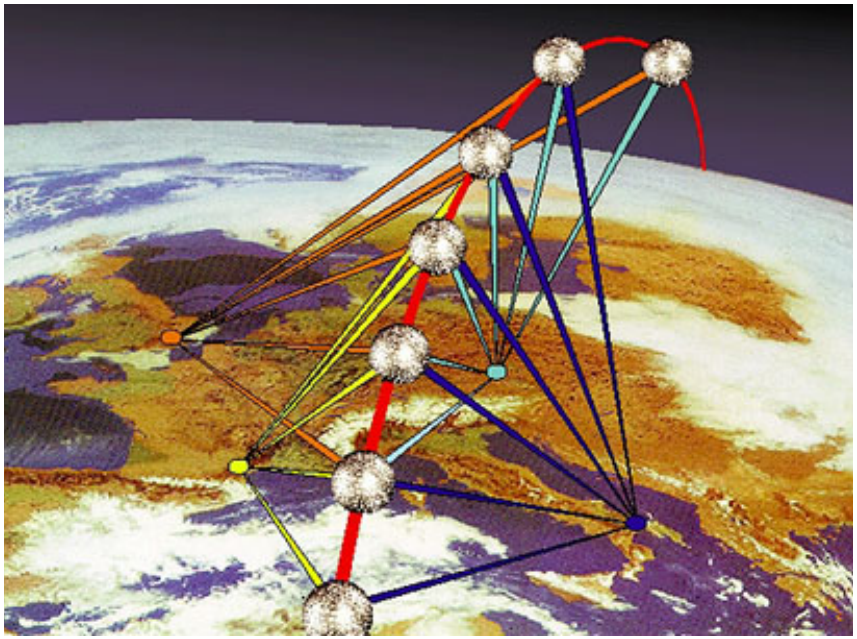

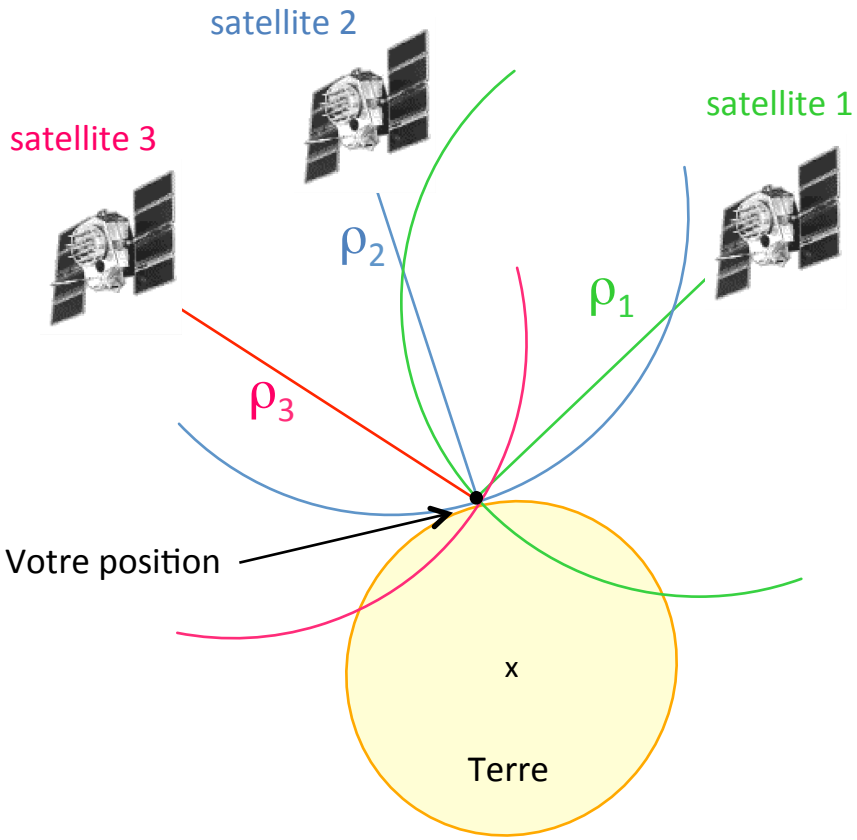
satellite 2
satellite 3
satellite 1
ρ2
ρ1
ρ3
Votre position
x
Terre

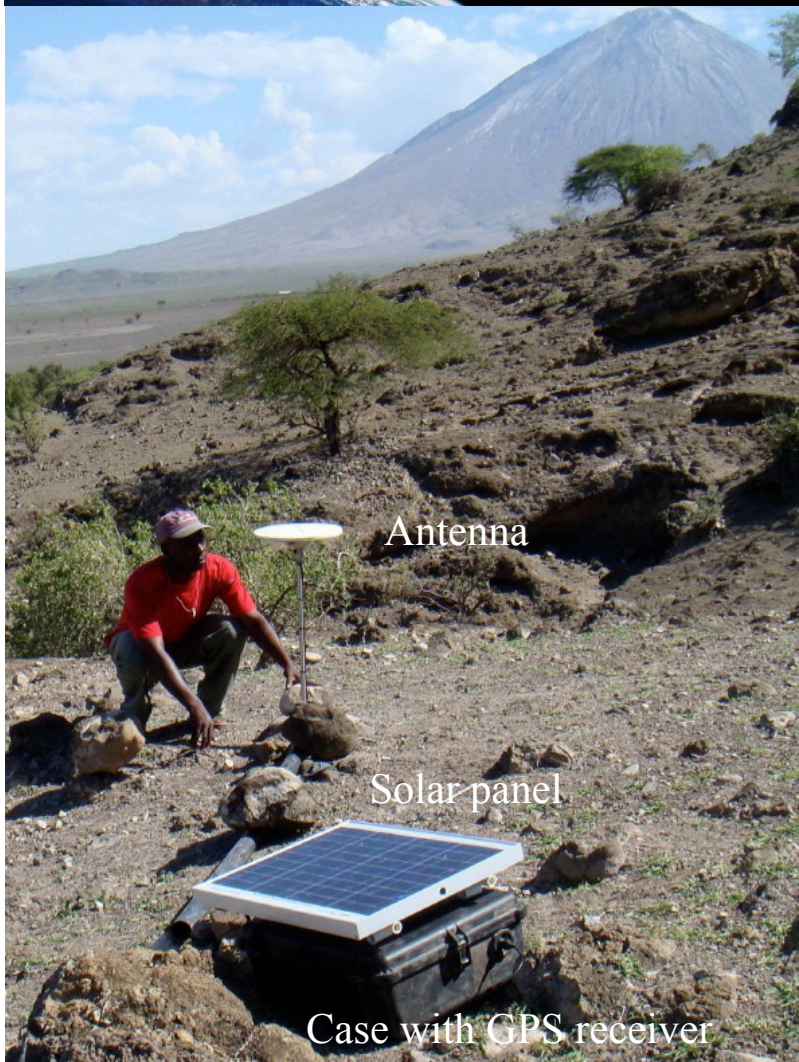
Antenna
Solar panel
Case with GPS receiver

Station GPS permanente

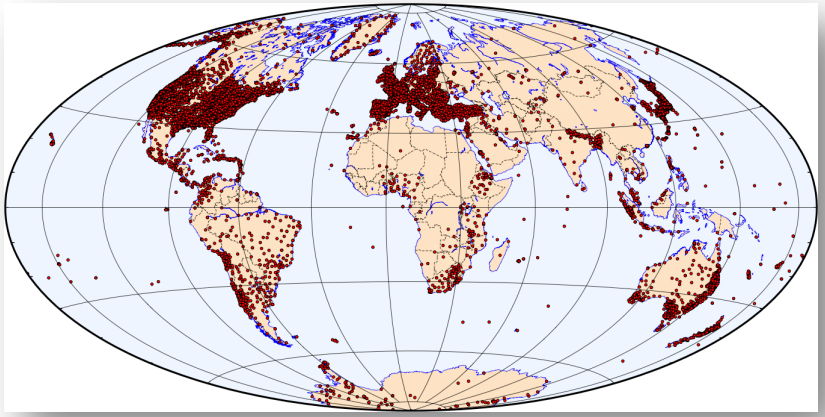

Distribution des stations GPS permanentes publiques (2015)

Algonquin, centre Canada

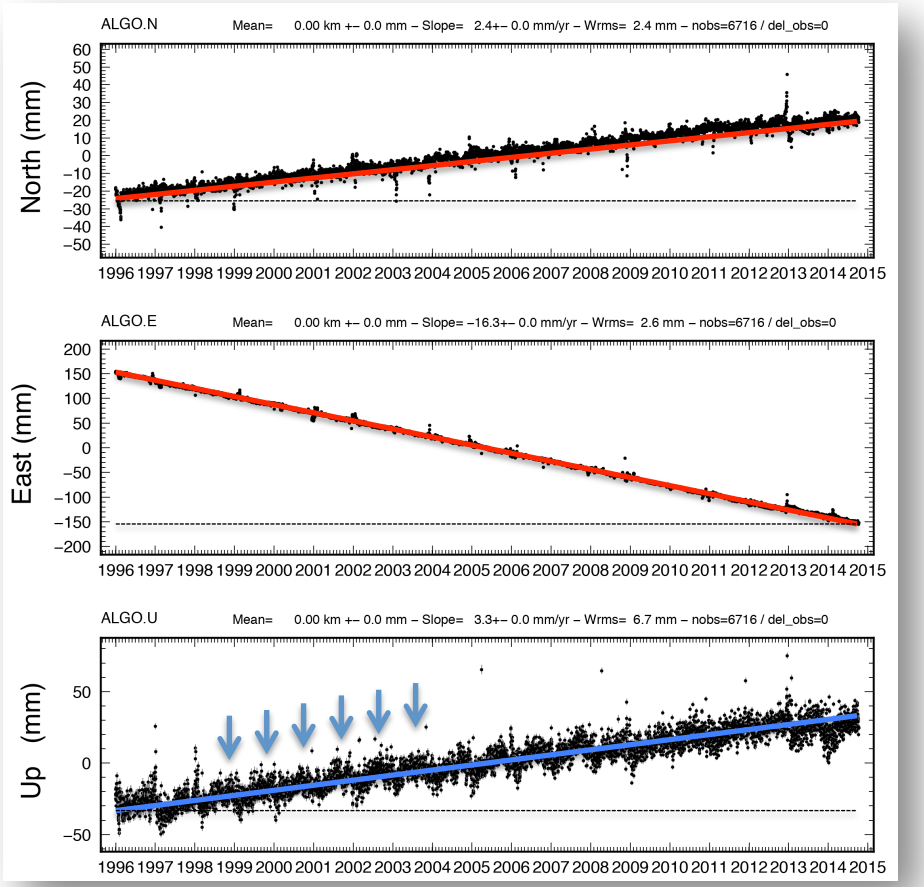

(1) Mouvement plaque nord américaine

(2) Rebond post-glaciaire

(3) Charge hydrologique saisonnière

Earthquakes M>6 (NEIC) - GPS velocities ITRF2005

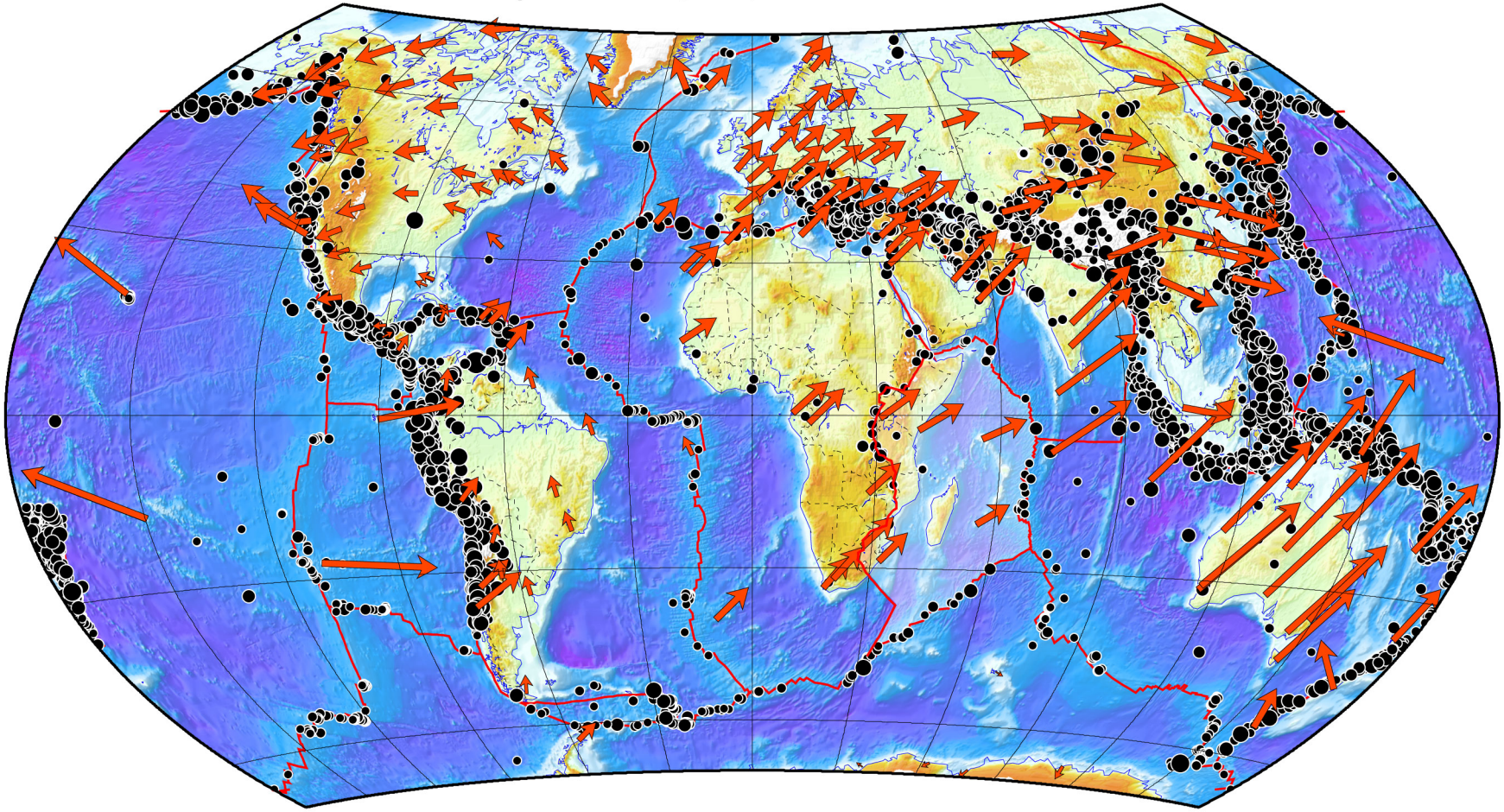

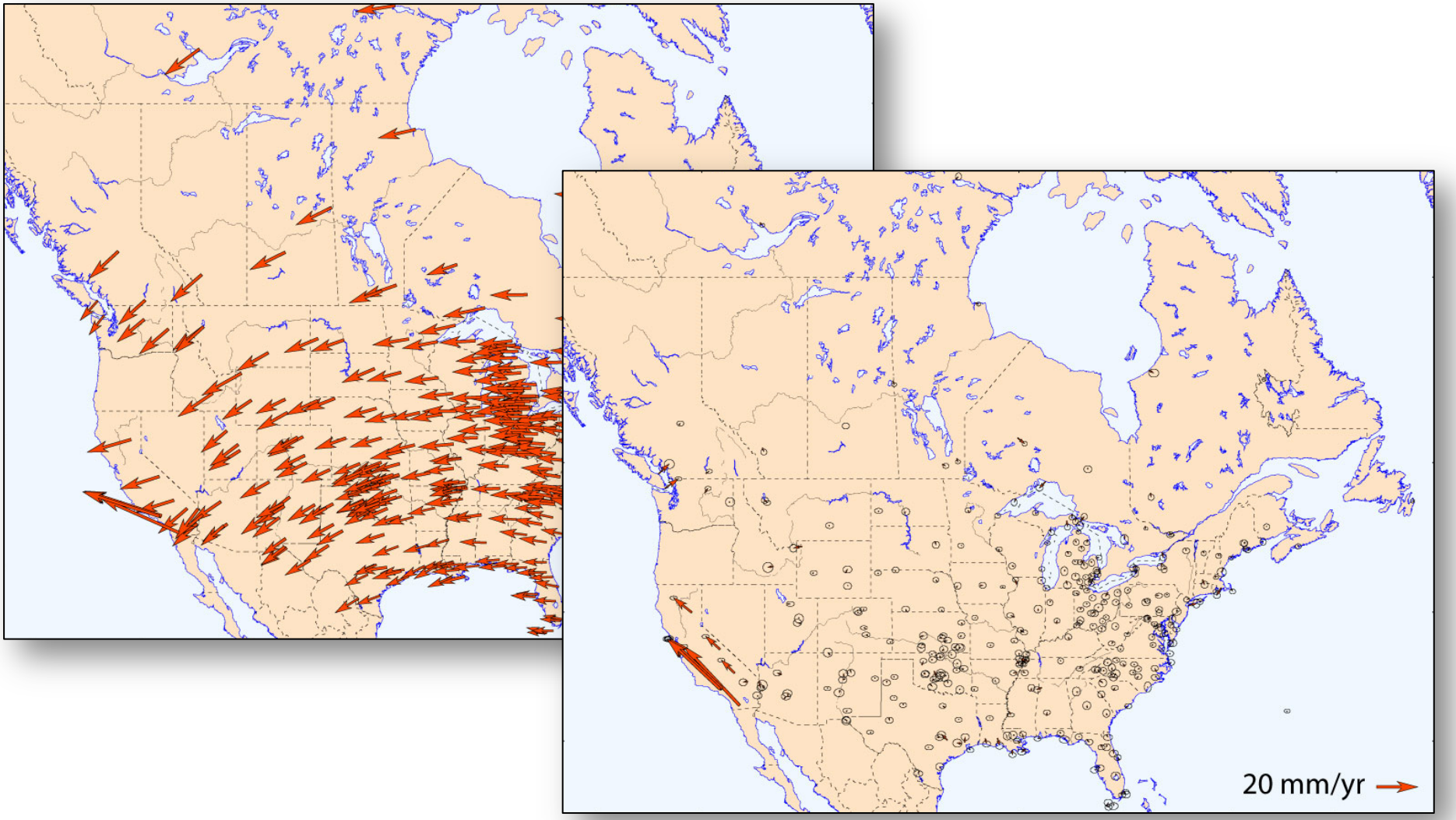
20 mm/yr

Plate Motions Are Steady

Richard G. Gordon Geophysics News, 1990

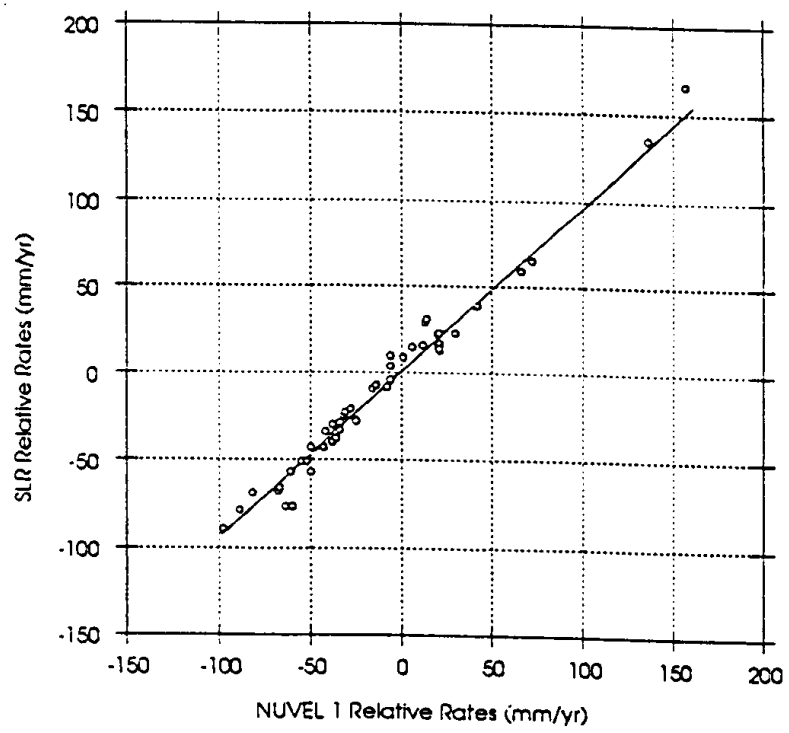

Fig. 11. Comparison of SLR determined geodesic rates with those implied by the NUVEL 1 geologic plate motion model for 54 lines connecting stations on five plates that are well within plate interiors and crossing at least one plate boundary. The slope of the line is 0.949 ± 0.019.

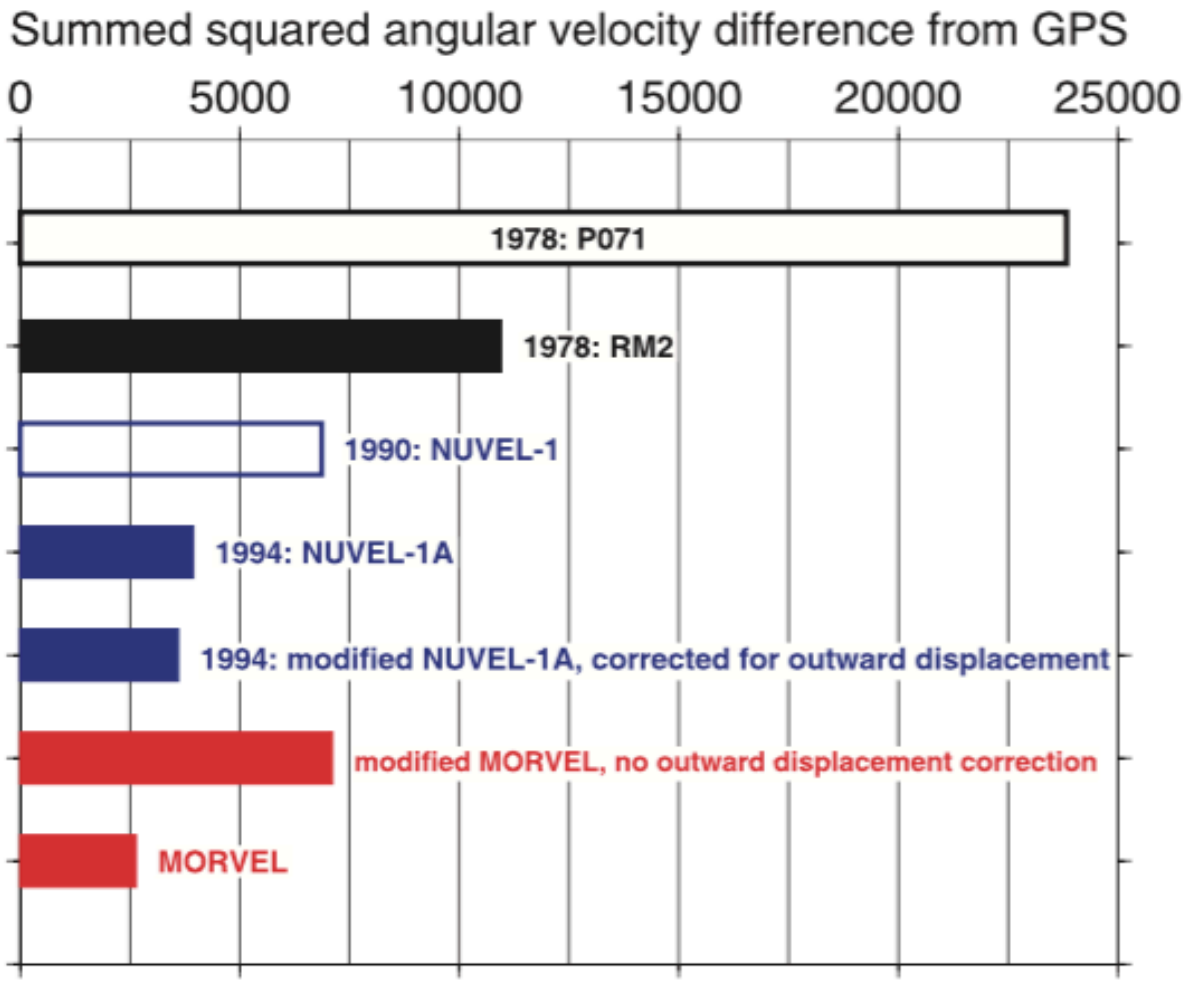

Figure 53. Sums of squared differences from eq. (2) between GPS-derived angular velocities from Table 6 and the closure-enforced angular velocities for seven geological estimates of global plate motions, as follows: P071 (Chase 1978), RM2 (Minster & Jordan 1978), NUVEL-1 (DeMets *et al.* 1990), NUVEL-1A (DeMets *et al.* 1994a), MORVEL and alternative estimates based on the NUVEL-1A and MORVEL data. Due to differences in how the original angular velocity uncertainties were computed for the different geological estimates, only the covariances for the GPS-derived angular velocities are used in eq. (2) to determine the weighted, summed-square difference. Angular velocity comparisons are limited to the plates for which both geological and GPS estimates are available, consisting of the Antarctic, Australia, Eurasia, India, Nubia (AF), Nazca, North America, Pacific, South America and Somalia (AF) plates. Locations of GPS stations used to estimate the plate angular velocities are shown in Fig. 54. Further details about the comparison are given in the text.

DeMets et al., 2010

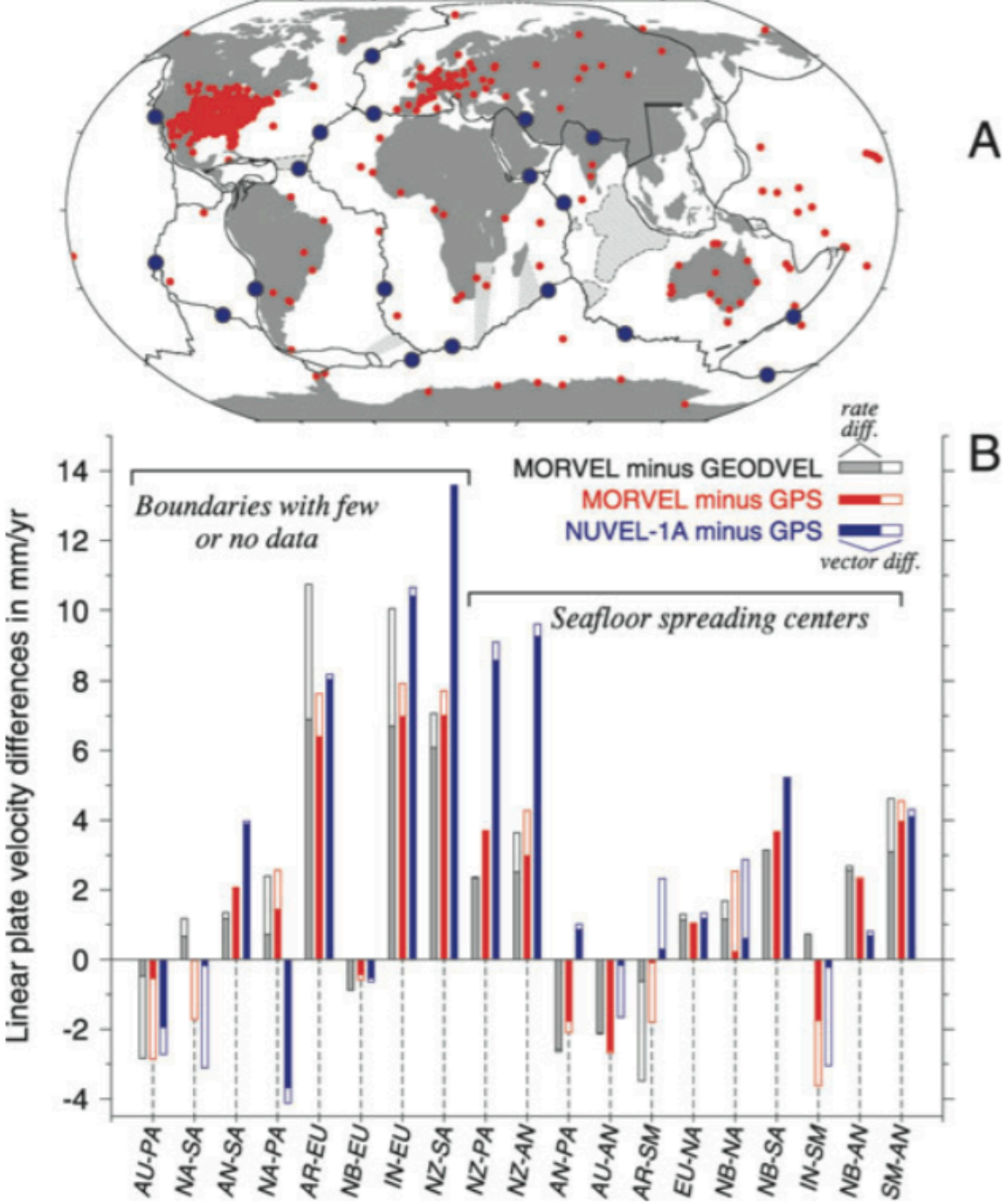

DeMets et al., 2010

(a) Locations of continuous GPS stations (red) that are used to estimate motions of designated plate pairs at locations shown by the blue circles.

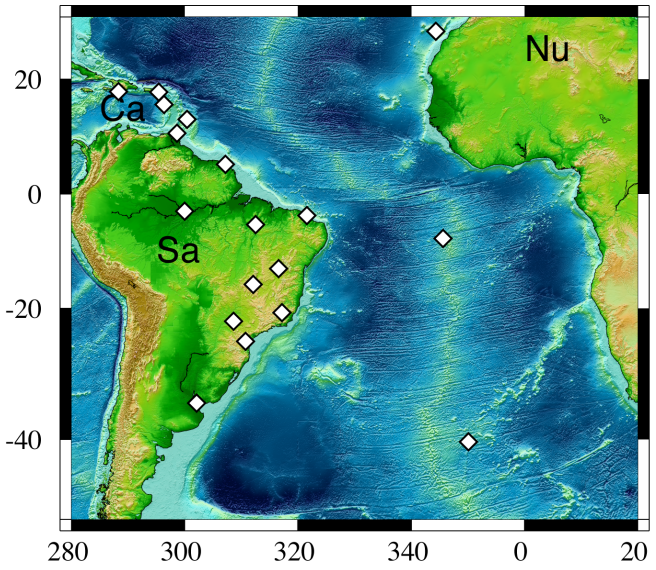

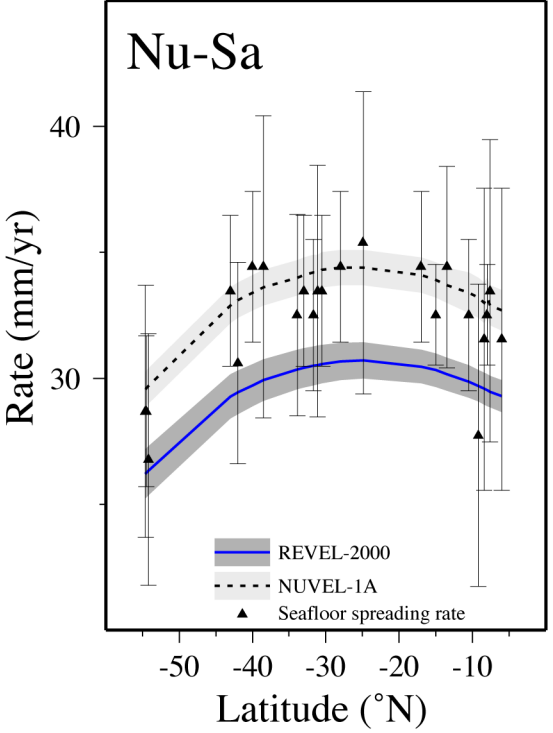

GPS rate slower than NUVEL (0-3 Ma spreading rate)

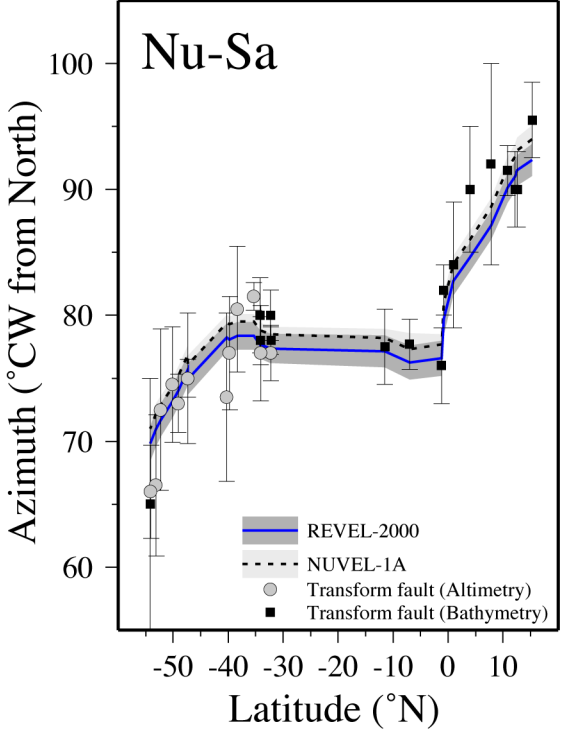

Azimuth has not changed (transforms match GPS)

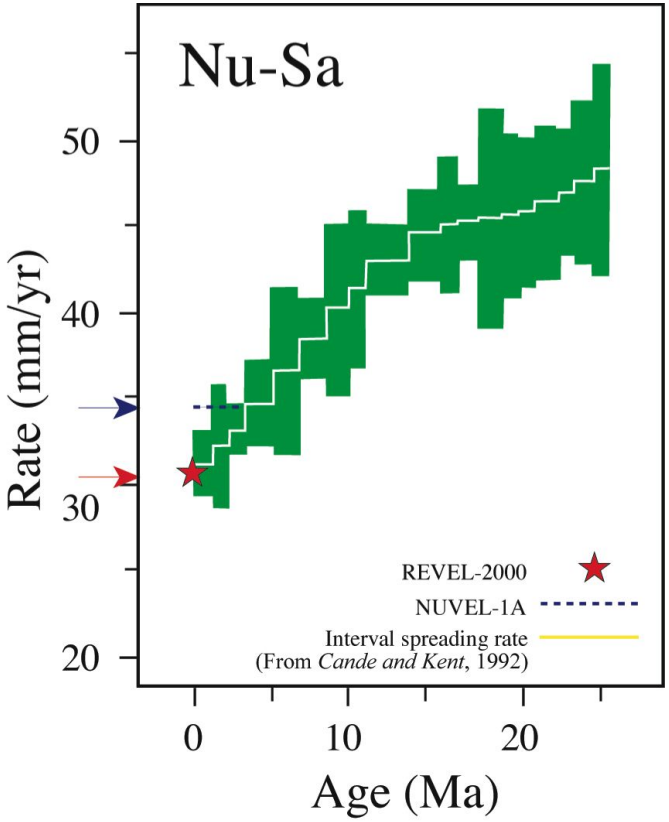

GPS rate slower than NUVEL-1 (0-3 Ma spreading rate) is part of long-term slowing shown by marine magnetic data

Sella et al., 2002

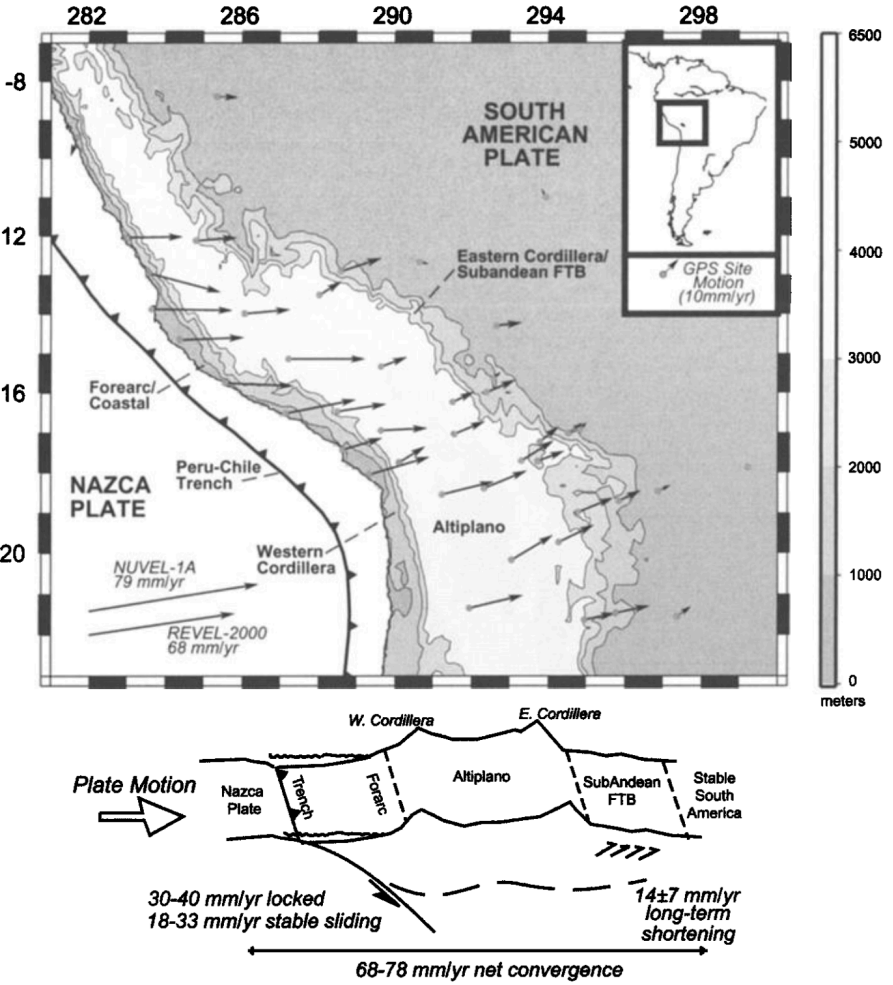

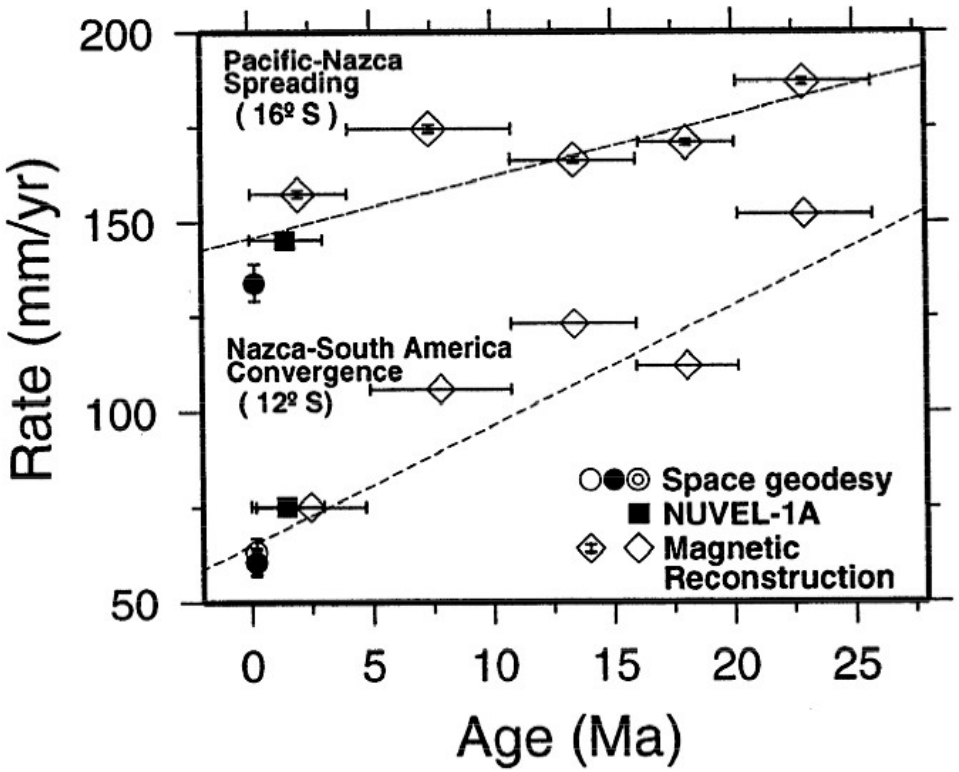

La décélération coïncide avec la croissance ce la topographie andine => augmentation de la friction interplaque et du frottement visqueux à la base de la lithosphère à mesure que la croûte s'épaissit?

Norabuena et al. (1999)

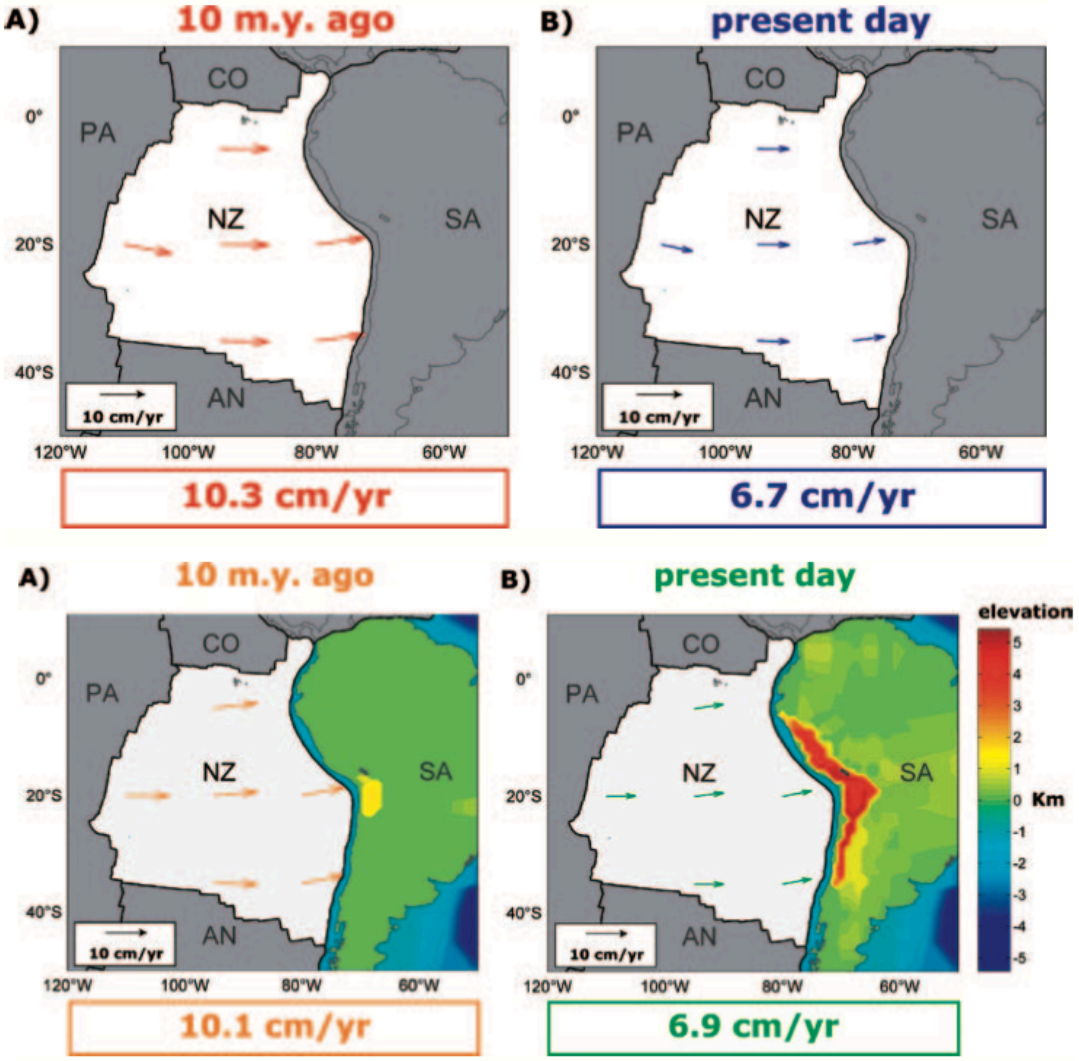

Observations du mouvement de la plaque Nazca (NZ) par rapport à l'Amérique du Sud à 10 Ma (Gordon and Jurdy, 1986), et à l'actuel (Norabuena et al., 1999)

Modèle géodynamique global avec paléotopographie des Andes à 10 Ma (A) et topographie actuelle (B)

2ème loi de Newton => équilibre entre poids de la topographie et forces aux limites
Poids de la topographie augmente => ralentissement de la convergence
La croissance de topographie « consomme » de l'énergie cinétique

Iafaldano et al., Geology, 2006

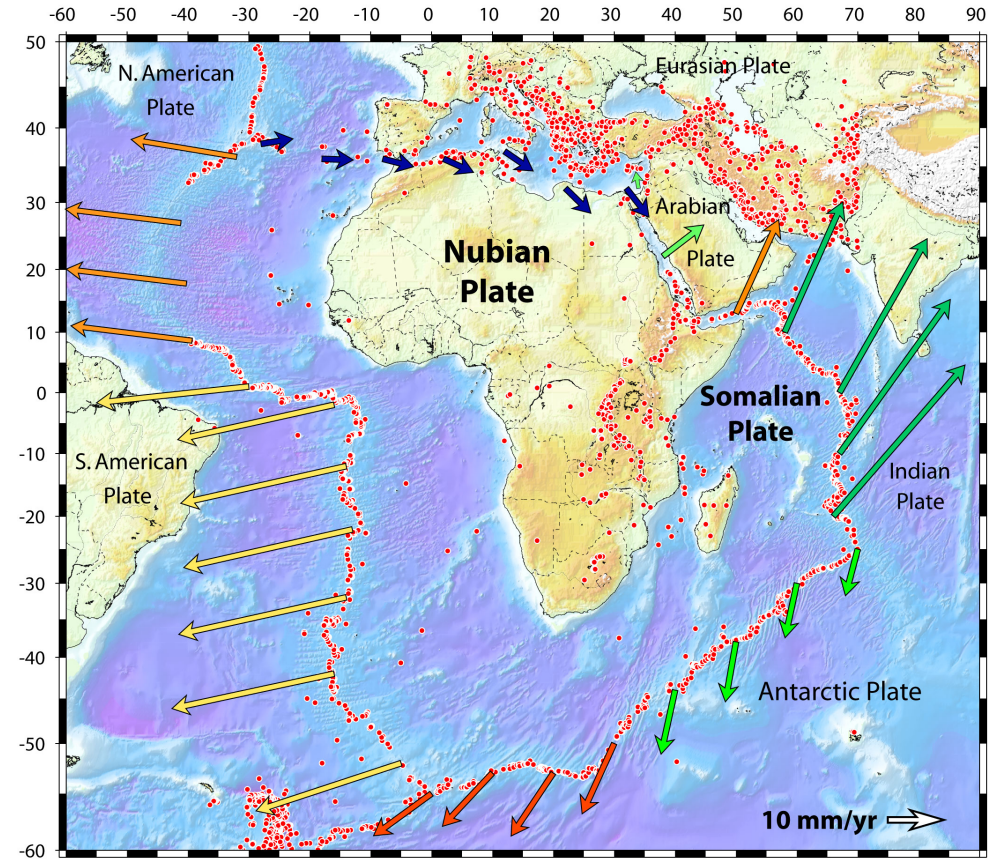
N. American Plate
Eurasian Plate
Nubian Plate
Arabian Plate
Somalian Plate
S. American Plate
Indian Plate
Antarctic Plate
10 mm/yr

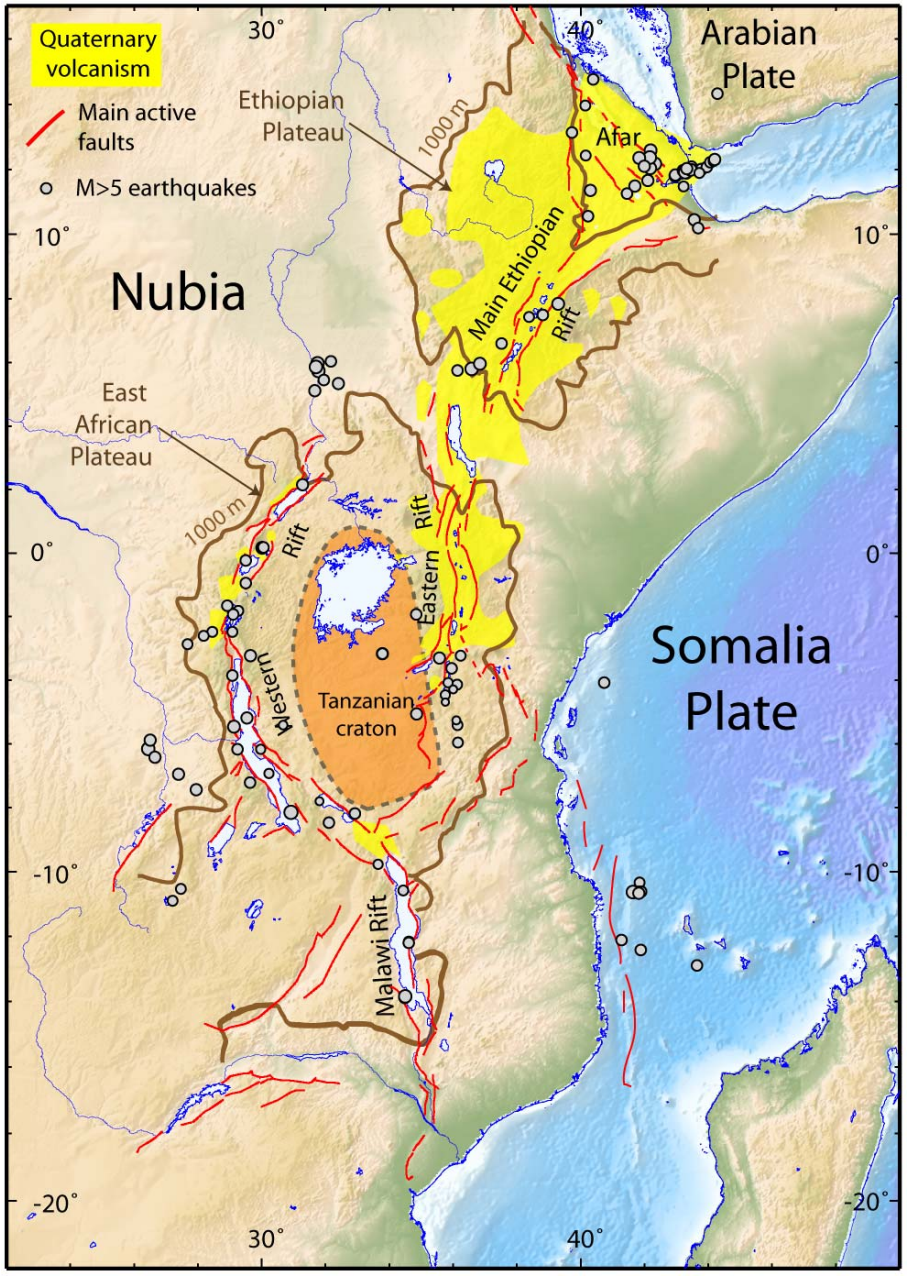
Quaternary volcanism
Main active faults
M>5 earthquakes
Arabian Plate
Ethiopian Plateau
1000 m
Afar
Nubia
Main Ethiopian Rift
East African Plateau
Rift
Eastern
Western
Tanzanian craton
Somalia Plate
Malawi Rift

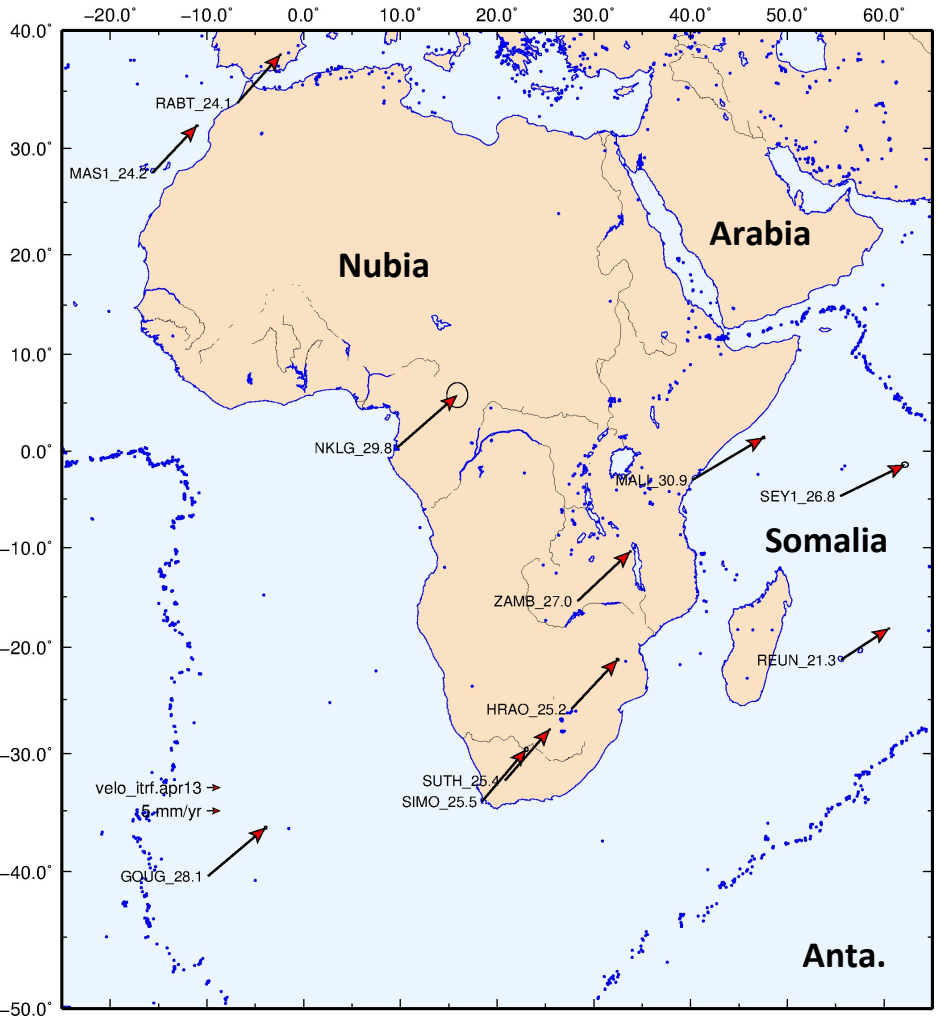
RABT_24.1
MAS1_24.2
NKLG_29.8
MAL1_30.9
SEY1_26.8
ZAMB_27.0
REUN_21.3
HRAO_25.2
SUTH_25.4
SIMO_25.5
velo_itrf.apr13
5 mm/yr
GOUG_28.1
Nubia
Arabia
Somalia
Anta.

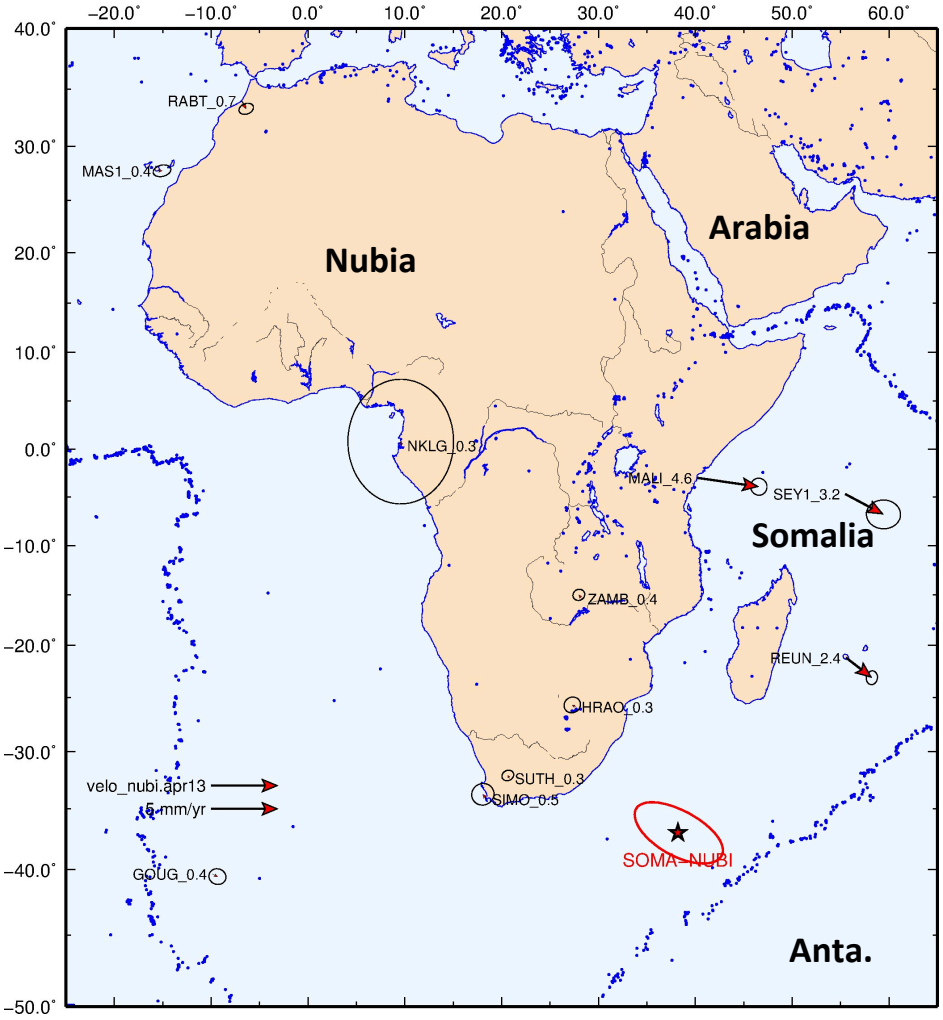
RABT_0.7
MAS1_0.4
NKLG_0.3
MAL1_4.6
SEY1_3.2
ZAMB_0.4
REUN_2.4
HRAO_0.3
SUTH_0.3
SIMO_0.5
velo_nubi.apr13
5 mm/yr
GOUG_0.4
SOMA-NUBI
Nubia
Arabia
Somalia
Anta.

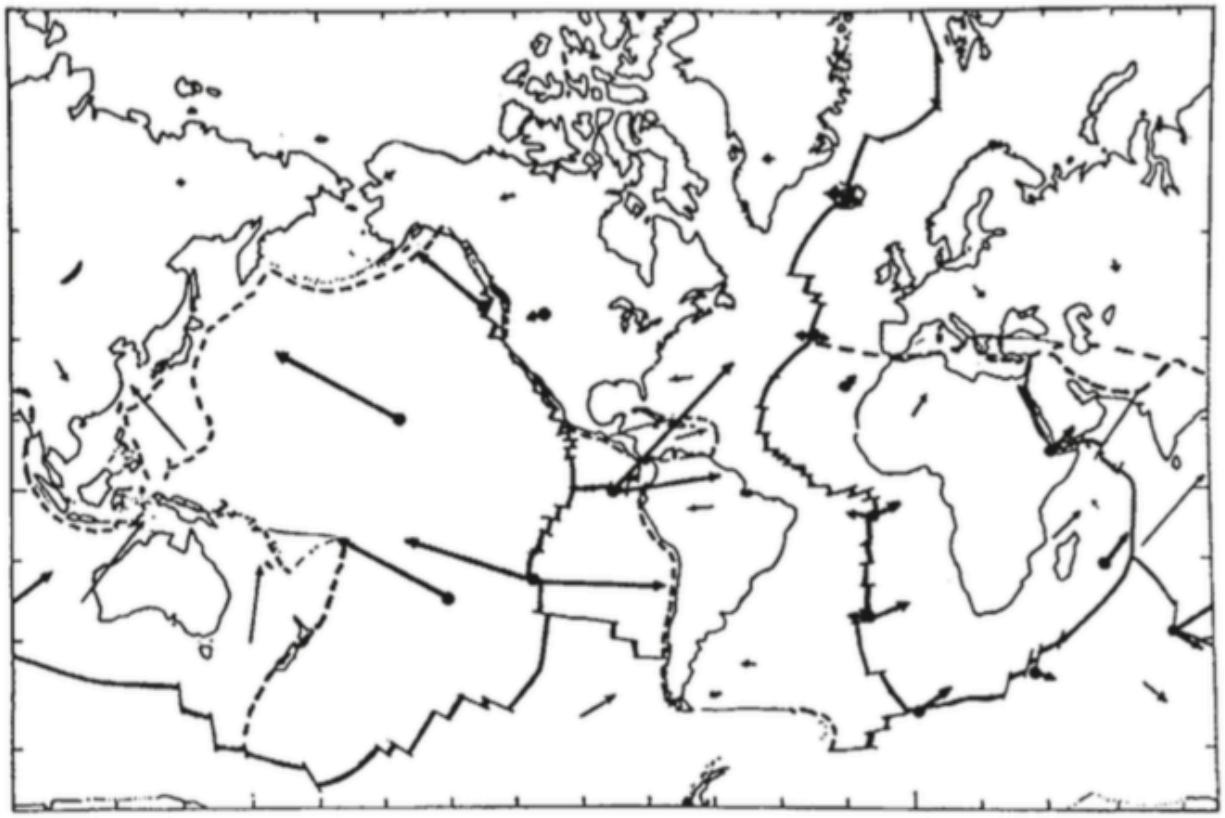

Fig. 1 The arrows show the direction and speed of the plates over the mantle; the heavier arrows show the plate motion at hotspots. This synthesis was based on relative plate motion data (fault strikes and spreading rates) and predicts the directions of the aseismic ridges/ island chains emanating from the hotspots.

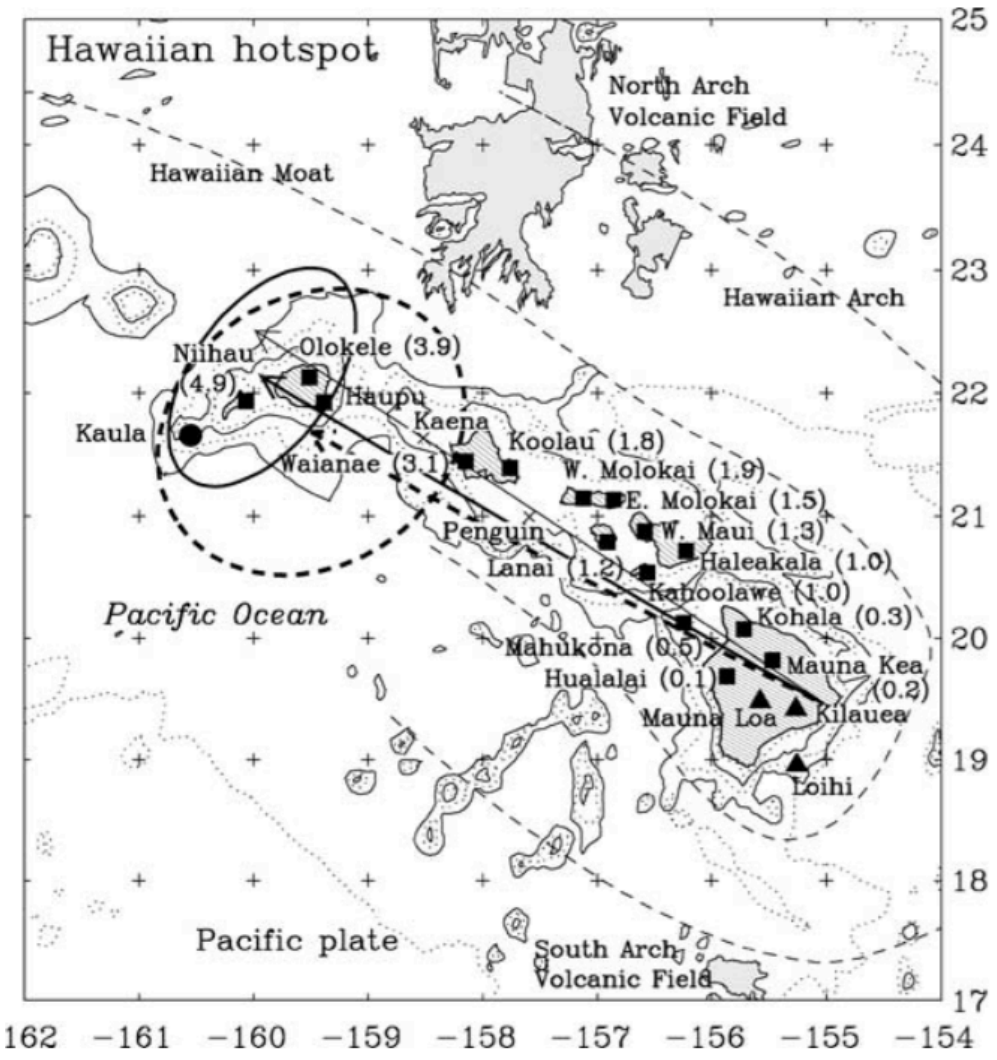

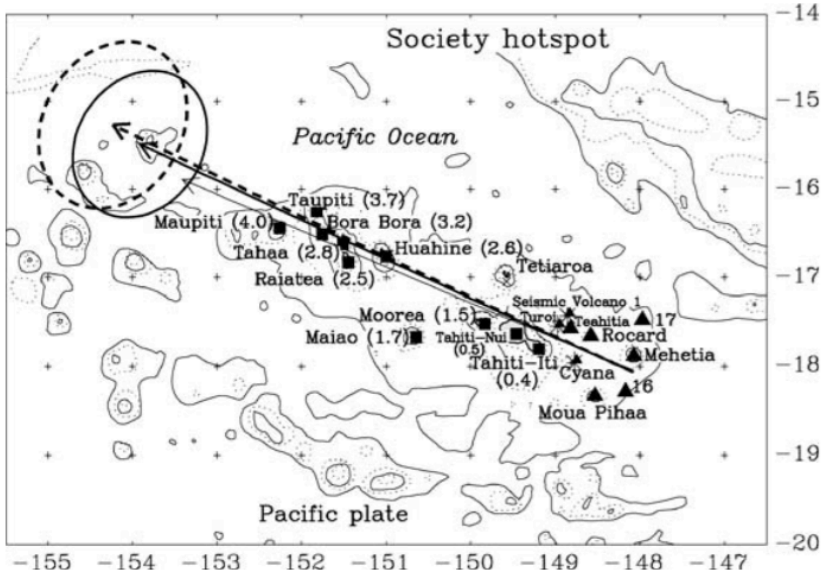

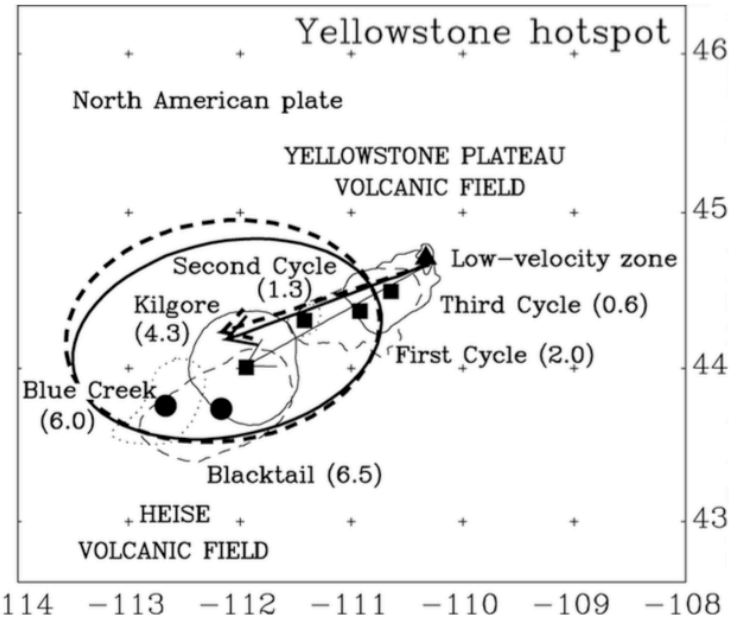

Gripp and Gordon, 2002

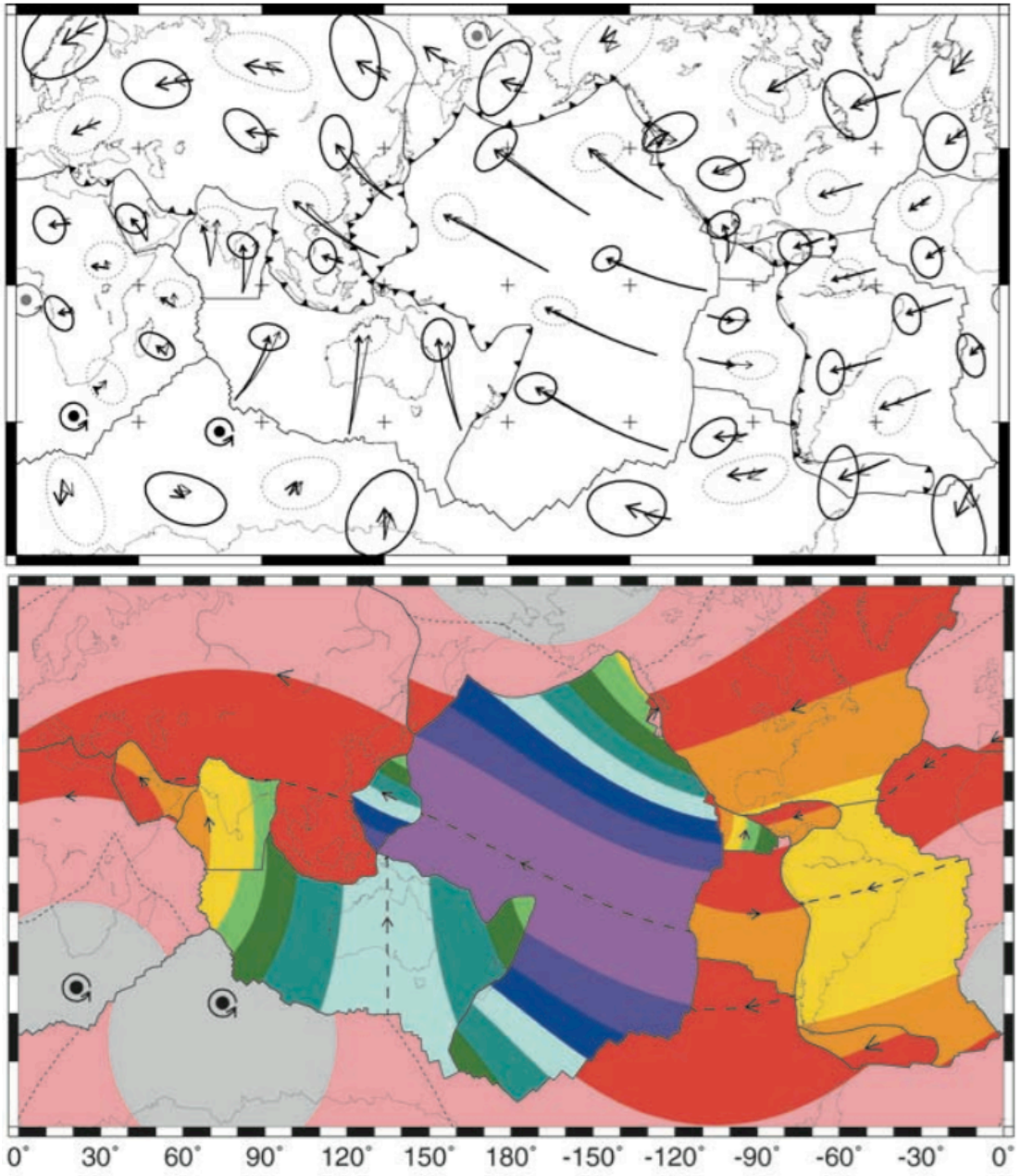

Gripp and Gordon, 2002

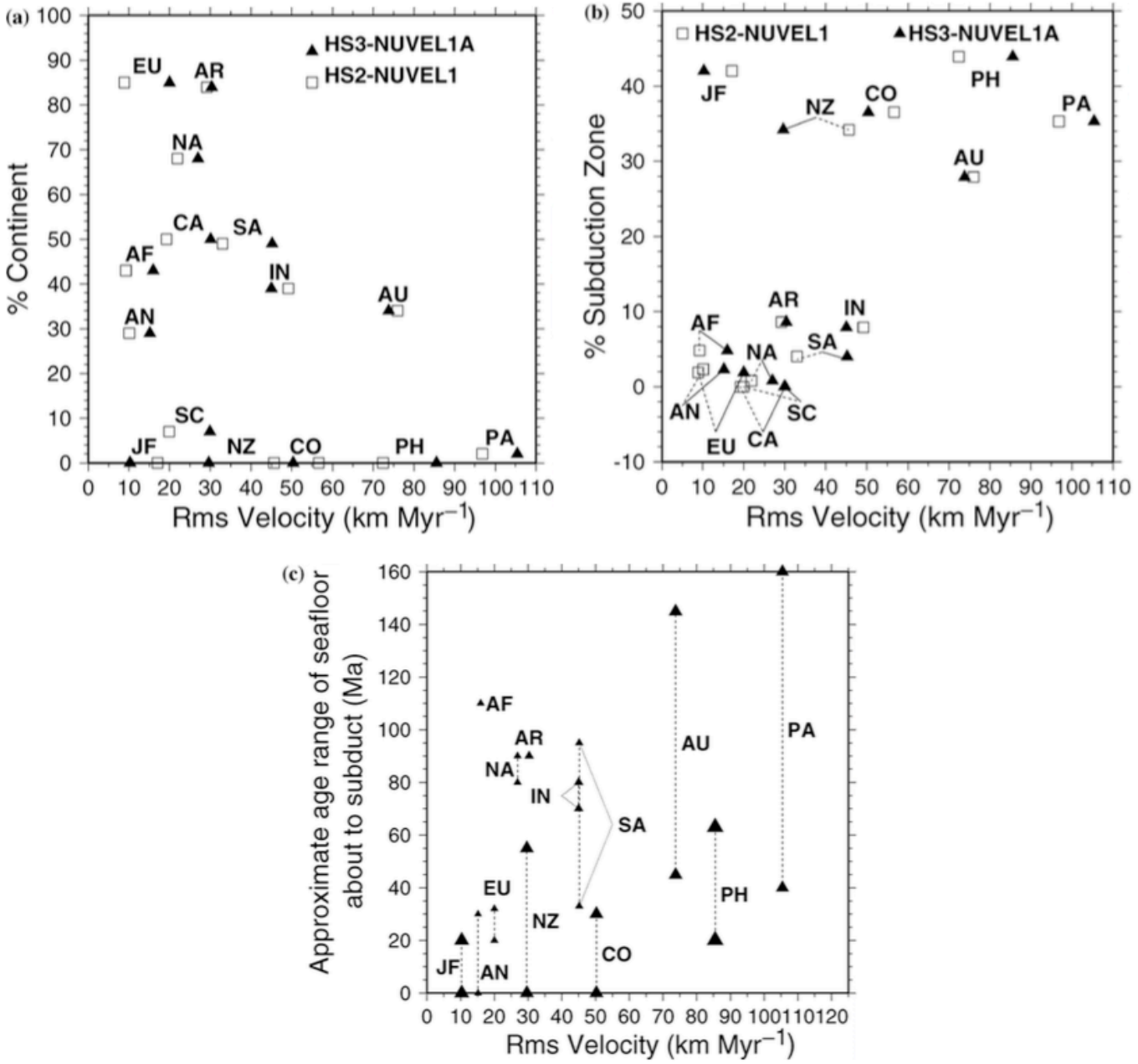

Gripp and Gordon, 2002